

Two-photon microscopic imaging in the vasculature – a sub-cellular window for imaging nitric oxide and thrombus

Von der Fakultät für Mathematik, Informatik und Naturwissenschaften der RWTH Aachen Universität zur Erlangung des akademischen Grades eines Doktors der Naturwissenschaften genehmigte Dissertation

vorgelegt von

M.Sc. Microbiology

Mitrajit Ghosh

aus Chittaranjan, India

Berichter: Univ.-Prof.Dr.rer.nat. Jürgen Bernhagen

Univ.-Prof.Dr.rer.nat. Marc A.M.J. van Zandvoort

Univ.-Prof.Dr.rer.nat. Ulrich Schwaneberg

Tag der mündlichen Prüfung: 09.09.2013

Diese Dissertation ist auf den Internetseiten der Hochschulbibliothek online verfügbar.

**"Many people say that it is the intellect which makes a great scientist.
They are wrong: it is character."**

- Albert Einstein

Table of Contents

Abbreviations	6
List of figures and tables	8
1. General Introduction	11
1.1 Nitric Oxide	11
1.1.1 Nitric Oxide biosynthesis.....	12
1.1.2 Intracellular mechanisms of NO action	14
1.1.3 Vascular effects of NO	16
1.1.4 Multimodal imaging of NO	17
1.2 Arterial wall structure	19
1.3 Thrombosis	21
1.4 Carbon dots	23
1.5 Two-photon laser scanning microscopy (TPLSM)	24
1.6 Scope of the study	27
1.6.1 Nitric oxide imaging in the vasculature.....	27
1.6.2 Investigation of arginine supplementation and effects of Arginase-1 deficiency on vascular NO production (various NOS mediated) during endotoxemia.....	30
1.6.3 In vitro thrombus imaging with carbon dot	33
2. Materials and methods	34
2.1 Materials	34
2.1.1 General equipments	34
2.1.2 Consumables.....	34
2.1.3 Buffers, Chemical Reagents, Dyes	34
2.2 Animal Care and Mouse strains	35
2.3 Methods	35

	4
2.3.1 Spectroscopic measurements	35
2.3.2 Cytotoxicity assay	36
2.3.3 Cell cultures and imaging	36
2.3.4 Griess assay	37
2.3.5 Tissue preparation	37
2.3.6 Mounting procedure	38
2.3.7 Wire myography	39
2.3.8 In vitro thrombus formation	40
2.3.9 Two-photon imaging	40
2.3.10 Two-photon ex vivo NO-production measurements in carotid arteries of endotoxemia mouse model.....	42
2.4 Image analysis	42
2.5 Statistical analysis	44
3. Results	45
3.1. Validation of the NO probe for vascular biology	45
3.1.1. Cu ₂ FL2E is more sensitive and specific than DAF-2-DA for NO detection	45
3.2. Visualization-analysis NO metabolism in vitro in endothelial cells	48
3.2.1. NO production can be imaged specifically in vitro in endothelial cells with Cu ₂ FL2E	48
3.3 Visualization of NO synthesis and vasomotor responses in the vasculature	54
3.3.1 NO production can be imaged and visualised ex vivo in non-precontracted murine carotid arteries and aortas with Cu ₂ FL2E.	54
3.3.2. Time-profile of changes in fluorescence intensity in ECs and SMCs of carotid arteries after stimulation.....	58
3.3.3. NO production can be imaged and visualized ex vivo in precontracted murine carotid arteries with Cu ₂ FL2E.....	59

3.3.4 Cu ₂ FL2E does not influence the contractile behaviour of carotid arteries after pre-contraction.....	61
3.3.5 3D reconstruction of the vessel.....	62
3.3.6 NO-mediated vasomotor response of arteries can be determined at end point and correlated with the change in fluorescence intensity	63
3.4. Visualization of NO synthesis and vasomotor response in the carotid artery in wild type and Arginase-1 deficient mice	65
3.4.1 NO synthesis in normal and endotoxemic carotid artery of wild type mice: effect of arginine supplementation	65
3.4.2 NO synthesis in normal and endotoxemic carotid artery of Arginase-1 -/- mouse (<i>Arg^{fl/fl}/Tie2-Cre^{tg/-}</i>): effect of arginine supplementation.....	69
3.4.3 <i>In vitro</i> assessment of arginine supplementation on human coronary arterial endothelial cells	72
3.5. <i>In vitro</i> thrombus imaging with carbon dot and TPLSM	73
3.5.1 Structure of the bilabeled peptide.....	73
3.5.2 Characterization of fluorescent properties of C-Dot.....	74
3.5.3 Thrombus imaging with TPLSM and c-dot-TAMRA conjugated A14 peptide reveal c-dot and TAMRA as FRET pairs	75
4. General discussion – future perspectives	77
5. Summary.....	83
6. Zusammenfassung	85
7. Acknowledgements	87
8. References.....	91
9. Curriculum Vitae	105

Abbreviations

ACh	Acetylcholine
ARG-1	Arginase-1
C-Dot	Carbon dot
DAPI	4',6-diamidino-2-phenylindole
DAF-2-DA	Diaminofluorescein-2-diacetate
ECs	Endothelial cells
EDHF	Endothelium derived hyperpolarizing factor
eNOS	Endothelial nitric oxide synthase
ECM	Endothelial cell medium
FRET	Fluorescence resonance energy transfer
Gd	Gadolinium
HCAECs	Human coronary artery endothelial cells
HMVECs	Human microvascular endothelial cells
HBSS	Hanks balanced salt solution
iNOS	Inducible nitric oxide synthase
L-NAME	L-N ^G -nitroarginine methyl ester
nNOS	Neuronal nitric oxide synthase
NA	Noradrenaline
NO	Nitric oxide
NOS	Nitric oxide synthase
PAECs	Porcine aortic endothelial cells
PBS	Phosphate buffer solution
PI	Propidium Iodide
PE	Phorbol ester

Abbreviations

Q-Dot	Quantum dot
ROS	Reactive oxygen species
SMCs	Smooth muscle cells
SNAP	S-nitroso-N-acetyl-D,L-penicillamine
TAMRA	Tetramethyl rhodamine
TPLSM	Two-photon laser scanning microscopy

List of figures and tables

Fig. 1 NO: the miracle molecule - **12**

Fig. 2 Intracellular mechanism of NO formation via NOS activation - **15**

Fig. 3 NO signaling pathway - **16**

Fig. 4 Simplified model of an arterial vessel wall - **20**

Fig. 5 Process of thrombus formation in a blood-vessel - **22**

Fig. 6 Carbon dots for imaging - **24**

Fig. 7 Representation of the Jablonski diagram - **26**

Fig. 8 Representation of the core of the study - **28**

Fig. 9 Scheme of NO detection by Cu₂FL2E in endothelial cells - **29**

Fig. 10 Experimental set up of the prolonged endotoxemia model - **31**

Fig. 11 Scheme of arginine metabolism by endothelial cell by various pathways - **32**

Fig. 12 Schematic representation of the perfusion chamber used to mount isolated arteries - **39**

Fig. 13 Two-photon microscopic setup (Leica TCS SP5) - **41**

Fig. 14 (a) Image analysis: Step1 - **43**

Fig. 14 (b) Image analysis: Step2 - **43**

Fig. 14 (c) Image analysis: Step 3 - **44**

Fig. 15 Sensitivity of Cu₂FL2E compared with DAF-2-DA - **45**

Fig. 16 Specificity of Cu₂FL2E compared with DAF-2-DA for NO and H₂O₂ - **46**

Fig. 17 Cytotoxicity assay - **47**

Fig. 18 Detection of NO with Cu₂FL2E produced by endothelial cells *in vitro* - **49**

Fig. 19 Griess assay - **50**

Fig. 20 HCAECs with eNOS phosphorylation - **51**

Fig. 21 NO detection in human coronary arterial endothelial cells (HCAECs) with PE - **52**

List of figures and tables

Fig. 22 Detection of NO with Cu₂FL2E produced by endothelial cells *in vitro* with flow - **53**

Fig. 23 Detection of NO produced in explanted murine carotid arteries *ex vivo* using Cu₂FL2E - **55**

Fig. 24 Detection of NO produced in explanted murine carotid arteries *ex vivo* using Cu₂FL2E with ACh - **56**

Fig. 25 DAPI staining of SMCs and ECs - **57**

Fig. 26 Detection of NO produced in explanted murine aorta *ex vivo* using Cu₂FL2E in aorta - **58**

Fig. 27 Profiles of NO occupancy in SMCs and ECs in carotid artery - **59**

Fig. 28 Detection of NO produced in explanted murine carotid arteries *ex vivo* using Cu₂FL2E with precontraction - **60**

Fig. 29 Original trace recordings of percentage of relaxation of mouse carotid arteries in a vessel myograph - **61**

Fig. 30 3D reconstruction of vessel - **62**

Fig. 31 Functional imaging of NO - **64**

Fig. 32 Effect of SNAP and CuCl₂ on integrity of Cu₂FL2E - **65**

Fig. 33 Detection and quantification of NO produced in explanted murine carotid arteries (normal) *ex vivo* using Cu₂FL2E for arg supplementation - **66**

Fig. 34 Detection and quantification of NO produced in explanted murine carotid arteries (endotoxemic) *ex vivo* using Cu₂FL2E for arg supplementation - **67**

Fig. 35 Functional imaging of NO in endotoxemic arteries - **68**

Fig. 36 *Ex vivo* NO production measured in carotid arteries of Control and Arg^{fl/fl}/Tie2-Cre^{tg/-} mice - **69**

Fig. 37 Detection and quantification of NO produced in explanted murine arg^{-/-} carotid arteries *ex vivo* using Cu₂FL2E - **70**

Fig. 38 Detection and quantification of NO produced in explanted murine arg^{-/-} carotid arteries (endotoxemic) *ex vivo* using Cu₂FL2E - **71**

List of figures and tables

Fig. 39 Assessment of arginine supplementation on survival of HCAECs using Cu₂FL2E - **72**

Fig. 40 Structure of A14 peptide conjugated with TAMRA (indicated with blue box) and C-dot (indicated with red circle) at the N-terminal of the peptide - **73**

Fig. 41 Fluorescent characteristics of C-dot - **74**

Fig. 42 Fluorescence from C-dot expressed on fibrin - **75**

Table 1: Mouse strains used in the study - **35**

1. General Introduction

1.1 Nitric Oxide

In Sir John Vane's words endothelium is a "marvelous factory". This endothelium indeed opened a major new chapter in cardiovascular physiology. In 1980, Furchgott and Zawadzki found that vascular endothelium is indispensable for the vasodilator action of acetylcholine in isolated arterial strips or rings **(1)**. Removal of the endothelium prevented the relaxant effect of acetylcholine and even led to a contraction. Thus, stimulation of the endothelial cells caused the release of a substance, which Furchgott named "endothelium derived relaxing factor" (EDRF). This was an "Eureka" moment in science as it defined a novel endogenous intercellular signaling system, whose further characterization and physiological and pathophysiological consequences were to grow exponentially over the years to come. In 1987, EDRF was shown to be nitric oxide (NO), as independently pointed out by Moncada and Ignarro **(2, 3)**. This increasing interest in NO led to its nomination as molecule of the year by Science in 1992 **(4)**.

The fundamental discoveries in NO research led to the awarding of Nobel prize for Physiology and Medicine to Robert F. Furchgott, Louis J. Ignarro, and Ferid Murad in 1998 **(5)**. NO is now known to serve a multitude of physiological roles throughout mammalian cardiovascular systems, let alone in other systems and other organisms. Nitric oxide discovery was indeed a landmark in biology. This simple, free radical gas mediates various biological phenomena and seems to regulate diverse processes. NO is involved in various vascular phenomena such as vascular relaxation **(2, 3)**, inhibition of platelet adhesion and aggregation **(6, 7, 8, 9)**, and inhibition of vascular smooth muscle cell mitogenesis **(10)**. The bioavailability of nitric oxide is decreased in many cardiovascular complications, which contribute to vasospasm, thrombus formation, and intimal thickening, ultimately leading to ischemia and infarction. Prevention of identified predisposing conditions is crucial, and hence, NO is an important molecule to study in this perspective.

1. General Introduction

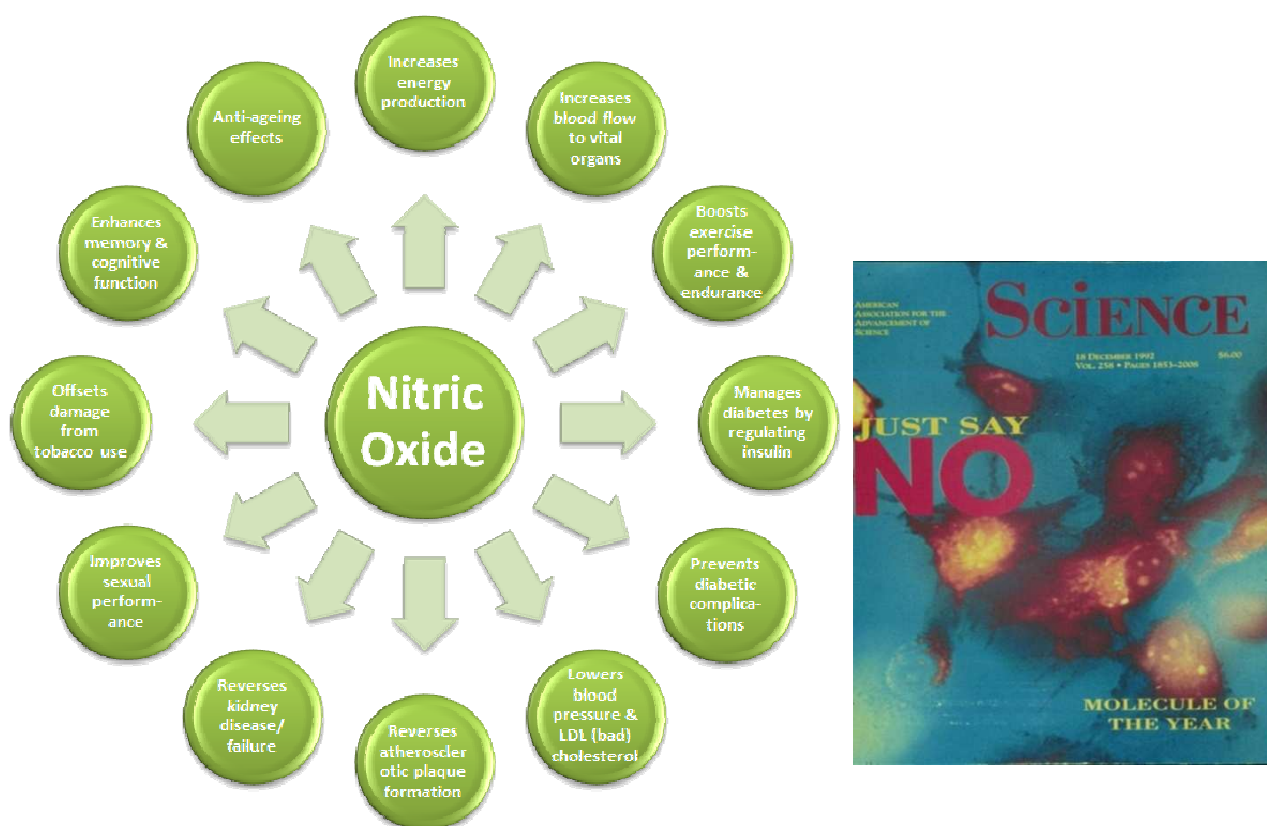


Fig.1 NO: the miracle molecule. *Left:* Flow chart of many benefits of NO (adapted from www.whatistremeno.net), *Right:* Science magazine's cover page (1992) displaying NO as the "molecule of the year" (adapted from Koshland Jr. *Science* 1992).

1.1.1 Nitric Oxide biosynthesis

Shortly after 1987, the amino acid L-arginine was found to be the substrate for endogenous NO synthesis **(11)**. NO synthase (NOS) was identified as the enzyme system responsible for the conversion of L-arginine to NO **(11)**. NOS exists in three distinct established isoforms; n-NOS (originally identified as constitutive in neuronal tissue, also known as type I NOS), i-NOS (originally identified as being inducible by cytokines or bacterial lipopolysaccharide [LPS] in macrophages and hepatocytes, also known as type II NOS) and e-NOS (originally identified as constitutive in vascular endothelial cells, also known as type III NOS). All three NOS isoforms share similar, if not identical, cofactor

1. General Introduction

and prosthetic group requirements and they all utilize L-arginine as the substrate for NO generation. The various NOS isoforms are distributed in different cells and tissues. Along with these differences in tissue or cellular origin, the three NOS isoforms do differ significantly with regard to their biophysical properties and mechanisms of physiological regulation. The constitutive enzymes (cNOS (nNOS and eNOS), [also known as NOSI and NOSIII]) were originally described as being Ca^{2+} and calmodulin dependent **(12)**. eNOS is responsible for the NOS activity of vascular endothelium in blood vessels of all sizes and types (i.e. arteries, arterioles, capillaries, venules, and veins), in different tissues and organs (eg. heart, brain, lung, liver, and kidney) and in various species **(13)**. However, eNOS is not uniquely expressed by endothelial cells, but is also constitutively expressed in megakaryocytes, platelets, T-cells, erythrocytes, cardiomyocytes **(14)**, epithelial cells, and rat hippocampus **(15)**. nNOS has a widespread distribution in the central and peripheral nervous system **(16)**, but has also been detected in non-neuronal cell types, such as rhabdomyocytes, epithelial cells, mast cells, and neutrophils **(15)**. It is widely expressed in different tissues. The high activity of nNOS in brain and skeletal muscle, plays an important role in physiological neuronal functions. It is also an integral player in various neurological disorders in which excessive NO production leads to neural injury **(17)**. There are two basic pathways for the stimulation of cNOS, both of which involve calcium ions from subsarcolemmal storage sites. First, forces acting on the vascular endothelium generated by blood flow cause release of calcium and subsequent cNOS activation. Therefore, increases in blood flow stimulate NO formation (flow-dependent NO formation). Second, endothelial receptors for a variety of ligands stimulate calcium release and subsequent NO production (receptor-stimulated NO formation). Included are receptors for acetylcholine, bradykinin, substance-P, adenosine, and many others vasoactive substances.

The inducible enzyme iNOS [also known as NOSII] is clearly different from cNOS as it is fully active in the absence of Ca^{2+} or calmodulin. Various cell types and tissues that are exposed to cytokinines (eg, tumor necrosis factor-alpha [TNF-alpha], interleukin-1 [IL-1] or bacterial products [eg, endotoxin or LPS] induce iNOS. They are also expressed in certain cells/tissues such as the mouse ileal mucosa **(18)**, human airway epithelium **(19)**, and human B lymphocytes **(20)**. The main characteristic of iNOS is that it releases

1. General Introduction

large amounts of NO continuously; the amount released per unit of time from fully activated macrophages is a thousand times higher than that released from NOS in endothelial cells. These high concentrations of NO are cytostatic and cytotoxic on parasitic microorganisms and tumor cells. Consequently, NO is an essential component of the nonspecific immune defense system **(21, 22, 23)**.

1.1.2 Intracellular mechanisms of NO action

NO is a unique messenger. Being uncharged, NO is soluble both in water and lipid and can diffuse freely across membranes. When it reaches the bloodstream, most NO is quickly bound to hemoglobin and converted to nitrate. After conversion to nitrate it is eliminated in the urine with a half life of few hours **(24)**. However, NO itself has a half life of few seconds in solutions *in vitro* and its biological half life is in the order of few minutes **(25)**. NO diffuses out of the cell that generates it into the target cells, where it interacts with specific molecular targets. The best characterized receptor of NO is iron, contained in certain proteins in heme group or as an iron-sulphur complex. On NO binding to the iron in the heme group of soluble guanylate cyclase (sGC), the enzyme is activated **(26)**. The binding of NO to sGC results in the conversion of guanosine tri-phosphate (GTP) to cyclic guanosine mono-phosphate (cGMP). Subsequently, the increase in cGMP activates other cellular processes, thereby acting as a second messenger, activating cGMP-dependent protein kinase, which decreases cytosolic Ca²⁺ concentration and modulates ion channel function leading to inhibition of platelet activity or relaxation of vascular smooth muscle cells. NO also acts independent of the sGC/ cGMP system, such as activation of Ca²⁺ dependent K⁺ channels in vascular smooth muscle cells to produce hyperpolarization and relaxation **(27)**. Thus, by both sGC-dependent and sGC-independent mechanisms, NO not only dilates blood vessels, but also inhibits platelet function, inhibits stimulated neutrophils adhesion, and has antimitogenic effects in vascular smooth muscle cells.

1. General Introduction

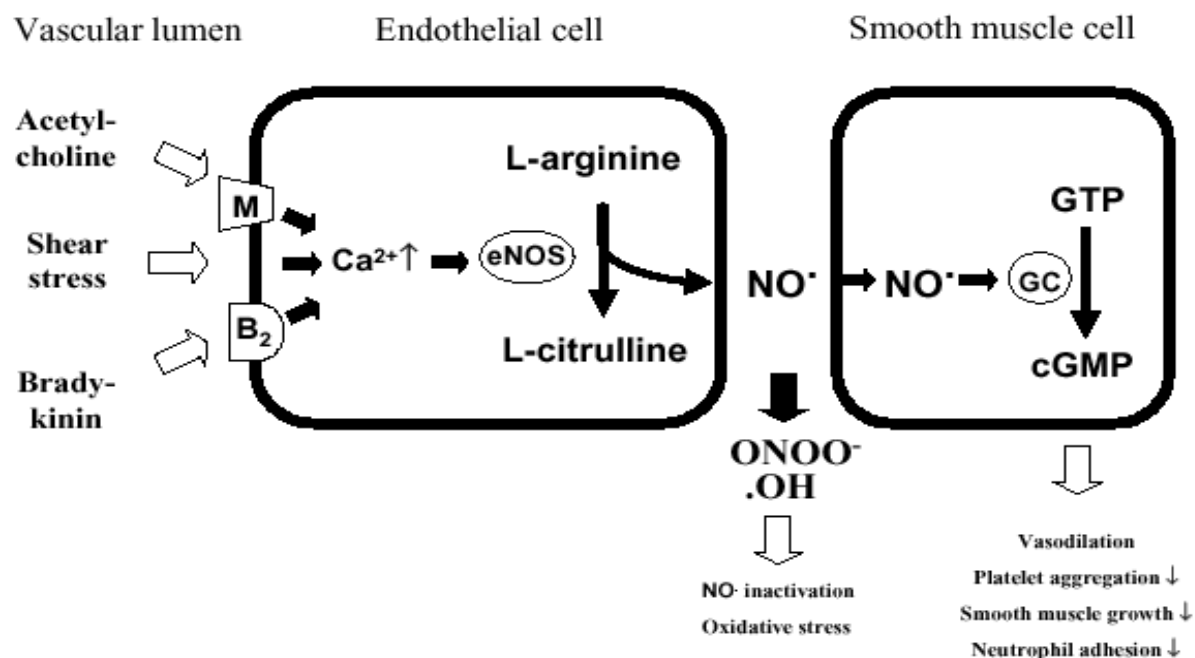


Fig.2 Intracellular mechanism of NO formation via NOS activation (adapted from Lassila 2000, www.ethesis.helsinki.fi)

Endogenous production of NO by native and cultured endothelial cells in response to shear stress is associated with only a transient and minimal increase in calcium ion. In the absence of extracellular Ca^{2+} and in the presence of a calmodulin antagonist, shear stress stimulates a continuous production of NO (28). The ability of the EC to sense shear stress involves an array of signaling pathways and cellular components, including G proteins, caveolae, integrins and the cytoskeleton, which may all participate in the mechanotransduction that lead to the activation of eNOS. Several agonists can induce the production of nitric oxide. Simultaneous measurements of calcium and NO in bradykinin stimulated ECs *in vitro* reveal that a transient increase in calcium was rapidly followed by an increase in NO that outlasted the calcium transient (28). VEGF is a potent vascular EC-specific mitogen that stimulates EC proliferation, microvascular permeability, vasodilation and angiogenesis (29). Stimulation of beta-adrenoceptors on vascular SMCs results in vasorelaxation, through adenylate cyclase activation and a consequent increase in cyclic adenosine monophosphate (cAMP) intracellularly (12).

1. General Introduction

1.1.3 Vascular effects of NO

Constitutive NOS isoforms are regulated by Ca^{2+} via the Ca^{2+} -binding protein calmodulin. Due to Ca^{2+} influx into the cell, this Ca^{2+} -calmodulin complex is formed, which then binds constitutive NOS and most likely displaces the enzyme from its location to caveolae in the plasma membrane; which leads to activation of NOS and hence, increase in NO level (30, 31). Phosphorylation also plays a regulatory role in the activity of constitutive NOS. In comparison to constitutive NOS, iNOS activity is regulated primarily via the induction of *de novo* enzyme protein synthesis. The availability of substrate and cofactors (most notably BH_4) also play a role in iNOS regulation in macrophages and smooth muscle (21, 22, 23), as in constitutive NOS. NO derived from the constitutive NOS subtypes is involved in the maintenance of vascular tone and

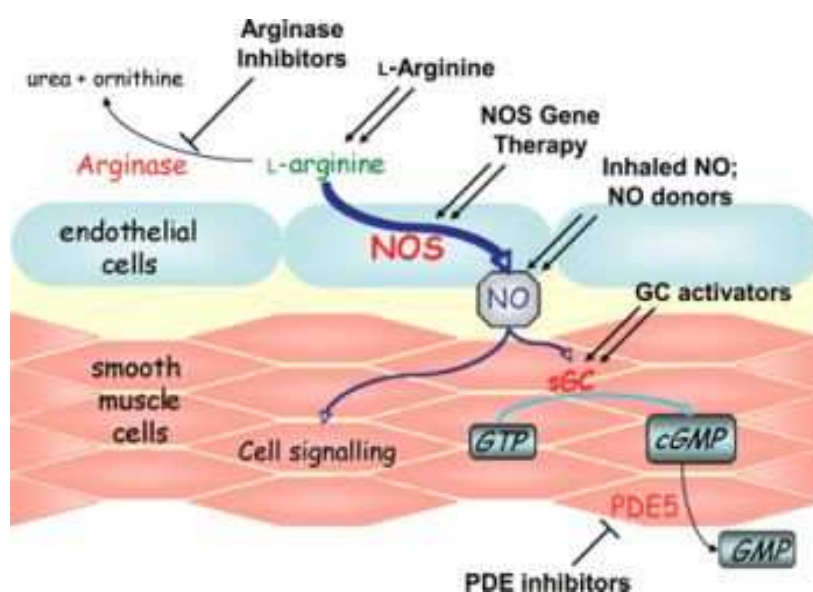


Fig.3 NO signaling pathway. A classic arginine-nitric oxide synthase-nitric oxide synthesis pathway highlighting the multiple levels of this pathway (adapted from Zuckerbraun *et al. Cardiovasc Res* 2011). Activation of eNOS in ECs involves an array of signaling pathways and cellular components. Several agonists can induce the production of nitric oxide. The binding of NO to sGC in SMCs results in the conversion GTP to cGMP. Subsequently, the increase in cGMP activates other cellular processes,

1. General Introduction

neurotransmission, its physiological concentrations may be under stricter regulation than that of NO derived from iNOS which is made in large quantities as a cytotoxic agent.

Vascular actions of NO include direct vasodilation (flow mediated and receptor mediated), indirect vasodilation by inhibiting vasoconstrictor influences (by inhibiting angiotensin II and sympathetic vasoconstriction), anti-thrombotic effect (inhibits platelet adhesion to the vascular endothelium), anti-inflammatory effect (inhibits leukocyte adhesion to vascular endothelium), anti-proliferative effect (inhibits smooth muscle hyperplasia) and scavenging of superoxide anion.

Impaired NO production and bioavailability results in causing thrombosis due to platelet aggregation and adhesion to vascular endothelium, vasoconstriction (coronary vasospasm, elevated systemic vascular resistance), inflammation due to upregulation of leukocyte and endothelial adhesion molecules, and also, vascular hypertrophy and stenosis. These abnormal NO availability conditions are associated with cardiovascular complications like hypertension, diabetes, obesity, atherosclerosis, dyslipidemia, heart failure etc.

1.1.4 Multimodal imaging of NO

NO governs a myriad of physiological and pathophysiological processes. NO is an important participant in various vascular diseases. Noninvasive imaging of NO or NOS can provide new insights in understanding these diseases and facilitate the development of novel therapeutic strategies. An imaging platform integrates and assimilates various techniques for visualization of NO with better spatial resolution and sensitivity. To this end, the most important imaging techniques in application are optical imaging (fluorescence and chemiluminescence), electron paramagnetic resonance (EPR) imaging, and magnetic resonance imaging (MRI).

Fluorescence imaging of NO requires various agents for fluorescent NO detection that include: diaminonaphthalene (**32, 33, 34**), dichlorofluorescein (**35, 36**), iron-based sensor (**37**), cytochrome C based sensor (**38**), cobalt complex (**39, 40**), fluorescent nitric oxide chelotropic traps (FNOCTs) (**41, 42**), diaminofluoresceins (**43**), diaminorhodamines (**44**),

1. General Introduction

diaminoanthraquinone **(45)**, porphyrin based sensors, copper-based compounds **(46, 47)**, FRET-based NO sensors **(48)**, and nanoengineered sensors **(49)**. All these compounds exhibit certain advantages and certain disadvantages, consequently limiting their application in various systems. Diaminofluoresceins (DAFs) are the most extensively used agent for NO imaging. These compounds react with NO in the presence of oxygen to form the fluorescent products quantitatively in an aqueous medium, even under physiological conditions. However, there are serious limitations for using DAFs. They only react with NO in the presence of oxygen, which is not an ideal condition to study interplay of NO in various conditions (like hypoxic tumor etc.). Also, they are not specific for NO and react with oxidized NO products rather than with NO itself, which may not truly reflect the status of NO in some diseases. Certain nitrogen-containing radicals or reducing agents can also cause fluorescence enhancement of these compounds. Hence, these compounds are not highly selective and exclusive for NO imaging, and thus are not the best choice for measurement of endogenous NO formation. However, the latest intervention with copper-based compounds looks promising for future application in terms of specificity and sensitivity. The stability and toxicity aspects are to be optimized further for potential application *in vivo*. In the present study, we evaluated the feasibility and characteristics of a specific, cell-trappable, copper-based fluorescent NO probe (Cu₂FL2E) for vascular NO analysis both *in vitro* and *ex vivo*. Cu₂FL2E, developed by McQuade L.E. *et al.* **(47)**, has highly desirable properties in comparison to conventional fluorescent NO probes. The Cu₂FL2E probe is non-toxic and readily internalized by cells *in vitro*. Moreover, it reacts with NO directly and specifically rather than with its oxidation products. Upon reaction of Cu₂FL2E with NO, Cu(II) is reduced to Cu(I) with concomitant formation of highly fluorescent, N-nitrosated FL2E-NO **(46, 47)**. These characteristics of Cu₂FL2E make it a useful intracellular sensor for NO. In terms of high spatial resolution, high sensitivity, and experimental feasibility, fluorescence imaging techniques still stand superior to other imaging modalities. We establish that Cu₂FL2E is a valuable tool for direct and specific imaging and visualization of NO in ECs *in vitro* and, in conjunction with TPLSM, *ex vivo* in intact vessels with high spatiotemporal accuracy.

1. General Introduction

Chemiluminescence imaging of NO is limited by its low specificity and time consuming procedure. EPR is a very powerful imaging tool in NO research, but the heavy instrumentation, high cost, small sample size, and the potential toxicity of the spin trapping agents are the major roadblocks for future clinical applications. Despite good resolution of MRI, its measurement is questionable due to its low sensitivity. Other imaging techniques like ultrasound, time-resolved photoelectron imaging, Hb spectral alteration imaging, laser induced fluorescence detection, and calcium amplification imaging have been used for NO detection. The future of molecular imaging, based on multimodal imaging approach may provide more accurate information on NO detection like EPR-CT **(50)**, EPR-MRI, EPR-chemiluminescence **(51)**, and PET/MRI **(52, 53)** imaging have been attempted, but further research/optimization is necessary for its potential successful application.

1.2 Arterial wall structure

The arterial wall of murine large arteries is anisotropic, multi-storey, and non-linearly elastic. It consists of three different layers; tunica intima, tunica media, and tunica adventitia. The tunica intima or inner layer is relatively thin and mainly consists of the endothelium (a single layer of endothelial cells) that lines the vessel lumen, underlying connective tissue (the basal lamina), and the internal elastic lamina. Endothelial cells monitor and regulate many processes, such as vasoconstriction and vasodilation by releasing regulatory factors, permeability to specific molecules, and in case of inflammation, capturing and allowing trans- and paracellular migration of inflammatory cells **(54)**. The luminal side of endothelial cells is covered by a matrix of proteoglycans and glycoproteins called the glycocalyx. This matrix also regulates vascular permeability and may induce mechanotransduction **(55)**. The basal lamina connects the endothelial cells to the vascular wall; it is a structure of extracellular matrix components such as collagen. Collagen is a fibrillar protein that provides the strength of the vascular wall. The internal elastic lamina separates the tunica intima from the tunica media. It consists of elastin, an extracellular matrix protein that provides the elasticity of the vascular wall. The tunica media or medial layer primarily consists of several concentric layers of

1. General Introduction

helically arranged vascular smooth muscle cells. The number of layers depends on size and type of the artery. The vascular smooth muscle cells are separated by fibers of extracellular matrix (collagen, elastin). Interposed between these layers of vascular smooth muscle cells are intermediate elastic laminae (the number of intermediate laminae again depends on the size and type of the artery) (56). The main function of the tunica media is control of vascular tone. Moreover, the vascular smooth muscle cells are the cellular source of the extracellular matrix. The external elastic lamina (EEL) is the most outer elastic laminae of the tunica media and separates it from the tunica adventitia; it is composed of many elastin fibers that form a finely woven structure. The tunica media predominantly determines the mechanical properties of the arterial wall. The tunica adventitia is the outer most layer of the arterial vessel wall and its basal structure consists of collagen and elastin fibers. These fibers allow the arteries to stretch and to prevent overexpansion due to the pressure that is exerted on the walls by blood flow.

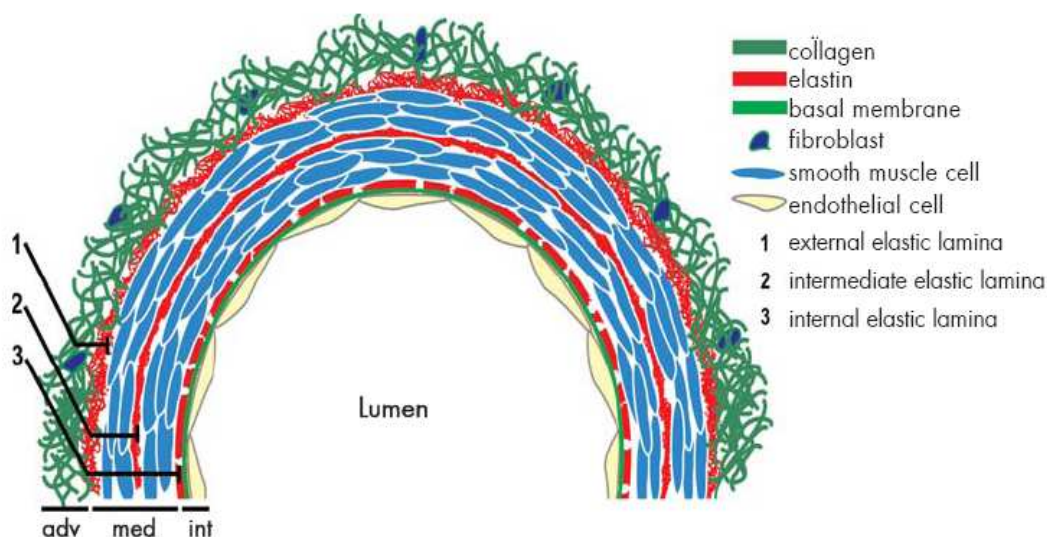


Fig. 4 Simplified model of an arterial vessel wall. The number of vascular smooth muscle cell layers and intermediate elastic laminae is dependent on type of artery and species. Note the fenestrations (white) in the internal elastic layer (adapted from R.T.A. Megens, Maastricht 2008, ISBN 978-90-9022535-7).

1. General Introduction

In between these fibers, fibroblast-like cells and vasomotor nerves are present. In the tunica adventitia of large arteries with a vessel wall that is too thick to be solely nourished by diffusion, a network of branched small blood vessels or vasa vasorum **(57)** is present that provides metabolites and oxygen to the tunica adventitia and abuminal parts of the tunica media. The vessel walls of various large arteries have a number of structural features in common although structural variations between comparable arteries can be considerable. Note that thickness, detailed structure, and function of these three tunicae strongly depend on total diameter, type of blood vessel, and species.

Based on their diameter and location, large arteries may be classified as elastic arteries (largest arteries) or muscular arteries (medium sized arteries). Elastic arteries are located directly downstream of the heart where blood is transported under high (pulsating) pressure. The vessel wall of elastic arteries is thick and elastic, and has a buffering function reducing the pulsations of blood flow. Muscular arteries are located more closely to organs and tissues and mainly have a conductive function and control the affluence of blood to the various organs **(56)**. The vessel wall of muscular arteries is thinner and their diameter (and, hence, resistance) is controlled by contracting or relaxing the vascular smooth muscle cells in the tunica media **(56)**.

1.3 Thrombosis

Thrombosis is the formation of a blood clot (thrombus) inside a blood vessel, obstructing the flow of blood through the circulatory system. Thrombus formation is the pathological hallmark of cardiovascular events such as myocardial infarction and stroke. Normal blood vessels are lined by a continuous layer of endothelium. When the lining is disrupted, subendothelial elements, such as extracellular collagen, are exposed to the circulation. Blood platelets draw a sharp distinction between endothelium and subendothelium. This distinction governs platelet function, keeping the surface of normal vessels free of platelets while encouraging platelet deposition on exposed subendothelium. Depending on the vascular insult, attached platelets initiate either

1. General Introduction

normal (i.e. haemostatic) or abnormal (i.e. thrombotic) events. For example, platelet plugs at sites of vascular injury limit blood loss (haemostasis), while platelet masses on diseased/ atherosclerotic vessels impair blood flow (thrombosis) and contribute to myocardial infarction and stroke. When platelets are activated, they acquire enhanced capacity to catalyze interaction between activated coagulation on factors **(58, 59)**. These factors circulated in the form of inactive precursors (zymogens). Rupture of the atherosclerotic plaque leads to activation of the coagulation cascade: each zymogen is converted into an activated coagulation factor, which in turn activates the next zymogen in the sequence.

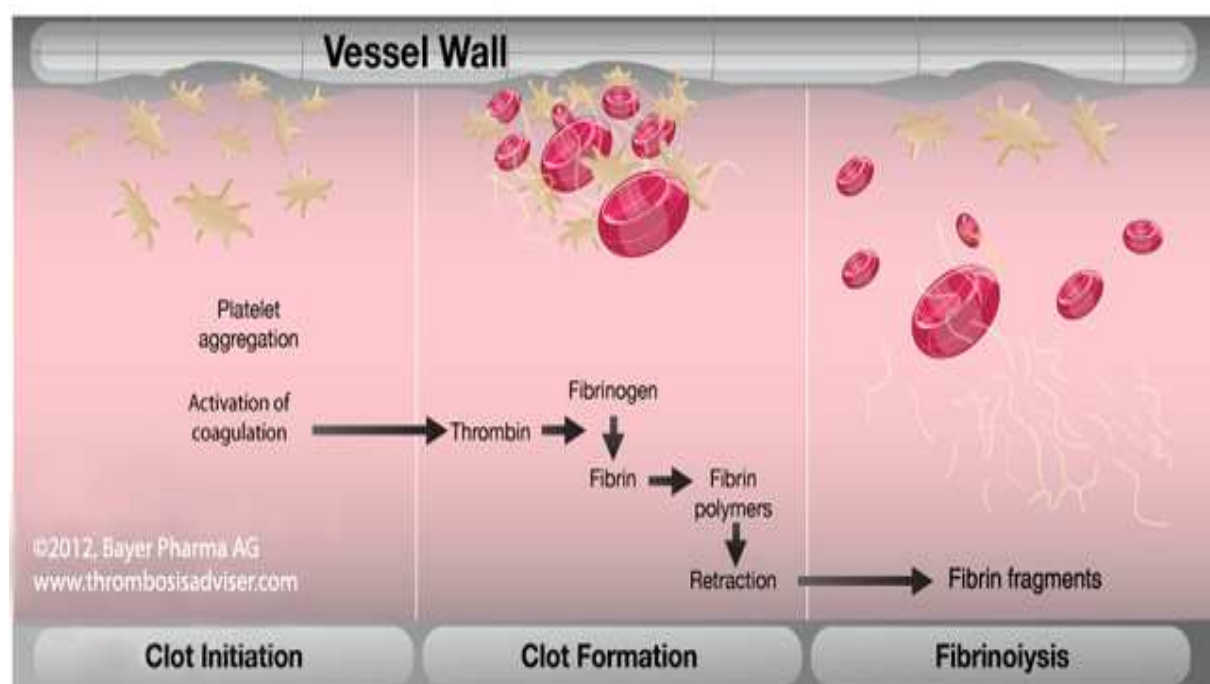


Fig. 5 Process of thrombus formation in a blood-vessel (adapted from Bayer Pharma AG, www.thrombosisadviser.com)

This process culminates in the generation of thrombin, an enzyme that converts the soluble protein fibrinogen to insoluble fibrin. This is followed by cross-linking of fibrin fibers under the influence of activated factor XIII forming a stabilized blood clot. Alpha2-antiplasmin is also cross-linked to fibrin under the influence of activated factor XIII,

1. General Introduction

making a clot more resistible to fibrinolysis. Eventually, over the course of hours, a stabilized clot develops consisting of activated platelets, erythrocytes, and leucocytes, in a matrix of cross-linked fibrin. This coagulation cascade gives rise to many molecular targets of thrombosis. Fibrin is perhaps the easiest target within a clot, and has been used in several studies. Later in this thesis, an alpha2-antiplasmin based agent is described which was used to target fibrin and visualize thrombus formation with two-photon microscopy **(60, 61)**.

1.4 Carbon dots

Carbon, an element of prehistoric discovery, is very widely distributed in nature. It is the sixth most abundant element in the cosmos, yet its abundance in the earth's crust does not even make it among the top ten elements on our planet. Carbon is a very special element because it plays a dominant role in the chemistry of life. With the revolutionary discoveries of the C molecule and carbon nanotube, carbon nanotechnology has become the building block of the entire field of nanotechnology. Whether it is deoxyribonucleic acid (DNA) or synthetic polymers, all are based on carbon backbones. Nature has been doing remarkably well by systematically organizing matter at nanometer-length scale in biological systems. It exhibits a unique property to form a wide range of structures. It is the chemical genius of carbon that it can bond in different ways to create a range of structures with entirely different properties.

Sun and colleagues prepared the carbon nanoparticles by laser ablation from a carbon target in the presence of water vapour. The resulting particles were around 5 nm in diameter. The team treated the particles with nitric acid solution before passivating their surfaces by adding a polymer coating **(62)**.

The polymer consisted of diamine-terminated oligomeric poly(ethylene glycol) PEG_{1500N} or poly(propionylethyleneimine-co-ethyleneimine)(PPEI-EI). When illuminated, the coated carbon nanoparticles photoluminesced, emitting light with visible and near-infrared wavelengths. These photoluminescent carbon dots (C-Dots) have attracted much recent attention for their promising application in the field of biomedical imaging,

1. General Introduction

as they have been found strongly two-photon active. Metal based nanoparticles have limited application in biological application for it raises serious concern on health and environment of the community.

Therefore, cDots are benign alternative, as carbon is hardly considered intrinsically toxic. On the application part, C-dots have been exploited successfully for *in vitro* and *in vivo* imaging (62, 63). cDots have been shown to be biocompatible, and non-toxic *in vivo*, while its strong fluorescent characteristics are not affected *in vivo*.

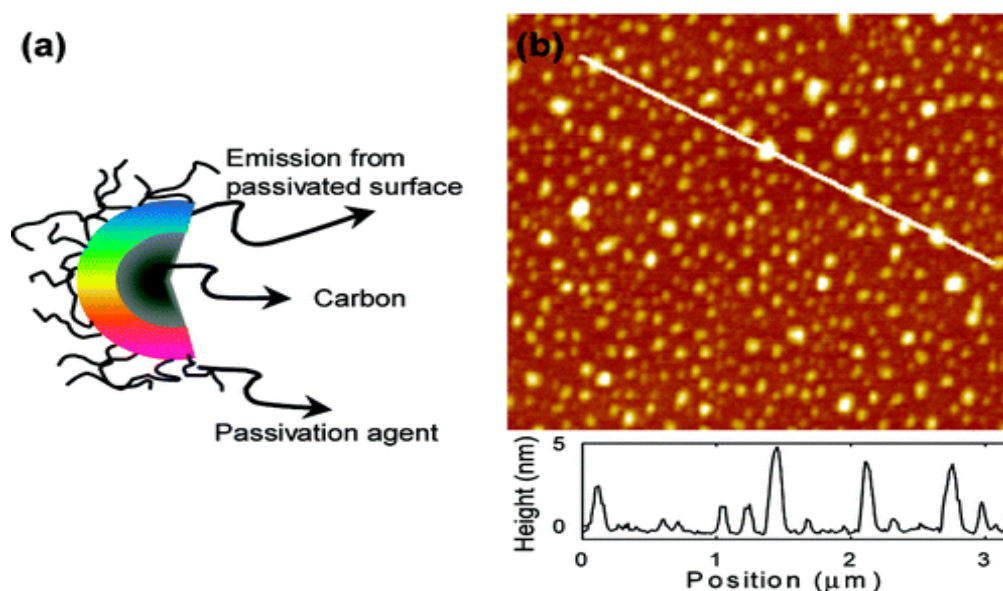


Fig. 6 Carbon dots for imaging. (a) The C-Dot structure; (b) AFM topography image of C-Dots on mica substrate, with the height profile along the line in the image (adapted from Li Cao *et al.* *J Am Chem Soc.* 2007)

1.5 Two-photon laser scanning microscopy (TPLSM)

The main theory of TPLSM came in 1931 from Maria Goppert-Mayer when she explained in her doctoral dissertation the concept of simultaneous absorption of two photons at a low energy state and emission of one photon at a higher energy state by a fluorophore in a single quantum event (64, 65). Later, in 1990, two-photon laser-scanning microscopy

1. General Introduction

(TPLSM) was developed by Webb and colleagues **(66)**. Since the probability of two-photon absorption depends on the square of the intensity of the excitation light, excitation only occurs in a very small volume at focal position of the microscope **(67)**. Therefore, out of focus absorption and excitation, as in normal or confocal fluorescence microscopy, are absent and as a result, emitted photons always originate from the focal position and thus are independent of scattering. Each photon carries approximately half the energy necessary to excite the molecule. An excitation results in the subsequent emission of a fluorescence photon, typically with a higher energy than either of the two excitatory photons. The probability of the near-simultaneous absorption of two photons is extremely low. Therefore a high flux of excitation photons is typically required, usually a femtosecond laser. The most commonly used fluorophores have excitation spectra in the 400–500 nm range, whereas the laser used to excite the two-photon fluorescence lies in the ~700–1000 nm (infrared) range. If the fluorophore absorbs two infrared photons simultaneously, it will absorb enough energy to be raised into the excited state. The fluorophore will then emit a single photon with a wavelength that depends on the type of fluorophore used (typically in the visible spectrum). Because two photons are absorbed during the excitation of the fluorophore, the probability for fluorescent emission from the fluorophores increases quadratically with the excitation intensity. Therefore, much more two-photon fluorescence is generated where the laser beam is tightly focused than where it is more diffuse. Effectively, excitation is restricted to the tiny focal volume (~1 femtoliter), resulting in a high degree of rejection of out-of-focus objects. This localization of excitation is the key advantage compared to single-photon excitation microscopes, which need to employ additional elements such as pinholes to reject out-of-focus fluorescence. Due to this excitation process, TPLSM possesses some interesting features; enhanced depth penetration, good optical sectioning, good resolution in three dimensions, and strong reduction of photobleaching, photo-damage, and photo-toxicity. This combination of features makes TPLSM better than other microscopic techniques for imaging of structures which are located deep in (scattering) tissues. The studies described in the present thesis were performed in order to visualize a variety of morphological and functional properties of healthy and diseased large arteries of mice using TPLSM.

1. General Introduction

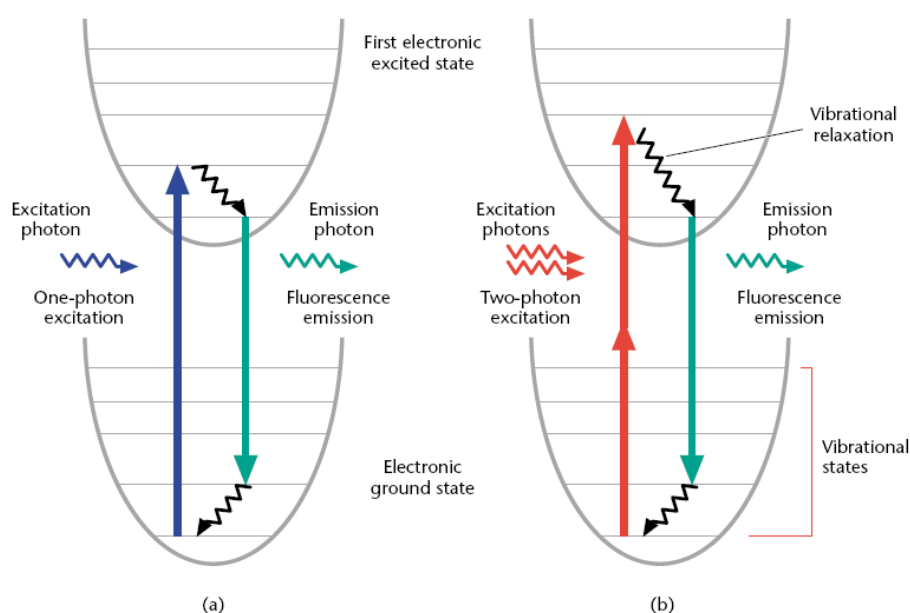


Fig. 7 Representation of the Jablonski diagram; showing one photon (a) and two photon (b) excitation. (adapted from Palikaras, K. and Tavernarakis, N. *Multiphoton Fluorescence Light Microscopy*. eLS, 2012)

However, TPLSM has also some drawbacks. (1) TPLSM is an expensive technique (68) and not yet routinely used for biological studies since it requires specific expertise for effective application (68, 69). (2) Due to the longer wavelengths used for excitation light (68), the spatial resolution in TPLSM is somewhat reduced when compared with CLSM. However, this only holds for imaging at shallow depths in the sample. Indeed, the size of the excited focal volume in TPLSM does increase with increasing depths (due to scattering and the consequent increase of the excitation light intensity), but the resolution of TPLSM deteriorates far less with increasing depth than that of CLSM (70). (3) Although photo-damage and photo-toxic effects are reduced, TPLSM can have negative consequences for the viability of biological samples (71, 72). Two photon excitation may cause heating of the sample, impaired cellular reproduction, oxidative stress, or apoptosis-like cell death. In order to avoid these effects, non-destructive imaging of live samples is limited to an optical window, dependent on the applied fluorophores, laser intensity, detector sensitivity, and the sample (72).

1.6 Scope of the study

NO is a tricky molecule to study due to its short half-life of a few seconds and high diffusibility. Serious limitation of current research methods is the ability to visualize the spatial and quantitative formation of NO. The available chemical assays and methods detect NO indirectly. Dearth of specific and selective tools to study NO directly is a challenge. However, in order to understand the role of NO in biology and medicine, its direct detection is indispensable.

Our imaging platform integrates and assimilates various techniques for visualization of NO with better spatial resolution and sensitivity.

The studies described in this thesis were performed to obtain more knowledge on the vascular structural production and functional analysis of NO in vasculature with emphasis on specific determination of NO with high spatial and temporal resolution. A novel fluorescent imaging technique is described to visualize vascular nitric oxide production at an unprecedented level. The second part of the thesis deals with translation of this research findings into a model of cardiovascular complication and illustrates the applicability of our technique in a disease system. In many cardiovascular diseases, the capacity of the L-arginine/NO system is decreased, an obvious therapeutic measure would be the pharmacological substitution of NO or stimulation of the L-arginine/NO system.

In the final part of this thesis, a novel carbon dot nanoparticle conjugated peptide is described that aids in thrombus imaging, showing future potential application. This thesis deals with two-photon microscopy in the forefront of technology to unravel the latest know-how in the vasculature.

1.6.1 Nitric oxide imaging in the vasculature

Endogenously produced vascular nitric oxide (NO) affects important biological processes such as platelet and leukocyte adhesion, smooth muscle cell (SMC) migration and endothelial regeneration in blood vessels (**3, 73, 74, 75**). Regulation of blood flow through induction of vasodilation is a major function of endothelial-derived NO. Cellular

1. General Introduction

NO is produced by three different enzymes (i.e. iNOS, eNOS, nNOS) (75), of which endothelial nitric oxide synthase (eNOS) is specifically expressed in endothelial cells (ECs) and is essential for the physiological NO (order of nanomolar range) (56, 76) production in healthy blood vessels. In response to increased shear stress, eNOS is activated in the endothelium (74, 75), with subsequent production of NO. NO then diffuses to the neighboring SMCs, where it actively induces vasodilation through SMC relaxation and subsequently increases vessel lumen diameter (3, 56) and blood flow.

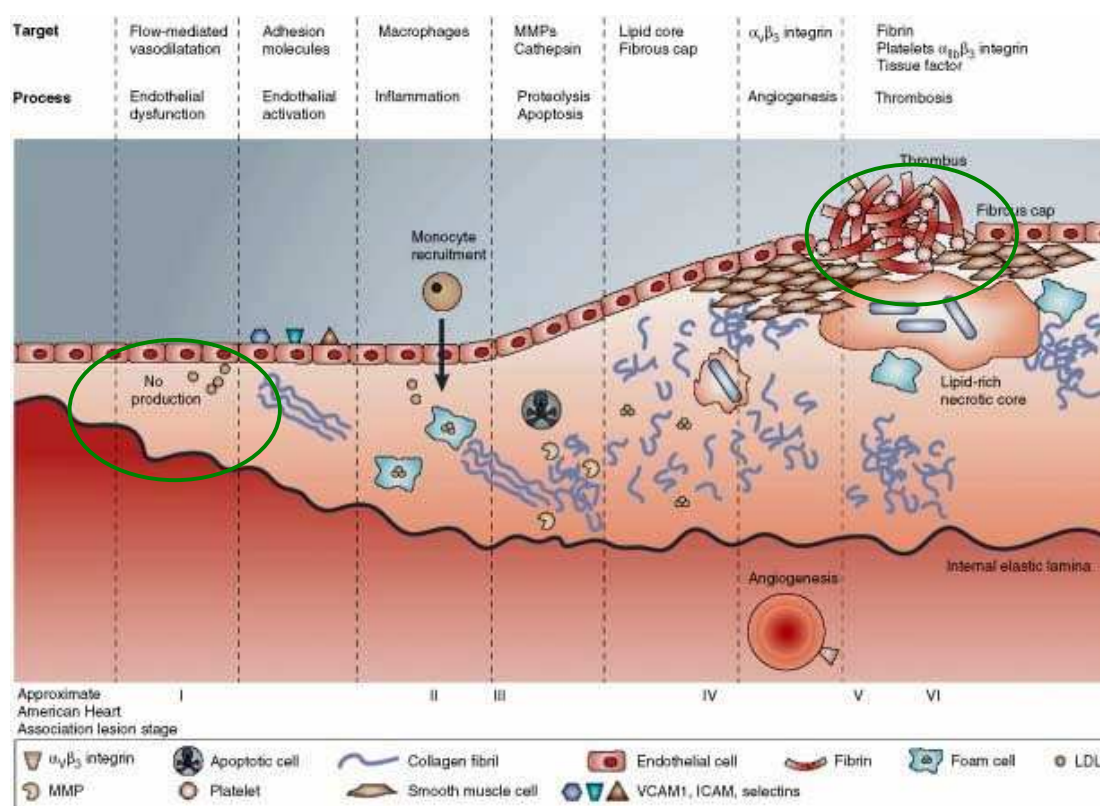


Fig. 8 Representation of the core of the study (marked in green circle): Scheme illustrating NO production in the vasculature and other molecular and cellular atherogenic players (from Robin P. Choudhury et al. *Nature Reviews Drug Discovery* **3**, 913-925, November 2004). Illustration of processes of atherogenesis ranging from pre-lesional endothelial dysfunction (left) through monocyte recruitment to the development of advanced plaque complicated by thrombosis (right). Various components shown here can be potential useful imaging targets.

1. General Introduction

Abrogation of NO production in dysfunctional endothelium is involved in numerous chronic cardiovascular diseases such as hypertension and atherosclerosis (**75, 76**), but also plays an important role in acute diseases such as sepsis.

The direct and specific detection of NO in living cells and tissues is a major hitherto unmet requirement for investigating the role and (sub) cellular NO constitution in various disease processes.

Ongoing research has been aimed at detecting and quantifying physiological NO levels (**74**), however the high diffusibility and short half-life (3-16 sec.) of NO complicate real time detection (**77, 78, 79**). Hence, little is known about the time course and diffusion profile of endogenously produced NO.

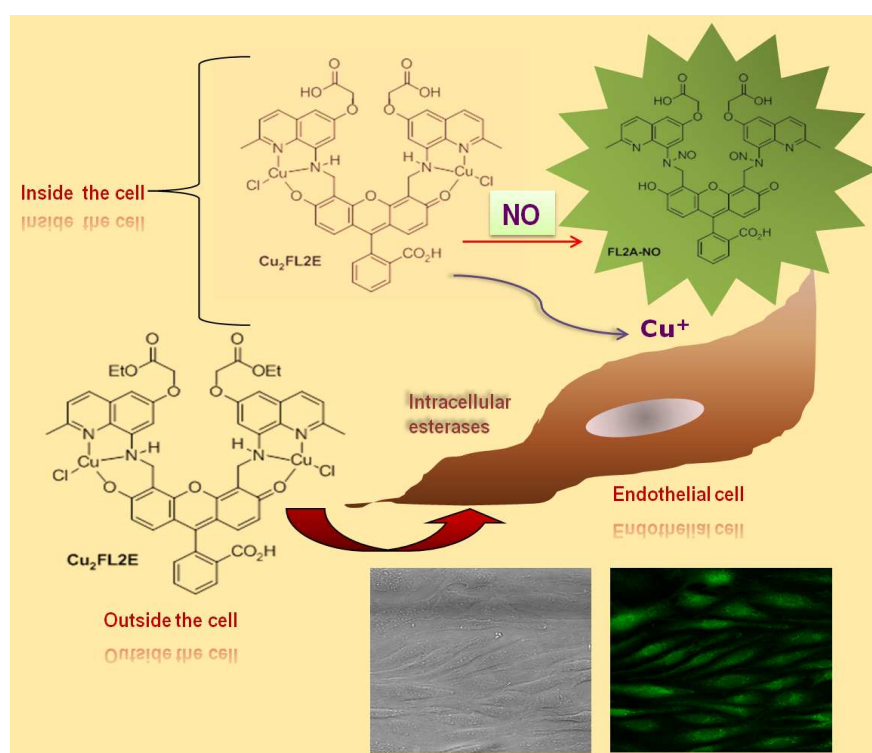


Fig. 9 Scheme of NO detection by $\text{Cu}_2\text{FL2E}$ in endothelial cells, showing the probe is trapped in the cell via hydrolysis of the pendant ester groups by intracellular esterases to give $\text{Cu}_2\text{FL2A}$ since the ester (E) is hydrolyzed to the acid (A). (Ghosh et al. submitted)

1. General Introduction

Several chemical methods are available to measure the oxidation products of NO, such as nitrite or nitrate but the detection of NO itself has proved challenging. We therefore used fluorescent probe-based imaging methods to study NO dynamics. The high sensitivity, spatial resolution, and experimental feasibility make fluorescent-based methods the preferred imaging modality **(76, 77, 78)**. An added advantage of this strategy is that structural and functional imaging can be combined simultaneously **(56, 80)**.

Determining the spatiotemporal relationship between vascular anatomy and NO production is crucial to unravel the role of NO in vascular pathologies. To address NO synthesis in vessel wall, two-photon laser scanning microscopy (TPLSM) was used, which enables fluorescent imaging of Cu₂FL2E with subcellular resolution, large penetration depth, and optical sectioning (to obtain 3D reconstructions of the tissue) **(56, 80)**.

We establish that Cu₂FL2E is a valuable tool for direct and specific imaging and visualization of NO in ECs *in vitro* and, in conjunction with TPLSM, *ex vivo* in intact vessels with high spatiotemporal accuracy. We also show that this methodology allows relative quantification of NO and exploration of NO-mediated vasomotor response *ex vivo*. The Cu₂FL2E probe offers unique possibilities for studying the spatial and temporal synthesis of NO in vascular biology and pathology.

1.6.2 Investigation of arginine supplementation and effects of Arginase-1 deficiency on vascular NO production during endotoxemia

Endothelial dysfunction, associated with imbalance in NO metabolism plays a crucial role in the development of endotoxemic conditions, such as in sepsis **(81, 82, 83, 84)**. A diminished NO bioavailability caused by depressed *de novo* synthesis or aggravated NO turnover is regarded key to this endothelial dysfunction **(85)**. Under normal conditions, endothelial NO is mainly generated by the endothelial nitric oxide synthase (NOS3; eNOS) mediated conversion of L-arginine to L-citrulline. The NOS3 activity is critically controlled by its substrate (L-arginine) availability. During pathological conditions such as inflammation, L-Arginine concentrations significantly decrease and a

1. General Introduction

diminished NO bioavailability in the microcirculation becomes evident (81, 86, 87). Inhibition (88) or uncoupling (89) of NOS3, impaired arginine *de novo* synthesis, or reduced cellular arginine uptake may all depress NOS3 derived NO production (87, 90) and as such vascular function. Another important contributor to depressed NOS3 derived NO is endotoxemia, as endotoxemia downregulate NOS3 and upregulates the inflammatory NOS (NOS2; iNOS), which competes with NOS3 for L-arginine (91, 92, 93). iNOS can produce excessive amounts of NO during endotoxemia, which contributes to the decreased arterial pressure and abnormal blood flow leading to cardiovascular complications (84, 94, 95). Simultaneously, eNOS-mediated NO production is decreased due to endotoxemia-induced eNOS downregulation, coupled with decreased substrate availability (88).

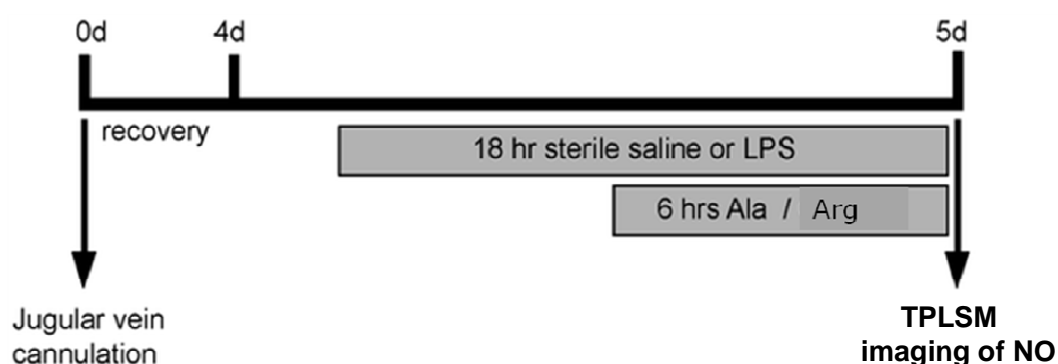


Fig. 10 Experimental set up of the prolonged endotoxemia model. Mice were fitted with a jugular vein cannula at $t = 0$ days. After 4 days ($t = 4$ days) an 18 hours continuous infusion with lipopolysaccharides (LPS) was started, which was combined during the last 6 hours with an infusion of Arginine (Arg) or an isonitrogenous quantity of the placebo Alanine (Ala) (modified from Wijnands KAP *et al.* PLoS ONE 2012).

An obvious approach would be pharmacological substitution of L-arginine. However, it has been demonstrated that L-arginine supplementation in prolonged endotoxemia and sepsis failed to increase the intracellular NO production despite increased arginine plasma availability (96, 97, 98, 99, 100). Thus, to investigate whether arginine supplementation during an ongoing endotoxemia rescues the eNOS-derived NO

1. General Introduction

production in endothelial cells is an interesting approach. Also, enhanced arginine catabolism by arginase-I (101, 102) significantly contributes to the arginine-NO deficiency found in inflammation and endotoxemia (83, 102, 103). Intriguingly, arginase-I mediated regulation of arginine availability subsequently affects NOS (2 and 3) activity and related NO synthesis in endothelial cells (NOS3) (102, 104, 105, 106) by depleting the arginine concentration. Reciprocally, lowering and depletion of total arginase-I activity significantly enhances NOS-related NO production during inflammation (104, 107, 108, 109, 110). This critical interrelation between arginase-I, substrate availability and NOS activity makes modulations of arginase-I activity an interesting therapeutic option for treating inflammatory diseases related to impaired NOS3 dependent NO production.

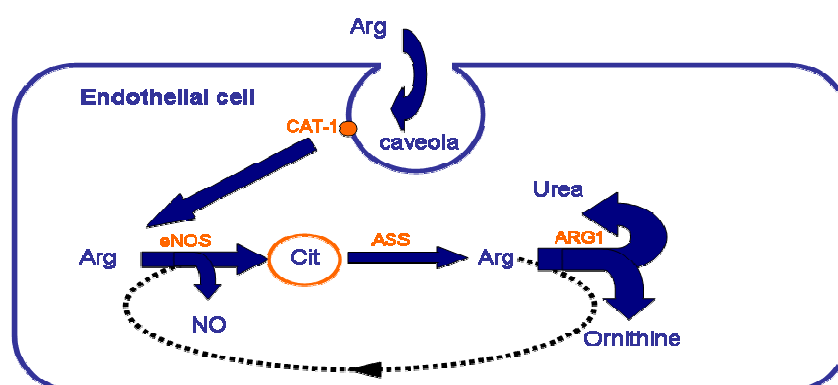


Fig. 11 Scheme of arginine metabolism by endothelial cell by various pathways; showing arginine metabolism by endothelial eNOS to convert arginine to citrulline, which then by use of ASS enzyme converts to arginine to be used in urea or ornithine cycle.

To demarcate the therapeutic potential of selective arginase-I modulation in enhancing NOS3 associated NO synthesis and in counteracting vascular dysfunction during inflammation, a prolonged endotoxemia model was inflicted in endothelial / hematopoietic arginase-I deficient knockout mice (111) and Cu₂FL2E-TPLSM approach was used to address these issues.

1. General Introduction

1.6.3 *In vitro* thrombus imaging with carbon dot

The convergence of nanotechnology and bioimaging opens the door to a revolution in molecular imaging. Medical imaging has evolved from a marginal role in healthcare to become an essential tool of diagnostics over the recent years. The convergence of nanotechnology and medical imaging opens the doors to a revolution in molecular imaging. Molecular imaging is based on the molecular and cellular fingerprints of the disease, requiring disease-specific molecular targets as well as target-specific nanoparticles. The remarkable properties of nanoparticles have resulted in their use as an alternative to both small-molecule and protein fluorophores in innumerable biological applications. In this study, a Factor XIII specific ligand (peptide A14) coupled to cDots are being used which will help to visualize thrombi with two-photon microscopy. This novel bimodal alpha2-antiplasmin-based contrast agent (peptide A14) binds to fibrin exposed during thrombus formation and visualization can be done with two-photon microscopy with intense fluorescence signal resulting from the nanoparticles at the target. Activated factor XIII (FXIIIa) plays an important role in regulating the resistance of thrombi against fibrinolysis. Upon activation, FXIII becomes capable of cross-linking fibrin alpha and gamma chains of neighboring fibrin molecules, providing stability of the thrombus. Moreover, FXIIIa covalently cross-links alpha2 antiplasmin, a key inhibitor of plasmin-mediated fibrinolysis, to fibrin **(61)** showed that contrast agent based on alpha2- antiplasmin (peptide A14) provides specific visualization of fresh thrombi. cDots are potentially nontoxic and smaller as compared to other frequently used nanoparticles like heavy metal-based quantum dots. Therefore, they hold good promise for clinical translation. In our case, the peptide was bilabeled with TAMRA for control of cDot efficacy. Imaging was performed by TPLSM.

2. Materials and methods

2.1 Materials

2.1.1 General equipments

Balances (Sartorius, Göttingen, Germany); centrifuges Hettich Universal 320R and Mikro 200R (Hettich, Tuttlingen, Germany); laminar flow hood Clean air technique (PMV, Utrecht, Netherlands); microscopes Leica DMI 3000B (Leica, Mannheim, Germany); Nikon E600FN microscope (Nikon Corporation, Tokyo, Japan), multiphoton system LeicaTCS SP5 (Mannheim, Germany) and Biorad 2100MP (Biorad, Hemel Hempstead, GB); pH-meter Lab 850 (Schott, Mainz, Germany); spectrometer NanoDrop (Thermo scientific, Erlangen, Germany), automated cell counter (Invitrogen), Big ben sphygmomanometer (Reister, Germany), MC60 heating stage (Linkam scientific instruments, UK), waterbath (Hettich, Tuttlingen, Germany); CO2 incubator (Laborgerate, Heidelberg, Germany)

2.1.2 Consumables

Disposable scalpel (Feather Safety Razor Co., Osaka, Japan); microscope slides (Thermo Scientific, Braunschweig, Germany); microtubes EDTA, with clot activator for sera (Sarstedt, Nümbrecht, Germany); glassware (Schott, Mainz, Germany); reaction cups 1.5ml, 2.0ml (Sarstedt, Nümbrecht, Germany); reaction tubes 15ml, 50ml (Greiner Bio-one, Frickenhausen, Germany); serological pipettes 5ml, 10ml, 25ml (Laborgerate, Heidelberg, Germany); syringes 2ml, 5ml, 10ml, 20ml (Terumo, Leuven, Belgium), 1ml (Braun, Melsungen, Germany); flasks, petridishes and petriplates (Greiner Bio-one, Frickenhausen, Germany); forceps (Fine Science Tools, Heidelberg, Germany)

2.1.3 Buffers, Chemical Reagents, Dyes

S-nitroso-N-acetyl-D,L-penicillamine (SNAP) [Sigma Aldrich], acetylcholine [Sigma Aldrich], L-N^G-nitroarginine methyl ester (L-NAME) [Sigma Aldrich], phorbol 12,13 dibutyrate ester [Sigma], endothelial cell medium (ECM) [Lonza], Hanks balanced salt solution (HBSS) [Lonza], propidium iodide (PI) [Invitrogen], 4',6-diamidino-2-

2. Materials and methods

phenylindole(DAPI) [Invitrogen], SIN-1 [Invitrogen], DAF-2-DA [Calbiochem], hydrogen peroxide [Merck].

2.2 Animal Care and Mouse strains

The local ethics committee (FHLM, Maastricht University) on use of laboratory animals approved all experiments. Procedures were in accordance with institutional guidelines. For ex vivo experiments euthanasia was performed by applying a mixture of CO₂ and O₂, after which arteries were isolated. Carotid artery segments (common part) and aorta segments were excised from 20-22 weeks old C57BL6/J (n=6) mice (Charles River, Maastricht, the Netherlands). For isolation of PAECs, dutch landrace pigs of 40 to 50 kg were euthanized using pentobarbital.

Gene Name	Abbreviation	Background	Description of transgene
Wildtype	None	C57BL6	None
Wildtype	None	Tie2Cre	None
Arginase-1	Arg-1	C57BL6	Targeted mutation (knock out)
Nitric Oxide synthase 2	NOS2	C57BL6	Targeted mutation (knock out)

Table 1: Mouse strains used in the study

Note: All knockout mouse models were developed by Matijn Poeze and KAP Wijnands; original questions are addressable by them.

2.3 Methods

2.3.1 Spectroscopic measurements

Spectroscopic measurements were made on a Nanodrop (ND3300, Thermo Scientific) fluorescence spectrometer. DAF-2-DA or Cu₂FL2E was used for determining spectral properties, SNAP was used to release NO in solution. HBSS was used for dissolving DAF-2-DA or Cu₂FL2E to make solutions of suitable concentration. Hydrogen peroxide (H₂O₂)

2. Materials and methods

was used to determine change in spectral characteristics of DAF-2-DA or Cu₂FL2E on reacting with this reactive oxygen species. Copper (II)-chloride dihydrate (99%, Sigma Aldrich) stock solutions of 1 mM were prepared in Millipore water. Stock solutions of 1 mM ligands (FL2E) were prepared in DMSO. Probe (Cu₂FL2E) concentrations were generated by combining stock solutions of CuCl₂ and FL2E in a 2:1 ratio. Cu₂FL2E or DAF-2-DA was dissolved in HBSS to get the desired concentration. Cu₂FL2E (2 μM) or DAF-2-DA (10 μM) was allowed to react with the NO-releasing chemical agent SNAP at pH 7. Replicate fluorescence measurements were taken at 1 min for 2 μL of solution of Cu₂FL2E probe or DAF-2-DA with or without SNAP. For the spectral measurements, a white LED (460-650 nm) was used for Cu₂FL2E and DAF-2-DA based on the detected maximum absorption.

2.3.2 Cytotoxicity assay

HCAECs were seeded into 24-well plates (500 μL total volume/well, 5000 cells/cm²) in complete ECM and incubated at 37°C with 5% CO₂ for 72 h until confluent. The medium was replaced and cells were incubated with or without Cu₂FL2E (2 μM-200 μM) in OptiMEM media for 1 h in triplicate. Nine wells were also incubated with DAF-2-DA (10 μM-200 μM) in triplicate. The medium was removed and replaced with HBSS and incubated with double stains; propidium iodide (1.5 μM) for dead/dying cells and DAPI (0.1 μM) for nuclear staining. The cells were then incubated for 30 min in the dark. Washing and imaging was done in HBSS. The percentages of cell survival values were calculated from 5 different images as ratio of PI/DAPI of nuclear staining.

2.3.3 Cell cultures and imaging

Porcine aortic endothelial cells (PAECs) were isolated from thoracic aorta **(112)**. PAECs, human microvascular endothelial cells (HMVECs; Lonza) and human coronary artery endothelial cells (HCAECs; Lonza) were cultured in EGM-2MV medium (ECM; Lonza). For imaging studies, cells were plated onto poly-d-lysine coated 6 wells plates, and cultured

2. Materials and methods

until confluency was reached at 37°C with 5% CO₂. To study NO production, the Cu₂FL2E probe was added in a concentration of 20 μM (40 μM CuCl₂ + 20 μM FL2E) in the case of PAECs and HMVECs, and 2 μM (4 μM CuCl₂ + 2 μM FL2E) in the case of HCAECs, diluted in OptiMEM (Invitrogen). Cells were co-incubated with Cu₂FL2E and stimulus (10 μM acetylcholine [Sigma] **(113)** or 150 μM H₂O₂ [Merck]) for 45 min and washed three times with HBSS prior to imaging. When stimulated with flow, HMVECs were cultured on Ibidi μ-slides I-Luer0.4, and cultured for 72 hours in the IBIDI flow system at a rate of 20 dynes/cm² shear stress, mimicking the blood flow, and then incubated with Cu₂FL2E for 5min, after which the cells were washed and imaged. For inhibitor studies, HCAECs were preincubated with 100 μM L-NAME for 1 h prior to addition of Cu₂FL2E and stimulus. For specificity and sensitivity studies, HCAECs and/or HMVECs were preincubated with 1 μM PE and 0.5mM SIN-1 for 5min and 10min respectively prior to addition of Cu₂FL2E and stimulus. Images were acquired on an inverted fluorescent microscope (Leica DMI3000B) equipped with FITC filter and a DFC350 FX camera (Leica). Images were taken after removing the DMEM media and washing the cells with Hanks buffered salt solution (HBSS). Additionally, two-photon microscopy was performed (see below) in some cases. All fluorescent images were corrected for background.

2.3.4 Griess assay

Cells were seeded in a 6-wells plate and grown until confluent. Medium was removed and 1.5 mL of fresh culture medium with or without 150 mM H₂O₂ was added and 200 μL was sampled at t = 0, 1, 6, and 24 h. Medium was centrifuged using 10,000 Da MWCO polysulfone filters (Sartorius). The supernatant was analyzed using the Total Nitric Oxide Assay Kit (Assay Designs).

2.3.5 Tissue preparation

Segments of murine common carotid arteries (length ~ 6-8 mm) were explanted and freed of adipose and connective tissue and carefully handled, only at their outer ends without stretching them, to keep them viable. To avoid contact with air, they were kept

2. Materials and methods

moist during the whole preparation procedure. Until further processing, arteries were stored (maximum 30 min) at 4°C in HBSS, pH 7.4, containing: NaCl 144mM, HEPES 14.9mM, glucose 5.5mM, KCl 4.7mM, CaCl₂ 2.5mM, KH₂PO₄ 1.2mM, and MgSO₄ 1.2mM.

2.3.6 Mounting procedure

The murine common carotid arteries were explanted and mounted on a perfusion chamber **(56)** filled with 10 mL ECM (37°C). The artery was mounted on two glass micropipettes (tip diameters 120-150 µm for carotid arteries) and residual luminal blood was carefully removed by gently flushing with HBSS. To correct for the shortening of the artery during isolation, a transmural pressure of 100 mmHg was applied (using a modified Big Ben sphygmomanometer, Riester, Germany) and the distance between the two pipettes was adjusted until the mounted artery was straight.

After this length adjustment, transmural pressure was set at 80 mmHg to mimic physiological conditions. All experiments were performed at 37°C (Linkam scientific instruments MC60 heating stage, UK) in the absence of luminal flow. Imaging was performed in vessels at a transmural pressure of 80 mmHg and was restricted to the central portion of the vessel segment.

Only weak elastin autofluorescence could be observed with TPLSM. After that the vessel was incubated with Cu₂FL2E probe (20 µM) for 5 min with luminal flushing of the probe. After washing excess probe from the solution and luminal washing, it was again imaged with TPLSM. The vessel was then incubated with: acetylcholine (10 µM) or H₂O₂ (150 µM) for 45 min and then washed and imaged and in case of measurements with L-NAME (100 µM) it was pre-incubated for 1 h. For precontraction and relaxation of vessels experiments, acetylcholine induced signal within 2minutes. For flow experiments, laminar flow (2.1Pa) was applied as stimulus for NO production.

For endotoxemic arteries studies, L-arginine supplementation was used for NO stimulation. Compared to carotid arteries, aorta was more difficult to mount and pressurize for our experiments because of its numerous side branches; nonetheless it was mastered successfully by ablation of side branches and NO signal was subcellularly studied along with vasomotor response.

2. Materials and methods

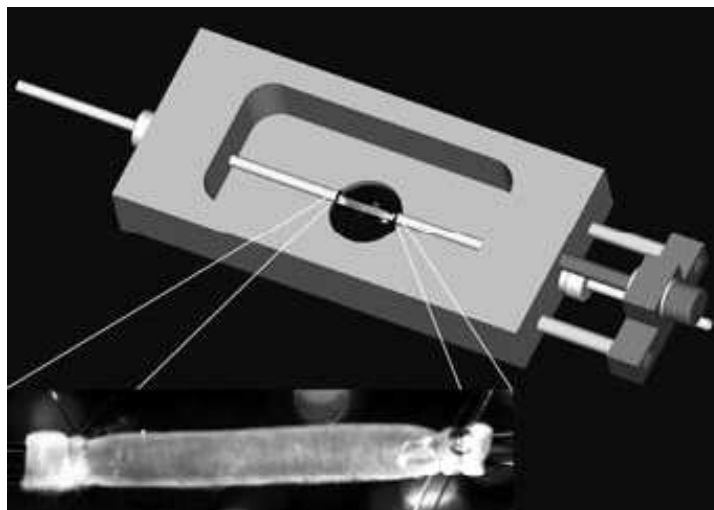


Fig.12 Schematic representation of a vessel perfusion chamber used to mount isolated arteries. The distance between the two pipettes is adjustable for correction of the arterial length after dissection. Fluid capacity is 10 ml. Inset: mouse carotid artery mounted on two glass pipettes with sutures, length-adjusted, and pressurized to 80 mmHg.

2.3.7 Wire myography

2mm segments of mouse carotid arteries were mounted between two stainless steel wires (40 μm in thickness) connected to a displacement device and an isometric force transducer (DSC6; Kistler Morse, Seattle, WA), respectively, in organ chambers (DMT, Aarhus, Denmark) filled with KRB solution at 37°C, and they were aerated with 95% O_2 , 5% CO_2 . The segments were progressively stretched to the diameter at which their contractile response to 10 μM noradrenaline was maximal. They were relaxed by administration of 10 μM acetylcholine. Experiments were repeated after addition of $\text{Cu}_2\text{FL2E}$ probe (20 μM) for 5 min in the chamber and washing.

2. Materials and methods

2.3.8 *In vitro* thrombus formation

Blood drawn from human volunteers was stored in vacutainer tubes with anticoagulant (trisodium citrate). 0.5ml of blood was used for thrombus formation (care was taken to form small thrombus, in order to save labeling expense). On addition of 7.5 μ l of CaCl₂ (1M) to 0.5ml blood for 90min at 37 degrees C, a thrombus is formed. Labeling of the thrombus with cDot-peptide-TAMRA conjugate and unconjugated cDots was done for 90min at 37 degrees C, with occasional shaking of the tubes to ensure non-sticking of thrombus on the wall of the tube and uniform staining of the thrombus. Followed by extensive washing with PBS, thrombi were dipped in PBS buffer for imaging.

2.3.9 Two-photon imaging

The perfusion chamber with artery or a 6-well plate with cultured endothelial cells was positioned on a Leica ultrafast TCS SP5 multiphoton microscope. The microscope was integrated with a DM6000 CFS (Confocal fixed stage) system, a DFC360FX camera system and an AOBS (Acousto optical beam splitter) [Leica, Mannheim, Germany] was used. The excitation source was a Chameleon Ultra Ti: Sapphire laser (690-1040 nm) (Coherent Inc. Santa Clara, CA, USA), tuned and mode-locked at 800 nm and producing light pulses of repetition rate 80 MHz with duration < 200 femtosecond. The pulses reached the sample through the Leica HCX APO L 20x/ 1.0W microscope objective (20 X, water dipping, numerical aperture 1.0, working distance 2 mm, access angle 39 degrees), connected to an upright Leica DM6000 CFS microscope. An optical zoom in the scan head achieved further magnification. Super Z-galvo was used for fast and accurate XYZ and XZY scan mode. External detectors were used for collecting emitted lights from the sample. When desirable the fluorescence was detected by one independent photomultiplier tube (PMT) for the green wavelength region (508-523 nm) and another independent photomultiplier tube (PMT) for the blue wavelength region (400-410 nm; for collagen and 450-480nm; for Syto 41). Images of 512 \times 512 pixels were obtained. For quantification purposes, the intensities in the green channel were used. The excitation wavelength of 800 nm was chosen since we found

2. Materials and methods

that at this wavelength both traps and adducts were effectively excited. No additional image processing was performed. For imaging of the endothelial cells and carotid arteries, an imaging speed of 50 Hz was used to improve signal-to-noise ratio. To prevent photochemical and thermal damage to the arteries, laser power was kept as low as possible(56).

Images were recorded in the XY-plane. Fluorescence images were taken after removing the EGV-2M media and by washing the cells or flushing the artery with Hanks buffered salt solution (HBSS). Inaccurate alignment of the pipettes in the perfusion chamber usually caused imaging of the artery in a slightly oblique plane. Series of XY-images at successive depths (Z-stack) were collected for reconstruction of 3D images. Luminal diameters were obtained from XZ or YZ-images. To obtain XZ- or YZ-images with square pixels, z-step distance was equal to the pixel dimensions in XY-direction. In case of vessels, the scanning takes place in the direction from adventitial layer to the intimal layer, making optical sections and compiling in Z-stacks.



Fig.13 Two-photon microscopic setup (Leica TCS SP5)

2. Materials and methods

For quantification of fluorescence intensity from the images, various regions of interests (ROIs) were selected and processed using LASAF-Lite (Leica Systems) software to calculate the fluorescence intensity (au) per ROI. Average measure of fluorescence intensities were taken for quantitative assessment, in every group of vessels.

2.3.10 Two-photon *ex vivo* NO-production measurements in carotid arteries of endotoxemia mouse model

To determine the endothelial NO production during endotoxemia, carotid arteries of control (n=6) and *Arg^{fl/fl}/Tie2-Cre^{tg/-}* mice (n=6) treated with LPS were measured. To specify the origin of the NO production in the *Arg^{fl/fl}/Tie2-Cre^{tg/-}* endothelial cells (NOS3 or NOS2), the NO production in carotid arteries with pharmacological inhibition (1400W; n=5) or genetic ablation of NOS2 (n=3) were additionally measured.

The 2-photon NO measurements and microscopic setup used for imaging has been described previously. In brief, carotid arteries were excised and mounted and pressurized in a perfusion chamber (IDEE BV, Maastricht, The Netherlands). Vessels were pre-loaded with the fluorescent copper-based NO probe for 5 minutes after which basal and arginine stimulated fluorescent measurements were performed using a Leica ultrafast TCS SP5 multiphoton microscope integrated with DM6000 CF system, DFC360FX camera system and AOBIS (Leica, Mannheim, Germany). Images were analyzed using LASAF acquisition software (Leica, Mannheim Germany)

2.4 Image analysis

Images were analyzed using LASAF acquisition software (Leica, Mannheim Germany). 3D reconstructions of images were made using Image-Pro Plus 6.3 software (Media Cybernetics Inc., USA). NO mediated vasomotor responses, i.e. functionality of arteries, in XZ- or YZ-scans of the vessel. Signal quantification was done by using LASAF software were determined in three carotid arteries and measured as changes in luminal diameter to check fluorescence intensity (au) in different regions of interest.

2. Materials and methods

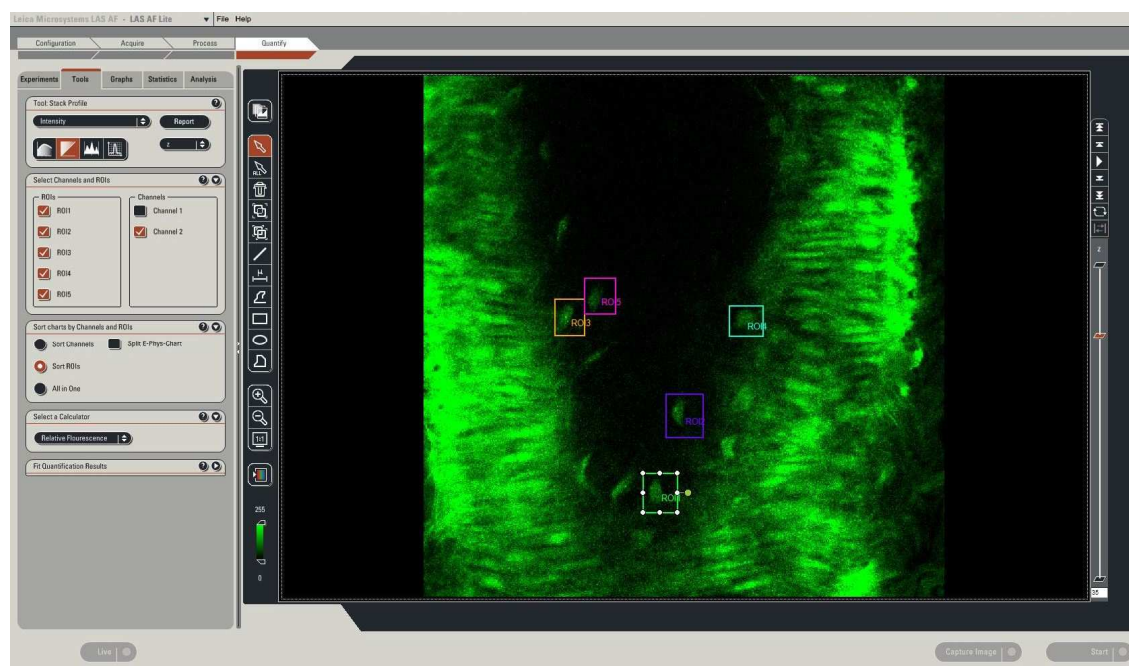


Fig.14 (a) Image analysis: Step1; selection of region of interests (ROI), setting right channel to quantify for relative fluorescence in each of ROI.

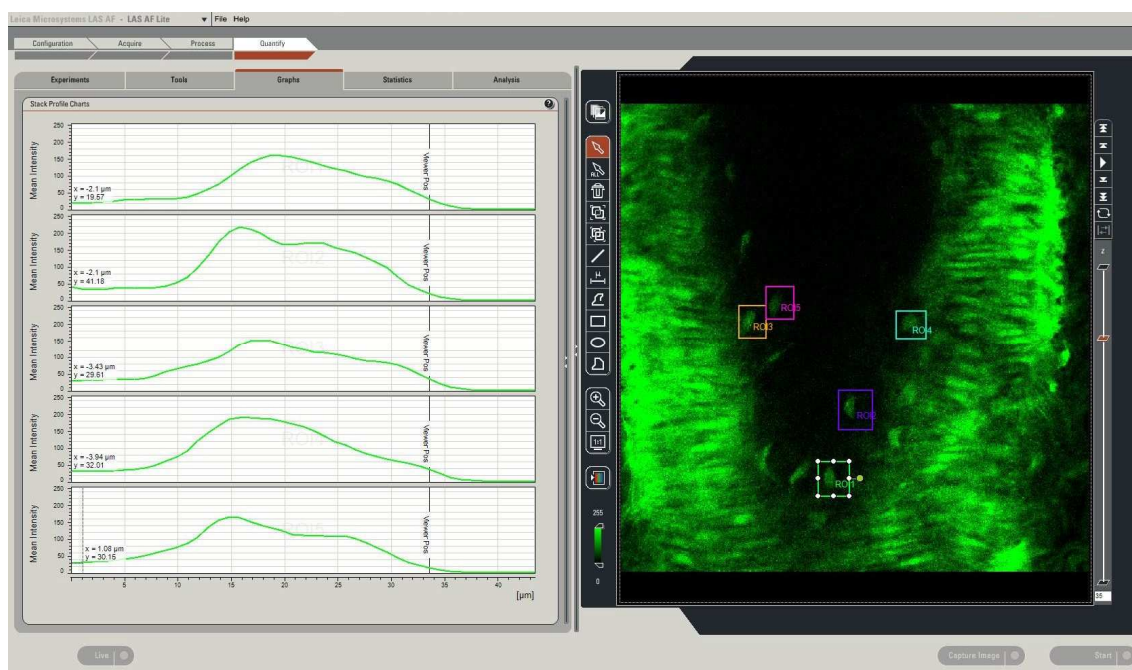


Fig.14 (b) Image analysis: Step2; checking individual profile for relative fluorescence; setting each ROI to obtain profile.

2. Materials and methods

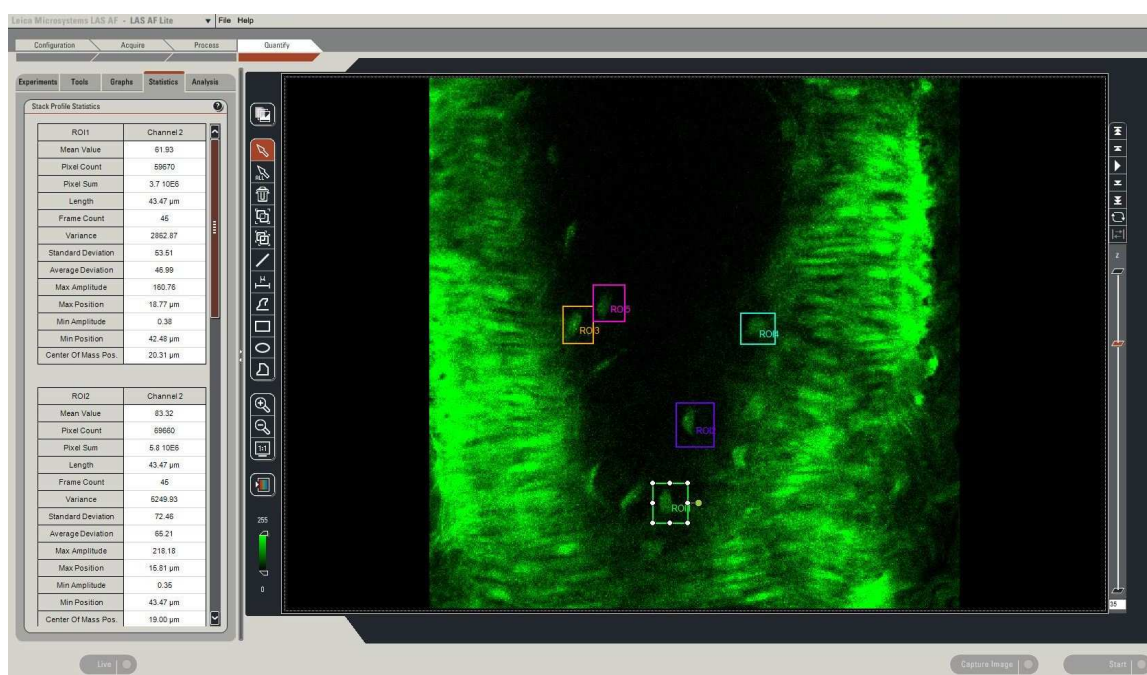


Fig.14(c) Image analysis: Step3; obtaining statistics (mean value) of relative fluorescence from each ROI.

2.5 Statistical analysis

Results were presented as mean \pm standard deviation and were tested for significance using the t-test (non-parametric test for two independent groups). A value of $P < 0.05$ was considered to be statistically significant. Linear regression analysis was performed to assess best fit relation, slope and correlation coefficient. R square value near to 1.0 shows best-fit predictability. All statistical analyses were performed using Graph Pad Prism software (GraphPad Software Inc. USA).

Statistical analysis of the endotoxemia data was performed using SPSS 15.0 (SPSS, Chicago, IL). One-way analysis of variance (ANOVA) was performed with post-hoc Bonferroni correction between groups to determine significant differences. Data are represented as mean and standard error of the mean (SEM). P-values below 0.05 were considered as statistically significant.

3. Results

3.1. Validation of the NO probe for vascular biology

3.1.1. Cu₂FL2E is more sensitive and specific than DAF-2-DA for NO detection

To underscore the sensitivity of Cu₂FL2E to NO, its behaviour was tested using various concentrations of SNAP as NO donor ¹⁷ and compared with that of the conventionally used DAF-2-DA. At a concentration of 100 μM in PBS at pH=7.4 and 37°C, SNAP produces 1.4 μM NO per min (114, 115). For Cu₂FL2E (2 μM) the lowest detectable concentration of SNAP after 1min was found to be 2.5 μM, corresponding to ~35nM NO, while for DAF-2-DA (10 μM) the lowest detectable concentration of SNAP was 5 μM, corresponding with an NO concentration of 70nM (Fig.15a). Subsequently, the concentration dependence of Cu₂FL2E and DAF-2-DA to SNAP was linearly fitted. The concentration dependence (Fig.15b) of Cu₂FL2E exhibited a higher correlation coefficient (R square = 0.9491 for Cu₂FL2E, R square = 0.6814 for DAF-2-DA), and higher steepness for Cu₂FL2E (Slope = 0.08824 ± 0.003864) while for DAF-2-DA (Slope = 0.02151 ± 0.002780) indicating best fit values for Cu₂FL2E.

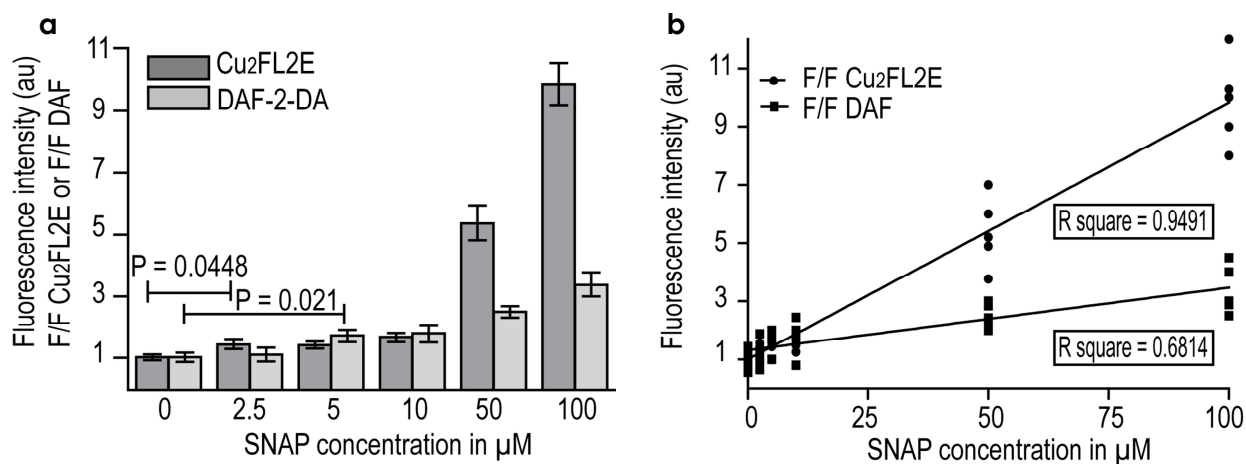


Fig. 15 NO sensitivity of Cu₂FL2E compared with DAF-2-DA; (a) Fluorescence response of DAF-2-DA and Cu₂FL2E (both 2 μM) to various concentrations of NO after 1 min of SNAP administration. n = 5, (b) Linear regression curve plotted from (a).

3. Results

Finally, the specificity and reaction speed of Cu₂FL2E for NO was compared with that of DAF-2-DA using 50 μM of SNAP. Additionally, although the specificity of Cu₂FL2E for NO over H₂O₂, HNO, NO₂⁻, NO₃⁻ and ONOO⁻ has already been shown before (46, 47), we compared the reaction of both probes to SNAP with that to H₂O₂ (150 μM), as the latter

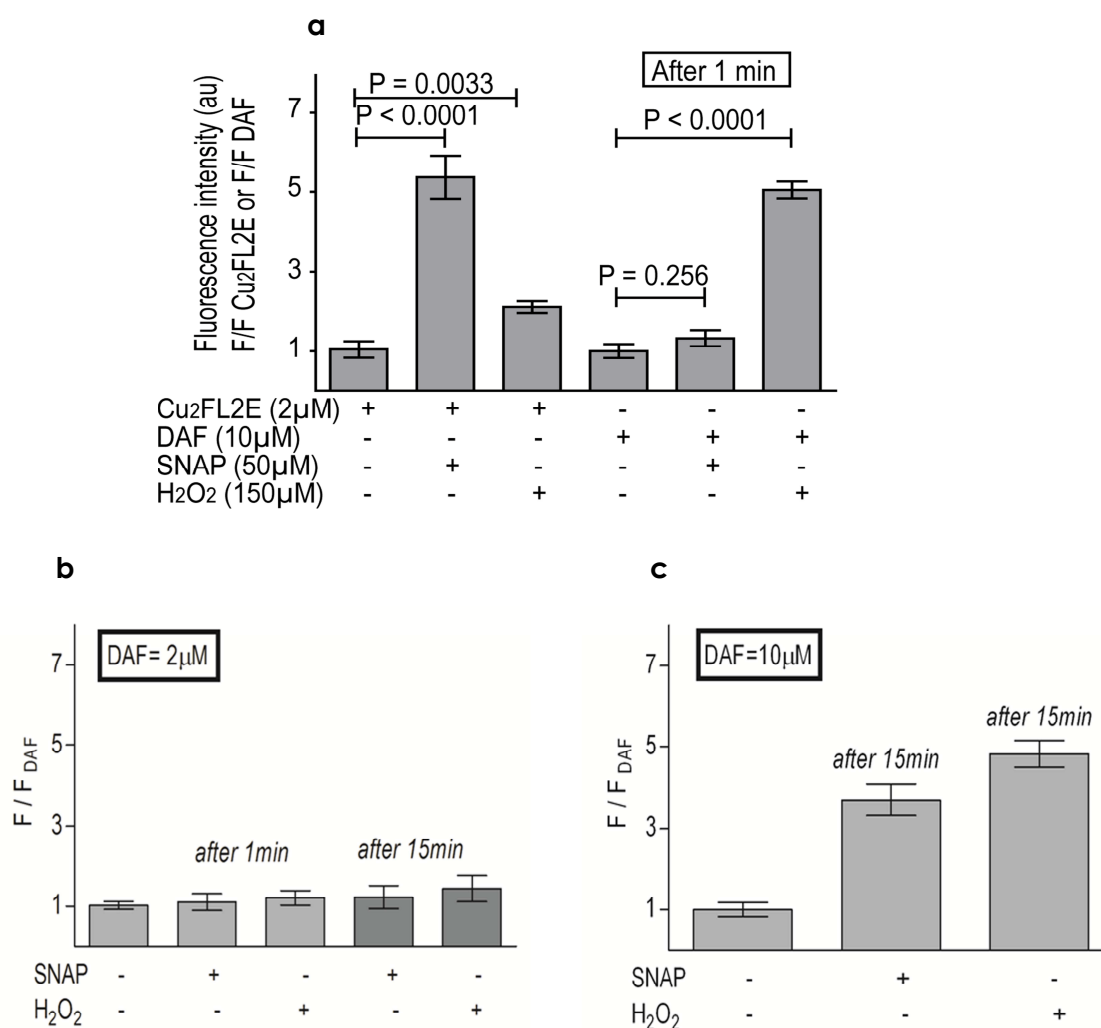


Fig. 16 Specificity of Cu₂FL2E compared with DAF-2-DA for NO and H₂O₂ ; Fluorescence response of (a) Cu₂FL2E compared with DAF-2-DA after 1 min and after 15 min, (b) DAF-2-DA (2 μM) response after 15 min, (c) DAF-2-DA (10 μM) response after 15 min 50 μM SNAP in PBS at 37°C, pH 7.4 was used to administer NO. The spectra were obtained 1 min /15min after SNAP addition. [H₂O₂] = 150 μM, [Cu₂FL2E] = 2 μM, [DAF-2-DA] = 2 μM / 10 μM, n = 5. Error bars indicate s.d.

3. Results

is used in our study as one of the stimuli for NO production in cells and vessels (**116, 117, 118**). **Fig.16a** shows that 1min after SNAP addition Cu₂FL2E (2 μ M) reacts with NO, resulting in a 5-fold increase in fluorescence intensity compared to background. Addition of H₂O₂ generated a smaller (2-fold) increase in fluorescence intensity. These data correspond with data of McQuade L.E. *et al* (**47**).

In contrast, the fluorescence of DAF-2-DA (10 μ M) after 1min increased only slightly in response to SNAP, and was 4-fold less than that of Cu₂FL2E. Addition of H₂O₂ to DAF-2-DA, however, resulted in a robust (5-fold increase in fluorescence) response. Upon increasing the incubation time of SNAP to 15min, DAF-2-DA (10 μ M) showed a 3-fold increase in fluorescence, but the same increase was also apparent for H₂O₂ (**Fig. 16b**). Lower concentrations of DAF-2-DA (2 μ M) failed to show any response under similar conditions or even after longer time periods (**Fig. 16c**). These findings underscores the superior NO detection characteristics of Cu₂FL2E over DAF-2-DA.

To study the cytotoxicity of the two probes, we loaded human coronary endothelial cells (HCAECs) with either Cu₂FL2E or DAF-2-DA. Toxicity at 2 μ M Cu₂FL2E, the regular concentration for cellular imaging of NO, was undetectable (**Fig.17**) and the upper limit for toxicity was 20 μ M. In contrast, the standard 10 μ M concentration of DAF-2-DA resulted in extensive cell death (< 10% viability). This excludes DAF-2-DA for further vital cell and vascular studies.

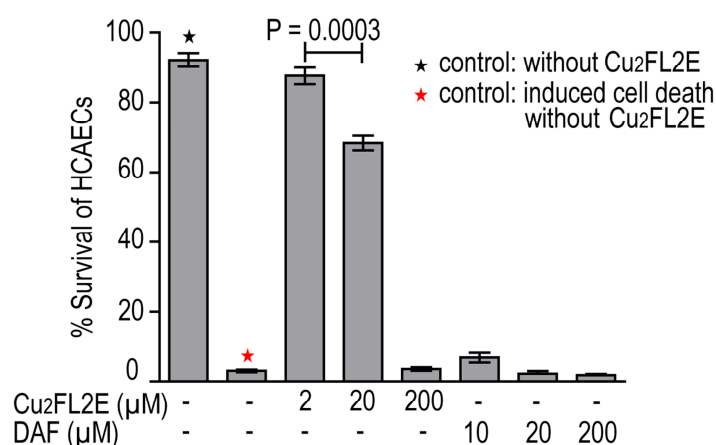


Fig. 17 Cytotoxicity assay; with different concentrations Cu₂FL2E and DAF-2-DA using ratio of PI/DAPI of nuclear staining (n=5).

3.2 Visualization-analysis of NO metabolism *in vitro* in endothelial cells

3.2.1 NO production can be imaged specifically *in vitro* in endothelial cells with Cu₂FL2E

The ability of Cu₂FL2E to detect NO produced in different EC types under the influence of various stimuli was investigated. Cu₂FL2E-loaded porcine aortic endothelial cells (PAECs) were stimulated with H₂O₂ and time-dependent fluorescence enhancement was monitored. From literature reports (119), it is known that H₂O₂-induced NO synthesis in ECs is a rather slow event. Indeed, H₂O₂ activates eNOS, and therefore NO production, through coordinated phosphorylation and dephosphorylation of eNOS amino acid residues between 15 to 45min after H₂O₂ supplementation. The activation is reported to last for 15min. Therefore, we followed NO production over 90 minutes after H₂O₂ supplementation (150 μM). In agreement with the above, we detected NO production as seen from a rise in fluorescence intensity above background in ECs, starting 5min after H₂O₂ exposure. After 45min the fluorescence intensity exhibited a plateau (Fig. 18a&b). Indeed, due to its chemistry, the NO-bound probe remains fluorescent (46, 47) and therefore over time the signal intensity increases. The result is a slow accumulation of fluorescence. Eventually, a signal plateau is reached when NO synthesis is reduced over time. To further address the specificity and sensitivity of the probe, we measured the NO response to H₂O₂-stimulated HCAECs with and without addition of SIN-1, a well-known eNOS-uncoupler (120) to specifically block eNOS activity. This resulted in abrogation of fluorescence signal in the presence of SIN-1 (shown later), reflecting potent uncoupling of eNOS. In presence of L-N^G-nitroarginine methyl ester (L-NAME) is a widely used non-specific nitric oxide synthesis inhibitor (77, 114, 116 117, 119), the fluorescence signal after various stimuli (H₂O₂ and Ach) was significantly weaker (2 to 3-fold, **p-value < 0.0001**) than in the absence of the inhibitor, indicating less NO production in HCAECs (Fig. 18c&d). NO detection with Cu₂FL2E was considerably faster (starting after 5 min) than the traditional Griess assay (121), which require hours of stimulation for significant detection. (Fig. 19)

3. Results

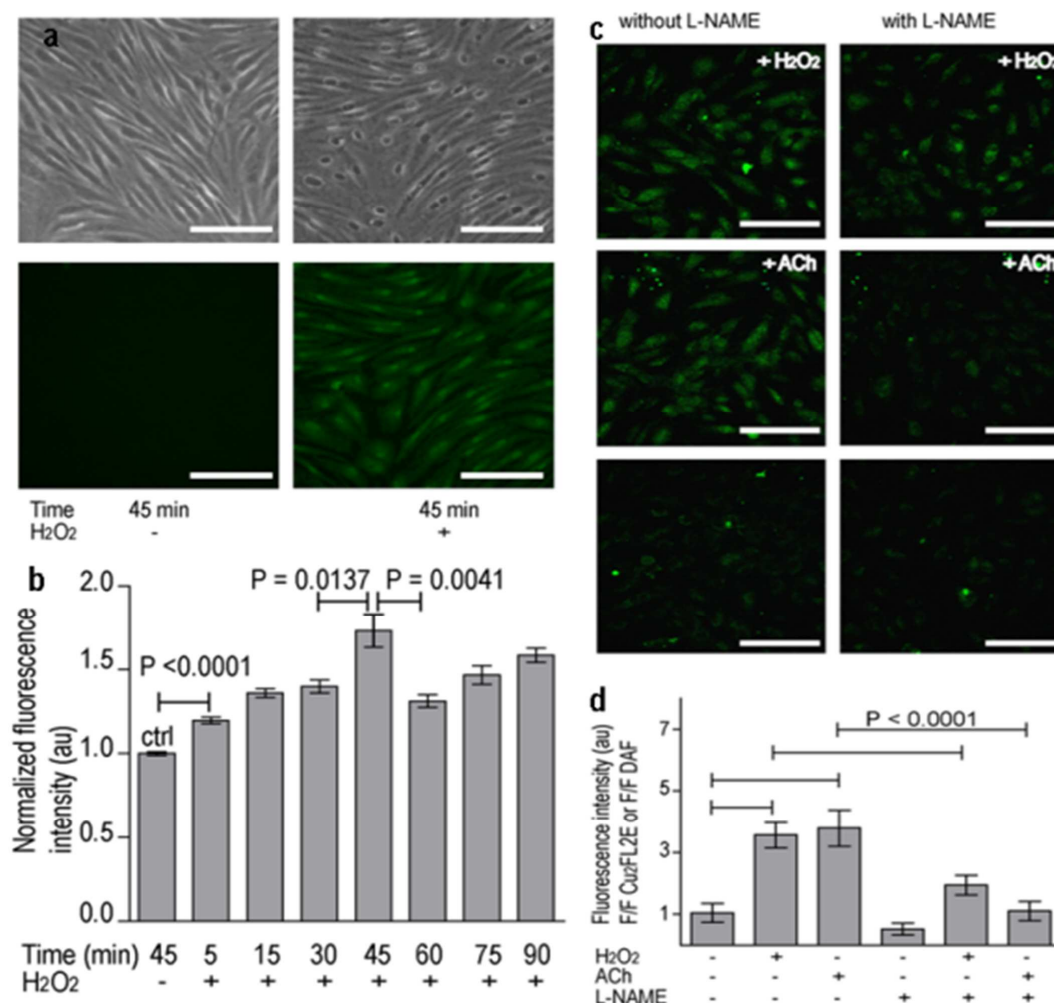


Fig.18 Detection of NO with Cu₂FL2E produced by endothelial cells *in vitro*. (a) NO detection in porcine aortic endothelial cells (PAECs); Left: 45 min incubation of Cu₂FL2E (20 μM). Right: 45 min incubation of Cu₂FL2E (20 μM) and H₂O₂ (150 μM). Top: bright-field images of cells. Bottom: fluorescence images of cells. Scale bars, 50 μm. (b) Quantification of fluorescence intensity plotted against incubation time. (c) Detection of NO with Cu₂FL2E in HCAECs cells, with or without NO-inhibitor (L-NAME). Shown are the fluorescence images after 45min co-incubation of the probe (Cu₂FL2E = 2 μM) with H₂O₂ (150 μM), L-NAME (100 μM), and/or ACh (10 μM) according to scheme. Scale bars, 75 μm. (d) Quantification of fluorescence intensity from (c) plotted against each condition mentioned in (c) (n = 5)

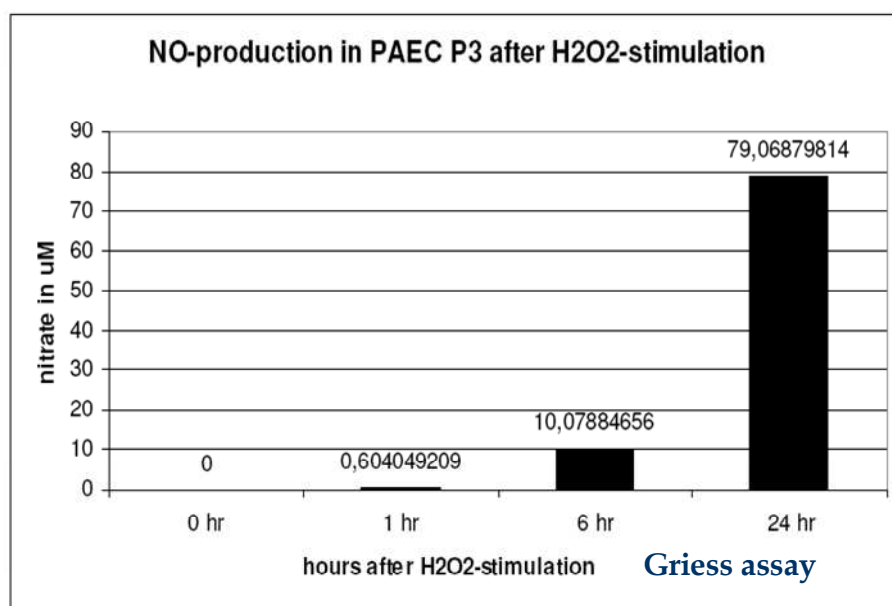


Fig. 19 Griess assay; for nitrate determination

In line with our experience we have been using low-mid passage HCAECs (passage <6), for our cellular studies. These data again pinpoint the NO specific response of the probe.

To demonstrate the efficacy of ACh stimulation on cellular signaling in HCAEC cells, we checked for colocalization of eNOS phosphorylation and NO production. Results show correlation of phosphorylated eNOS with the measured NO signal (**Fig. 20**), which again pinpoints at the non-toxic nature of the probe, since the probe does not interfere with cellular metabolic activity.

In order to address the specificity and sensitivity of the probe in a vascular setting, we challenged HCAECs with phorbol ester (PE). We observed an increase in NO production (high fluorescence intensity) when ECs were stimulated with phorbol ester (which activates NADPH oxidase). There was no significant additive effect of ACh or H₂O₂ stimulation (**Fig. 21**). NADPH oxidase is a major source of intracellular ROS production and could decrease NO availability by uncoupling eNOS. A decreased NO signal in ECs was therefore anticipated (activated by PE).

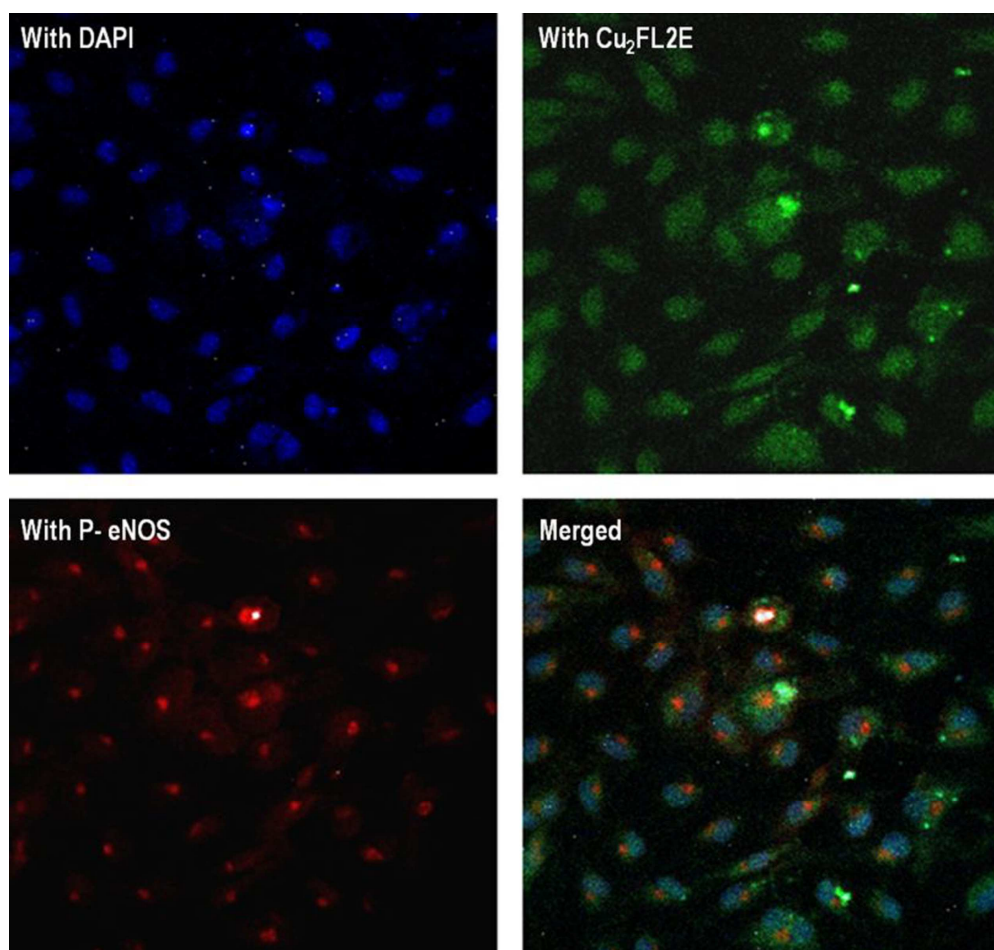


Fig. 20 HCAECs with eNOS phosphorylation; showing clear staining of phospho-eNOS (in red) with nuclear stain (DAPI, in blue) and NO signal (in green). This indicates the low-mid passage HCAECs (passage <6) have the ability to respond to ACh-induced NO synthesis.

Instead, we saw an increased NO signal, which can be explained by the observation **(122)** that ROS via NADPH oxidase activation can also enhance eNOS activity and subsequently enhances localized NO production. This effect was mechanistically attributed by ROS enhanced association of hsp90 with eNOS, thereby facilitating rather than inhibiting NO synthesis. In line with the positive effect of PE in our hands we consider a comparable mechanism to act in the increased NO signal detected with the Cu₂FL2E probe.

3. Results

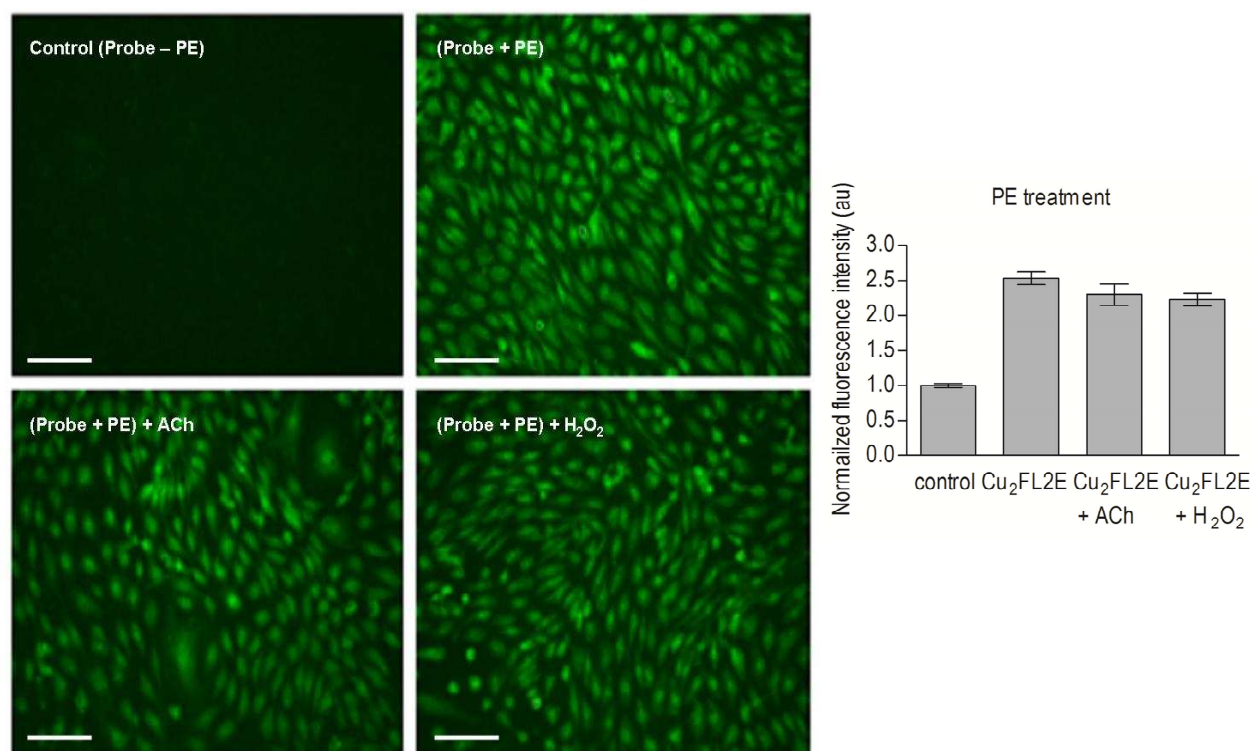


Fig. 21 NO detection in human coronary arterial endothelial cells (HCAECs) with PE; fluorescence intensities obtained with co-treatment of Cu₂FL2E (20 μ M) and PE (1 μ M), showing increase in fluorescence intensity when stimulated with PE due to ROS enhanced association of hsp90 with eNOS, thereby facilitating NO synthesis. No significant additive effect of ACh or H₂O₂ stimulation was observed.

Furthermore, we evaluated the ability of Cu₂FL2E to detect a more vascular and physiological stimulus, namely flow-induced **(116, 117, 123)** endogenous NO production in human microvascular endothelial cells (HMVECs). ECs subjected to flow adapt their NO production by activation of eNOS. After 72hrs of flow, cells will have increased their eNOS activity. In our setup, the probe is added to ECs (after 72hrs of flow) and the fluorescence intensity of the cells is monitored at 5min (the minimum time needed to establish the imaging), imaging carried out under flow. A rapid, 4-fold fluorescence increase was detected in cells that were cultured under flow (2.1Pa, 72 hrs) whereas

3. Results

cells cultured under static (no flow) conditions remained negative (**p-value = 0.0034**) (**Fig. 22a&b**). This underscores the immediate reaction of the probe to increased NO production.

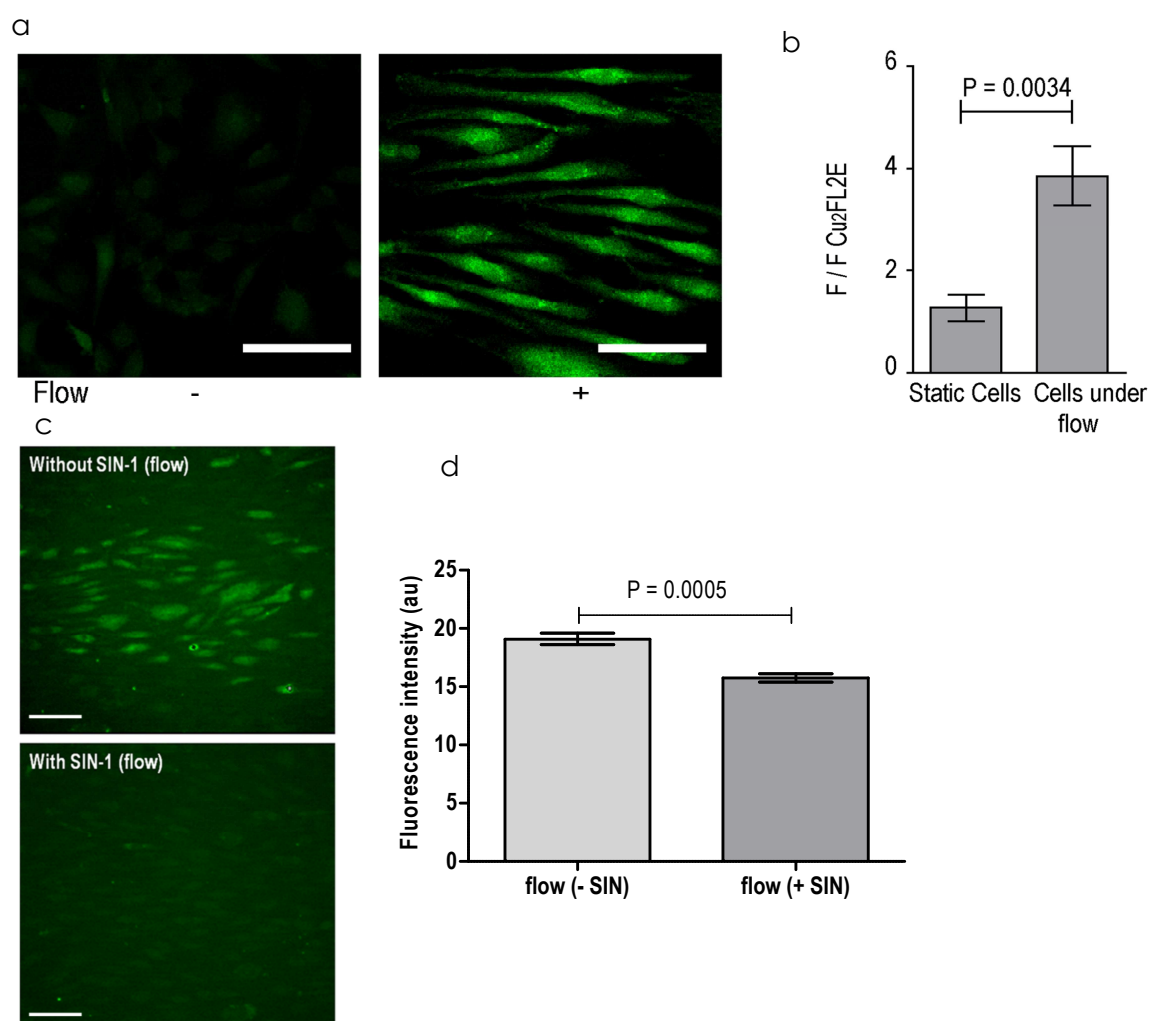


Fig. 22 Detection of NO with Cu₂FL2E produced by endothelial cells *in vitro* with flow. (a) Left: NO detection in HMVECs in static condition (i.e. without flow) with Cu₂FL2E (20 μM). Right: under flow condition (flow rate= 2.1 Pa, time=72 h) with Cu₂FL2E (20 μM). Scale bars, 50 μm. (b) Quantification of fluorescence intensity from (a). (c) NO detection in HMVECs in flow condition (flow rate= 2.1Pa, time=72 h) with Cu₂FL2E (20 μM) and without / with SIN-1 (0.5 mM). Scale bars, 50 μm, (d) Quantification of fluorescence intensity from (c). Error bars indicate s.d.

3. Results

When the cells under flow were concomitantly incubated with SIN-1, there was abrogation of fluorescence signal (p -value = 0.0005) (Fig. 22c&d), showing potent uncoupling of eNOS. These data again proves the NO specific response of the probe and its validity to study cellular NO synthesis.

3.3 Visualization of NO synthesis and vasomotor responses in the vasculature

3.3.1 NO production can be imaged and visualised *ex vivo* in non-precontracted murine carotid arteries and aortas with Cu₂FL2E

Murine carotid arteries were explanted and mounted in a custom-made perfusion chamber (56, 80). Weak autofluorescence was detected from elastin fibres of the vessel, presenting clearly distinguishable background fluorescence (Fig. 23a&b). This autofluorescence was independent of the presence of probe and can be used to locate relevant vascular layers. Individual SMCs and ECs could not be identified at the starting point of analysis (i.e. in absence of the probe or in the presence of the probe but without external stimulus) due to lack of sufficient cellular autofluorescence or basal NO signal above threshold of detection, respectively. When subsequently the vessel was incubated with ACh or H₂O₂ for 45 min, and subsequently washed, the fluorescence signal clearly reflected the presence of NO in ECs of the intimal layer and, to a lesser extent, in SMCs of the medial layer (Fig. 23c-f). Next, quantification of NO signal in vascular cells showed that after stimulation (here with H₂O₂), fluorescence increased more significantly over background levels in ECs (p value = 0.0091) than in SMCs (p value = 0.0481) (Fig. 23g).

Additionally, flow-mediated (2.1 Pa) stimulation of NO production in vessels after 45min of flow, could be seen in ECs. In this case, the increase in fluorescence over background levels for ECs was significant (p value = 0.0311), whereas the fluorescence change in SMCs was not significant (p value = 0.4664) (Fig.23h). Comparable results were obtained after ACh stimulation (Fig. 24). Proper labelling and focusing on the cells in different planes is demonstrated by nuclear staining (DAPI) in the merged images (Fig. 25).

3. Results

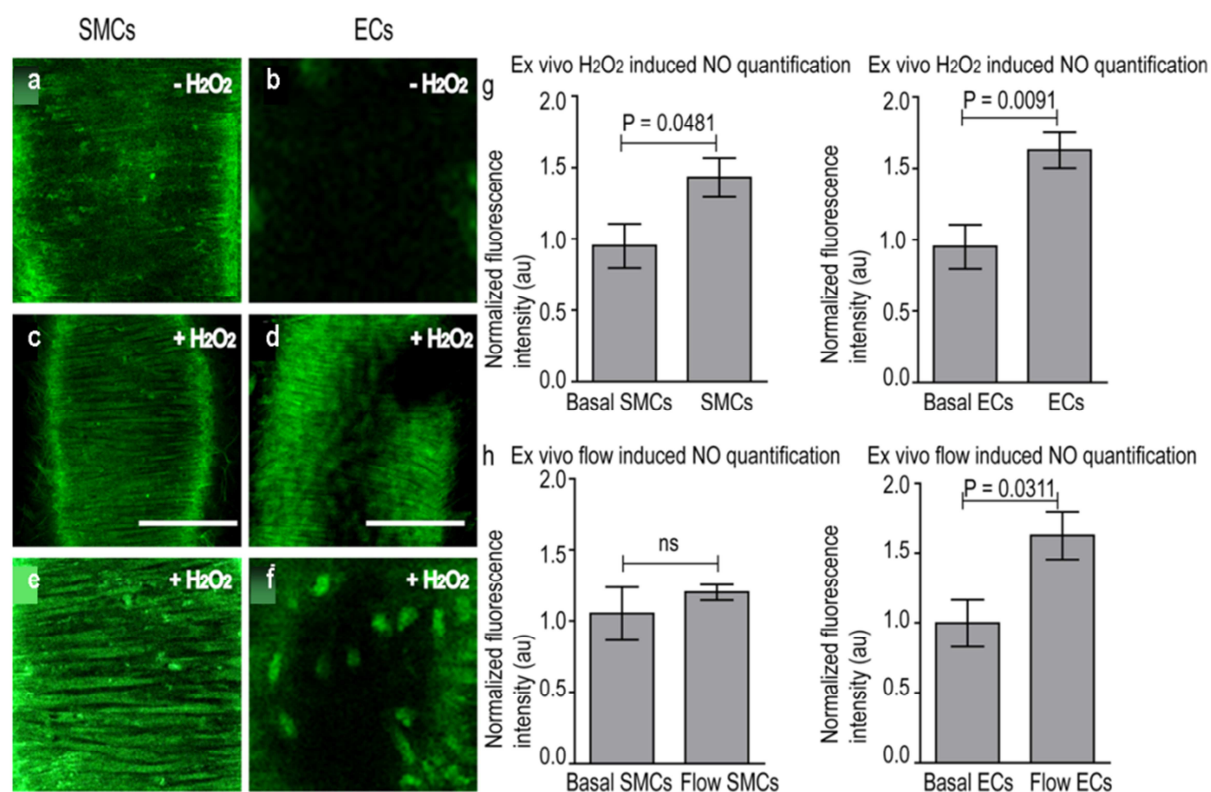


Fig. 23 Detection of NO produced in explanted murine carotid arteries ex vivo using Cu₂FL2E. (a) & (b) Magnified images of vessel showing basal NO signal detected after 5 min incubation of Cu₂FL2E (20 μM) without any stimulus at medial and intimal focal planes, respectively. (c) NO signal detected in smooth muscle cells (SMCs) and (d) endothelial cells (ECs) of the tissue with 5 min incubation of Cu₂FL2E (20 μM) and, subsequently 45min incubation of H₂O₂ (150 μM). Scale bars, 50 μm, (e) & (f) Magnified images of vessel showing NO signal detected after 5 min incubation of Cu₂FL2E (20 μM) and subsequently, 45 min incubation of H₂O₂ (150 μM) in SMCs at medial plane and in ECs at intimal plane respectively, (g) Quantification of spatial distribution of fluorescence intensity as measure of NO in cells of vessel wall stimulated with H₂O₂. (n = 5). (h) Quantification of spatial distribution of fluorescence intensity as measure of NO in cells of vessel wall stimulated with flow (flow rate= 2.1 Pa, time=45min), (n = 5).

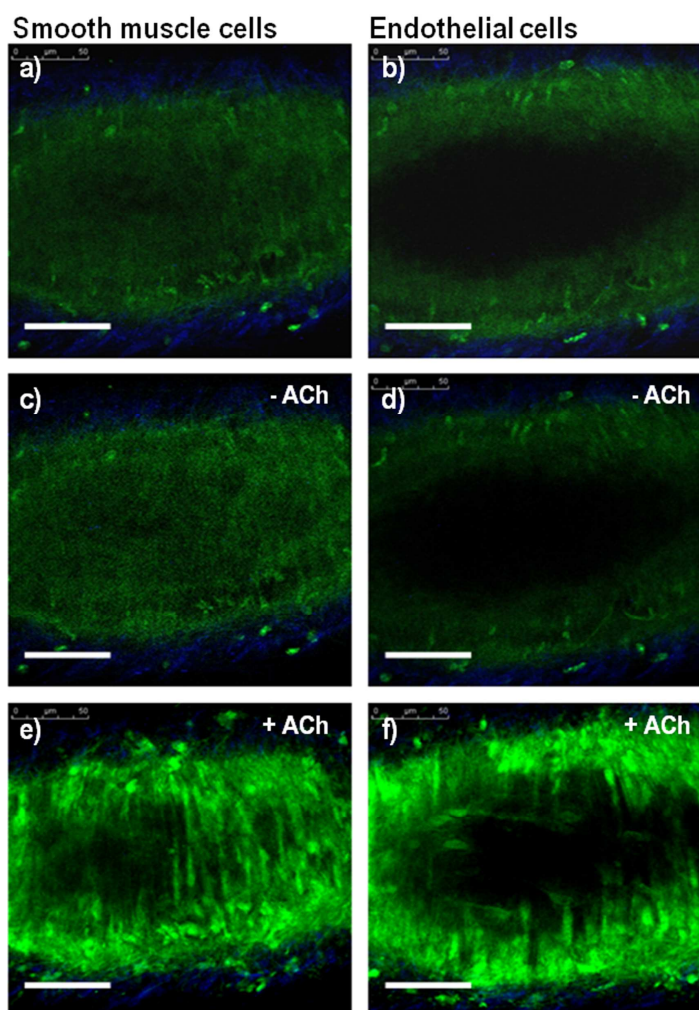
3. Results

Fig. 24 Detection of NO produced in explanted murine carotid arteries *ex vivo* using **Cu₂FL2E with ACh**. (a) & (b) Autofluorescence in SMCs & ECs of the tissue respectively, without Cu₂FL2E & ACh, (c) & (d) Basal NO signal detected after 5 min incubation of Cu₂FL2E (20 μM) without any stimulus in SMCs & ECs, respectively. (e) & (f) NO signal detected in SMCs & ECs of the tissue respectively, with 5 min incubation of Cu₂FL2E (20 μM) and 45min incubation of ACh (10 μM). Scale bars, 50 μm.

Compared to the carotid artery, the aorta was more difficult to mount and pressurize because of its numerous side branches; nonetheless proper mounting was mastered successfully by careful ablation of side branches.

3. Results

Fluorescence signal visualization in aortic endothelial cells was possible ex vivo, resulting in NO-mediated structural- functional imaging. This demonstrates limited capability of SMCs to directly respond to this physiological trigger. ECs were observed 45 minutes after probe addition and subsequent ACh stimulation (**p value = 0.0462**).

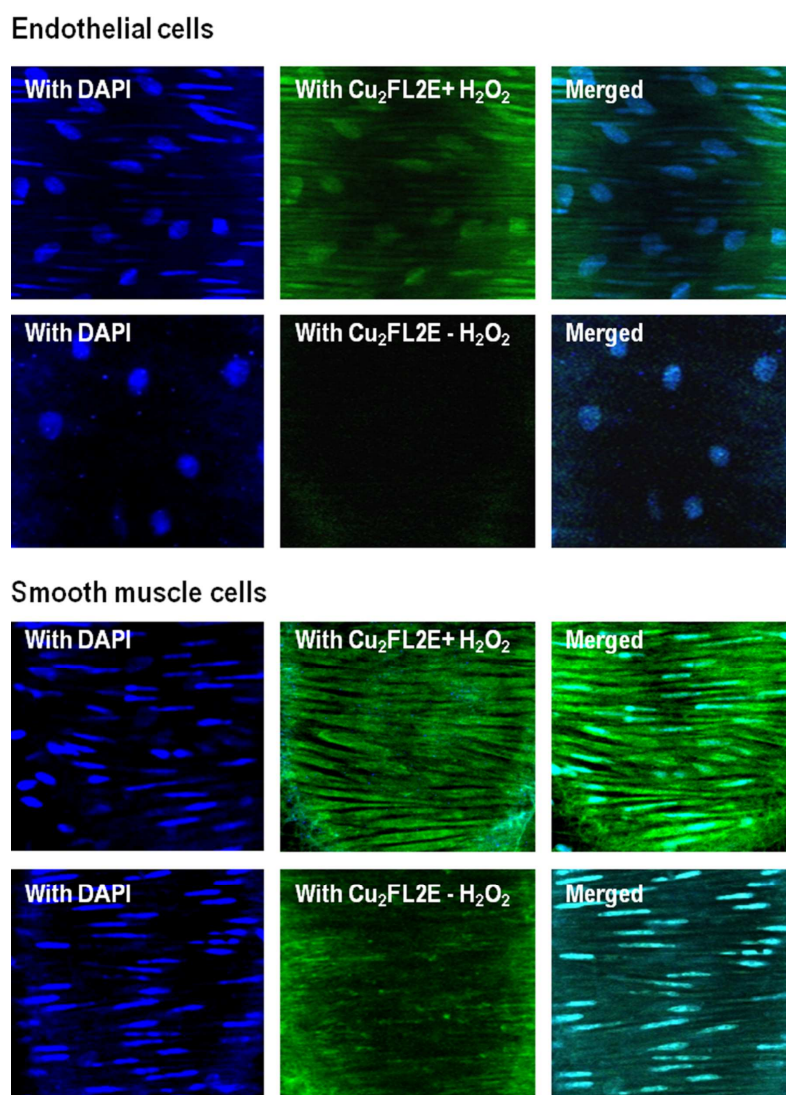


Fig. 25 DAPI staining of SMCs and ECs; Magnified images of vessel showing NO signal detected in smooth muscle cells (SMCs) and endothelial cells (ECs) of the tissue with 5 min incubation of Cu₂FL2E (20 μM) and, subsequently 45 min incubation of H₂O₂ (150 μM), in medial and intimal focal planes respectively. The cells are also stained with nuclear stain (DAPI) and merged images can be seen.

3. Results

In contrast to our findings in the carotid artery (stimulated with ACh) there was no apparent and significant NO production in SMCs, perhaps due to lower amount of NO generated in aorta (**Fig. 26**). However, 3D analysis and reconstruction of the aorta shows NO-mediated relaxation occurs with an increase in luminal diameter.

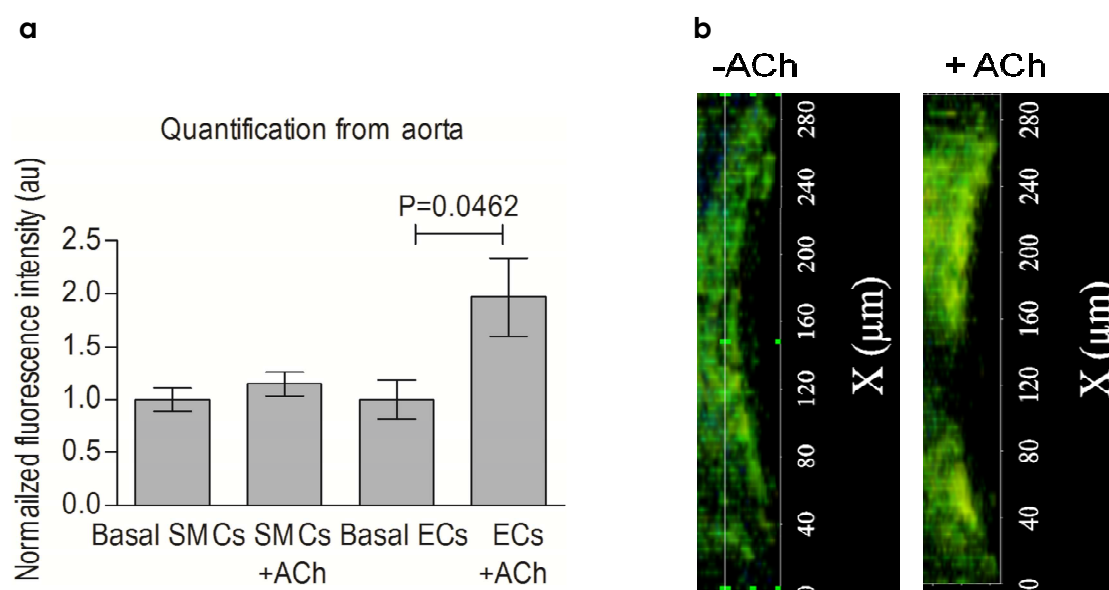


Fig. 26 Detection of NO produced in explanted murine aorta ex vivo using $\text{Cu}_2\text{FL2E}$ in aorta: (a) Quantification of spatial distribution of fluorescence intensity as measure of NO in cells of vessel wall stimulated with flow ($n = 5$), (b) Functional imaging of NO; 3D reconstruction of vessels with $\text{Cu}_2\text{FL2E}$ without/ with stimulus (here ACh) showing luminal diameter measured from arteries.

3.3.2 Time-profile of changes in fluorescence intensity in ECs and SMCs of non-precontracted carotid arteries after stimulation

Diffusion profile for NO in the vascular cells was obtained to investigate the duration of NO production and storage in these cells (**Fig. 27**), with monitoring at regular time points. Here, the cells were stimulated with H_2O_2 . A similar profile was obtained with ACh stimulations (data not shown). By obtaining diffusion profile, we specifically addressed compartments and temporal profiles of NO production in the vasculature. Indeed, due

3. Results

to its chemistry the probe remains fluorescent and thereby with time, signal intensity increases in SMCs due to this slow accumulation of NO passing from ECs. The decrease in NO signal in ECs most probably is the result of high NO-probe complex saturation and subsequent bleaching.

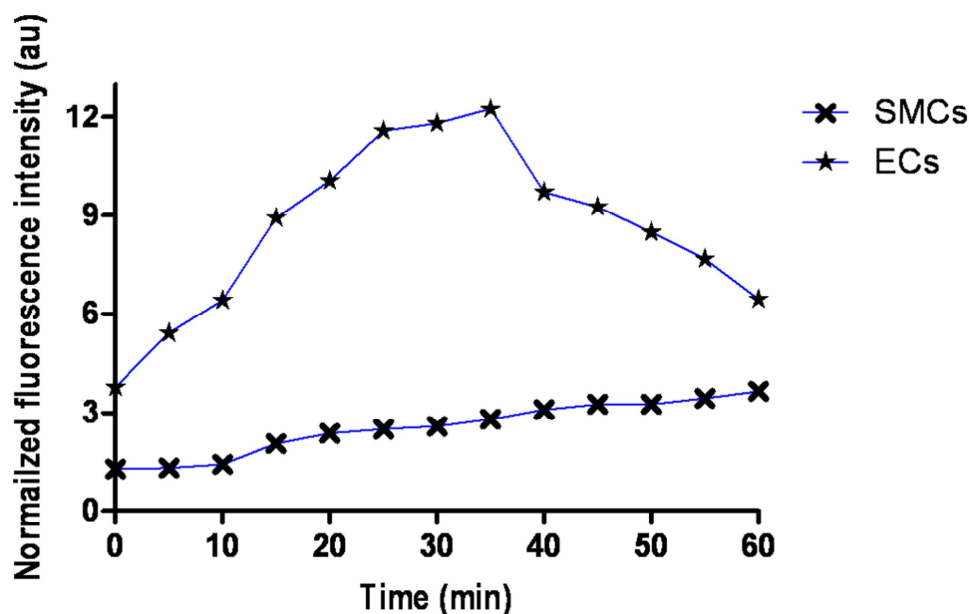


Fig. 27 Profiles of NO occupancy in SMCs and ECs in carotid artery, when stimulated with H_2O_2 . ($n = 5$). With time, signal intensity increases in SMCs due to slow accumulation of NO passing from ECs. The decrease in NO signal in ECs at longer time point is probably the result of NO-probe complex saturation and subsequent bleaching.

3.3.3 NO production can be imaged and visualized ex vivo in precontracted murine carotid arteries with Cu_2FL2E

In most physiological experiments, ACh is added after precontraction of the vessel. To visualize the NO production of carotid arteries after precontraction, we first applied Noradrenaline (NA) as a vasoconstrictor, after which the time curve of ACh-induced fluorescence response from NO signal was monitored in ECs and SMCs. In contrast to the results obtained in carotids without precontraction, where only a slow increase in NO signal was observed after ACh stimulation, here already after 2.5 min (the first

3. Results

possible measurement point) a detectable fluorescence change (**Fig. 28a, b & c**) was seen in ECs. In SMCs no significant increase in fluorescence was seen. The fluorescence in ECs continued to increase during 15min after ACh stimulation (**Fig. 28d**).

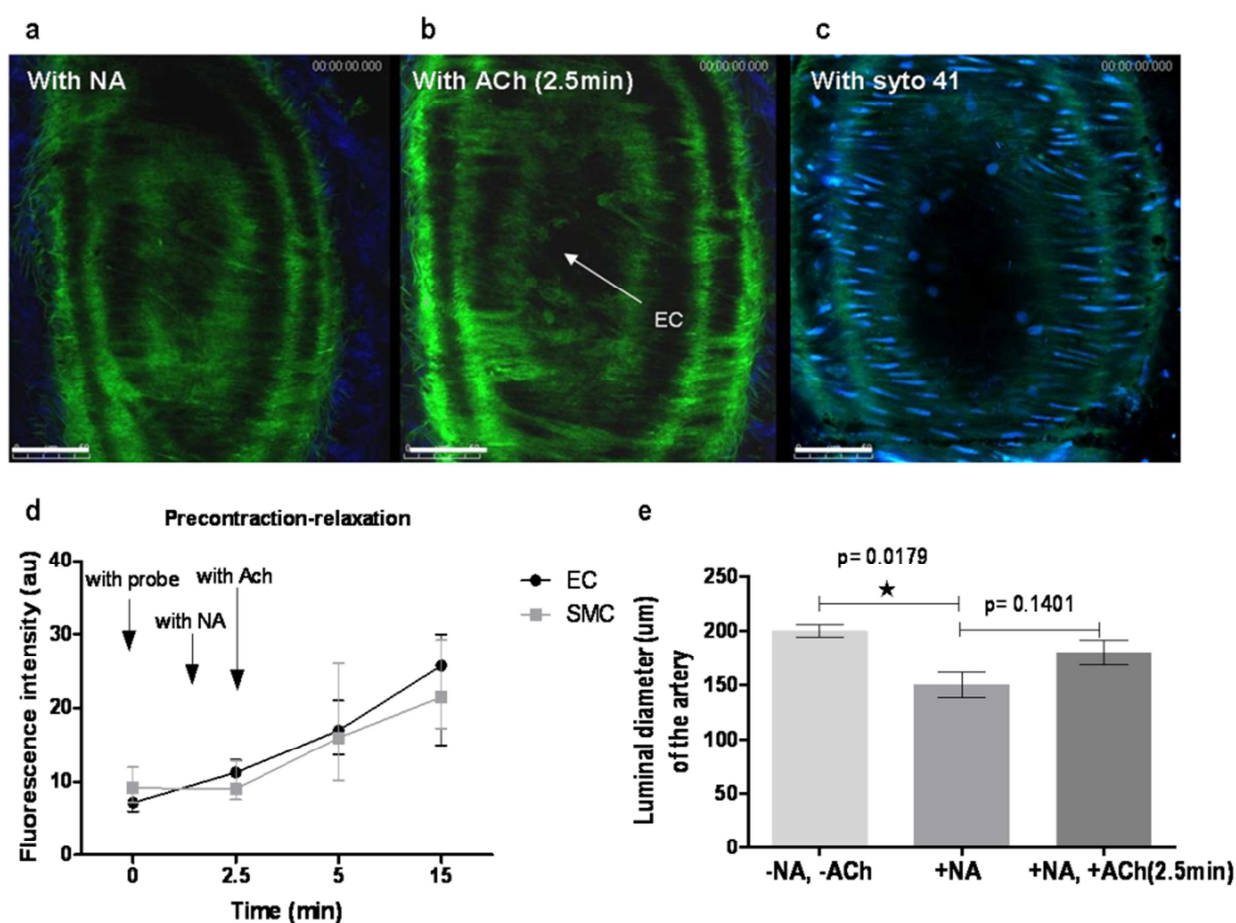


Fig. 28 Detection of NO produced in explanted murine carotid arteries *ex vivo* using **Cu₂FL2E** with precontraction. **(a)** Detection of NO in response to NA (ECs and SMCs are not apparent), **(b)** Detection of NO in post NA and ACh stimulation (2.5min) (ECs and SMCs are apparent), **(c)** Syto 41 staining of nucleus of ECs and SMCs, **(d)** plot of fluorescence intensities of the ECs and SMCs (from carotid artery) measured with NA and ACh stimulation for 15min, **(e)** luminal diameter measured from arteries with conditions mentioned in a & b, error bars indicate s.d. (n=3)

3. Results

3.3.4 Cu₂FL2E does not influence the contractile behaviour of carotid arteries after pre-contraction

In order to demonstrate the non-toxicity of Cu₂FL2E and to show the absence of an influence of Cu₂FL2E on contractile behavior of the carotid arteries, studies on arteries in the myograph were performed. In this experimental setup, the excised murine carotid artery was stretched in the myograph chamber and was challenged with noradrenaline (NA) (10 μ M) for precontraction.

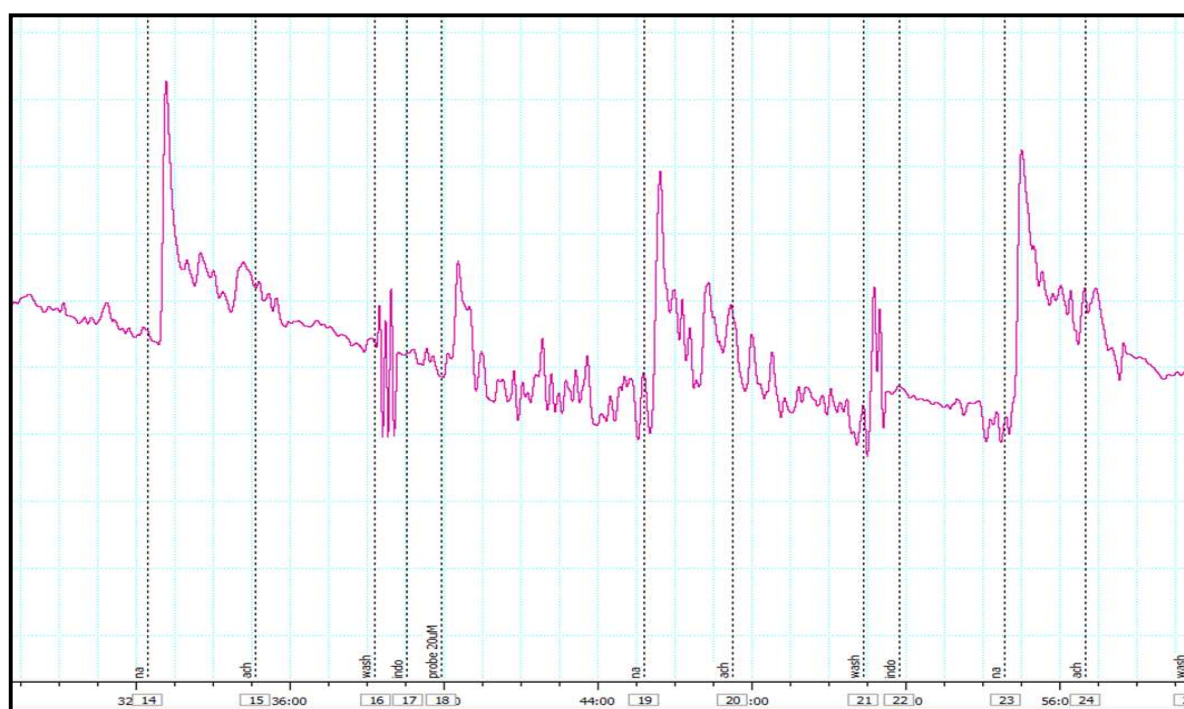


Fig. 29 Original trace recordings of percentage of relaxation of mouse carotid arteries in a vessel myograph. Segments of the carotid artery (2 mm long) from wild-type mouse and were mounted in a vessel myograph and vessel pretension was adjusted in steps to resemble an intraluminal pressure of 100 mm Hg. Vessels were first contracted with indomethacin, washed, and then contracted by 10 μ M noradrenaline. Acetylcholine (10 μ M) was then added in the vessel bath. ACh induced relaxation of the vessel. The same procedure was repeated, this time first with incubation of the vessel with Cu₂FL2E (20 μ M) for 5min, then NA and ACh were added. ACh induced relaxation was not influenced by Cu₂FL2E as could be seen from the percentage of relaxation.

Vasomotor response to ACh ($10 \mu\text{M}$) was then checked as positive control. Subsequently, the same experiment was performed several times in the presence of $\text{Cu}_2\text{FL2E}$ ($20 \mu\text{M}$). The result (**Fig.29**) revealed no change in the percentage of relaxation and time course of the dilation in the presence of $\text{Cu}_2\text{FL2E}$. Hence, this demonstrates the non-toxic nature of the probe and its utility in functional assessments.

3.3.5 3D reconstruction of the vessel

As shown before, in a non-stimulated control artery elastin layers are visible, while ECs and SMCs are not visible. On stimulation, SMCs and ECs become visible due to the NO-induced rise in fluorescence intensity. Series of XY-images at successive depths (Z-stack, step size $0.99 \mu\text{m}$) were collected for reconstruction of 3D images (**Fig. 30**). 2D and the 3D reconstructions expose the medial and intimal layer of the vessel wall. Thus, from every obtained optical section, a detailed study of delicate structures in the vessel wall was possible.

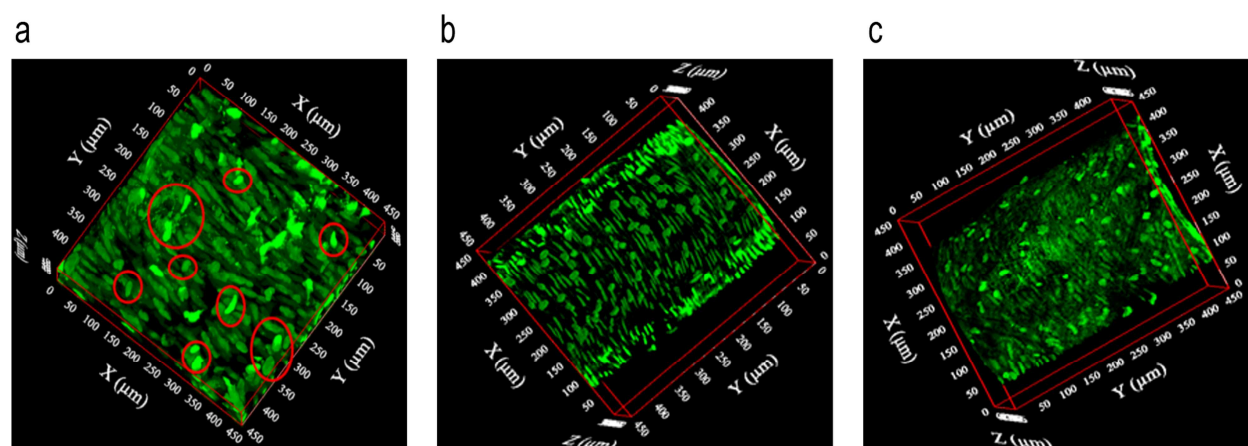


Fig.30 3D reconstruction of vessel; (a) 3D reconstruction of a section of the vessel showing “spindle shaped” smooth muscle cell and endothelial cell (several indicated by red circles) alignment with respect to the direction of flow, (b) 3D reconstruction of the intimal side of the vessel exposing smooth muscle cells and endothelial cells at the media-intima interface to assess the structure of the cells in relation to variable NO release, (c) 3D reconstruction of the adventitial side of the vessel showing thin elastin fibres and fibroblasts at the adventitia-media interface.

3. Results

The NO signal was apparent in SMCs and ECs at the medial-intimal interface of the vessel wall as could be seen with good spatial resolution. Furthermore, these 3D optical sections could be used for functional analysis, such as determining the luminal diameter. Unfortunately, this way of determining luminal diameters is rather slow, since 3D stacks have to be imaged. Furthermore, to carry out 3D stacking, the vessel diameter first needs to be stabilized. These two factors exclude “on the fly” diameter calculations during the intensity experiments.

3.3.6 NO-mediated vasomotor response of arteries can be determined at end point and correlated with the change in fluorescence intensity

Since changes in vascular diameter cannot be measured during the intensity experiments, vascular diameters of explanted carotid arteries were assessed before and after the dynamic intensity experiments. To that end, luminal diameters were obtained from XZ images after 3D reconstruction. On stimulation of non-precontracted carotids by ACh for 45 min, the luminal diameter of the ACh-stimulated arteries increased significantly when compared with non-stimulated arteries (p value = 0.0451) (**Fig. 31a&b**). Also the fluorescence intensity of the ACh-stimulated arteries increased significantly when compared with non-stimulated arteries (p value = 0.0427) (**Fig. 31c**). In contrast, when NO synthesis in the vessel was blocked by L-NAME, luminal diameter of arteries decreased significantly, (**Fig. 31d&e**) even after administration of ACh (p value = 0.0168) and also the fluorescence intensity decreased (p value = 0.046) (**Fig. 31f**). Functionality of the ECs and SMCs of mounted carotid arteries was also evaluated by testing the acute vasomotor responses (change in luminal diameter) to the vasodilator acetylcholine (10 μ M) during (10 μ M) NA- induced vasoconstriction. Both were administered extraluminally. The average luminal diameter of the arteries decreased (from 200 ± 10 μ m to 150 ± 20 μ m) upon administration of NA, and when ACh was added the average luminal diameter of the arteries increased (from 150 ± 20 μ m to 180 ± 20 μ m). These results not only establishes the viability of the mounted vessels, but also demonstrate that Cu₂FL2E does not crucially affect the enzymatic activity of NO synthesis, NO bioavailability or of downstream pathways involved in SMC-relaxation. This

3. Results

also establishes the importance of this method in the forefront of simultaneous structural-functional imaging of NO in the vasculature. We also evaluated the influence of removal of the NO donor SNAP (**Fig. 32a**) on the stability of the probe and the influence of copper ions on the sensitivity of the probe (**Fig. 32b**). Both showed no effects on the integrity of the probe.

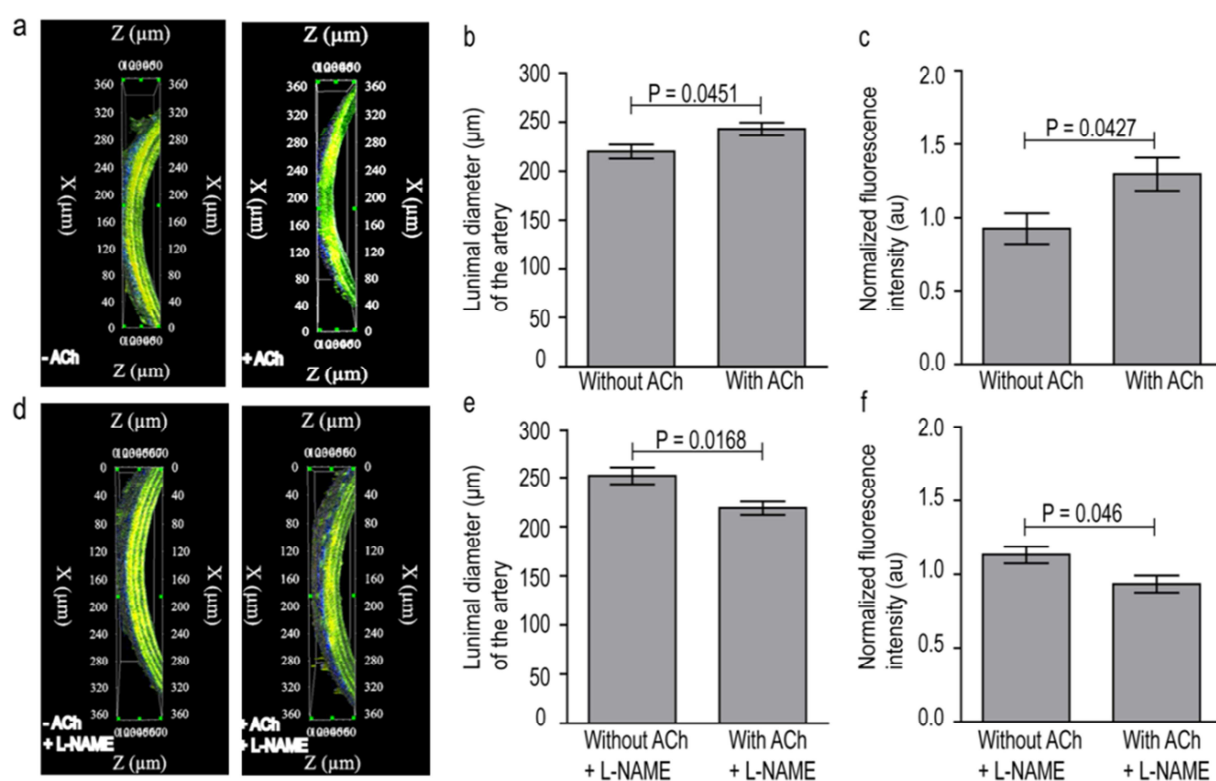


Fig. 31 Functional imaging of NO; (a) 3D reconstruction of vessels with $\text{Cu}_2\text{FL2E}$ without/ with stimulus (here ACh), (b) luminal diameter measured from arteries with conditions mentioned in (a), (c) normalized fluorescence intensities of the arteries with conditions mentioned in (a), (d) 3D reconstruction of vessels with $\text{Cu}_2\text{FL2E}$ without/ with stimulus (here ACh) and also in combination with L-NAME, (e) luminal diameter measured from arteries with conditions mentioned in (d), (f) normalized fluorescence intensities of the arteries with conditions mentioned in (c), error bars indicate s.d. ($n=5$)

3. Results

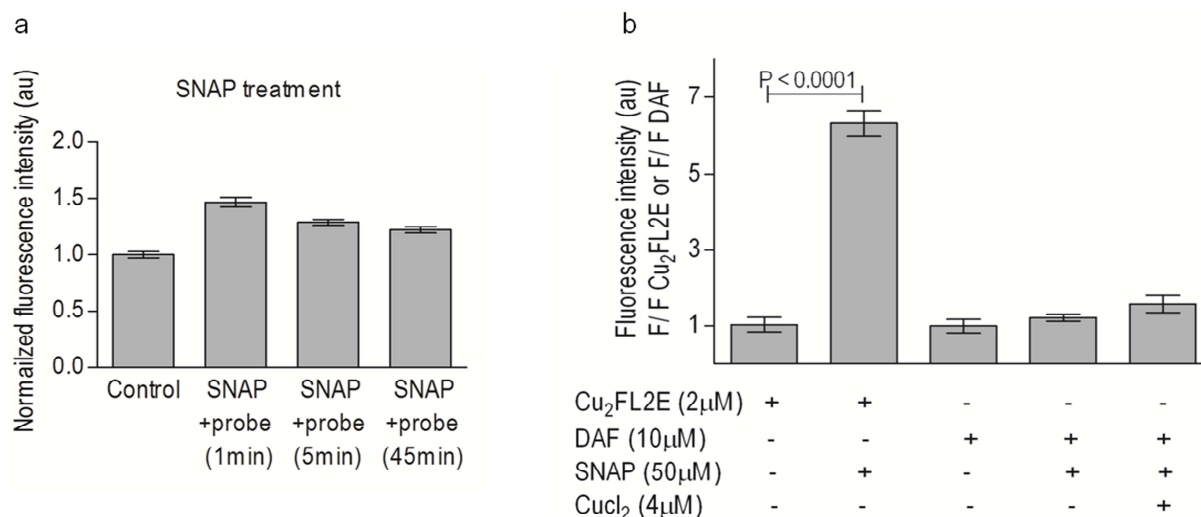


Fig. 32 Effect of SNAP and CuCl₂ on integrity of Cu₂FL2E (a) Fluorescence response of HCAECs with Cu₂FL2E to SNAP, (b) Fluorescence response of DAF-2-DA to SNAP in presence of CuCl₂, n = 5 (accumulations in both the cases). Error bars indicate s.d.

3.4. Visualization of NO synthesis and vasomotor response in the carotid artery in wild type and Arginase-1 deficient mice

NO imaging in a model of cardiovascular complication, where NO is a major regulator, is indispensable. Therefore, we applied our Cu₂FL2E-TPLSM approach to unravel the role of NO under vascular pathologic conditions. This methodology helped in determining the spatiotemporal relationship between vascular anatomy and NO production with relative quantification of NO and exploration of NO-mediated vasomotor response.

3.4.1 NO synthesis in normal and endotoxemic carotid artery of wild type mice: effect of arginine supplementation

In this study, a newly developed prolonged murine endotoxemia model (18 hours) **(123)** (**shown on page 31**) was used to visualize modulated NO production and also to investigate the effect of arginine supplementation during ongoing endotoxemia.

3. Results

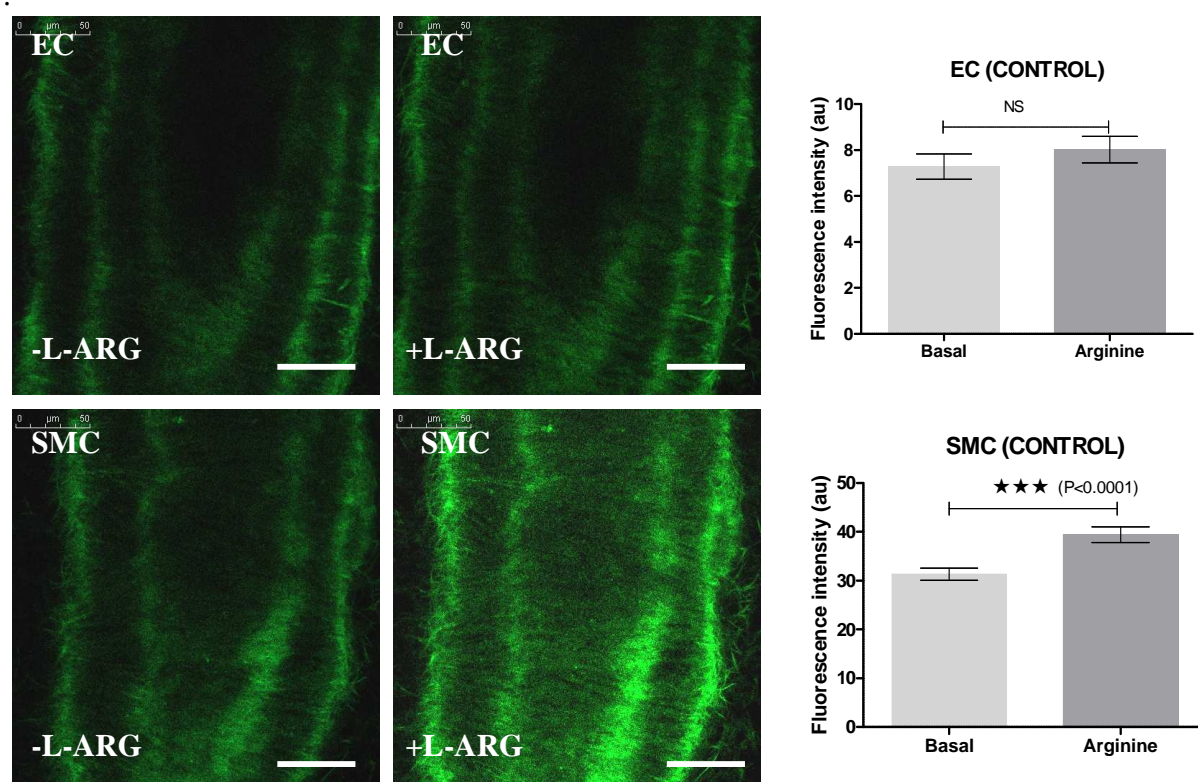


Fig. 33 Detection and quantification of NO produced in healthy explanted murine carotid arteries ex vivo with and without arg supplementation; NO signal detected in smooth muscle cells (SMCs) and endothelial cells (ECs) of the tissue with 5 min incubation of Cu₂FL2E (20 μM) and, subsequently 30min incubation of L-ARG (67 μM). Scale bars, 50 μm.

This murine model of prolonged endotoxemia mimics the human situation where the arginine-NO metabolism is disturbed due to prolonged exposure to endotoxin. Consequently, in this condition, arginine availability is reduced along with associated decreased NO production. Cu₂FL2E –TPLSM imaging modality was used as the tool to establish if extracellular arginine supplementation can restore NO production at sub-cellular level during endotoxemic condition. The results demonstrate that L-arginine supplementation under normal condition, does not improve the localized NO production in ECs (as no significant increase in fluorescence intensity can be seen),

3. Results

while in SMCs increased fluorescence intensity on addition of arginine (**Fig. 33**) can be observed. This observation can be explained, as it is known that extracellular arginine forms only arginine pool for iNOS induced NO production.

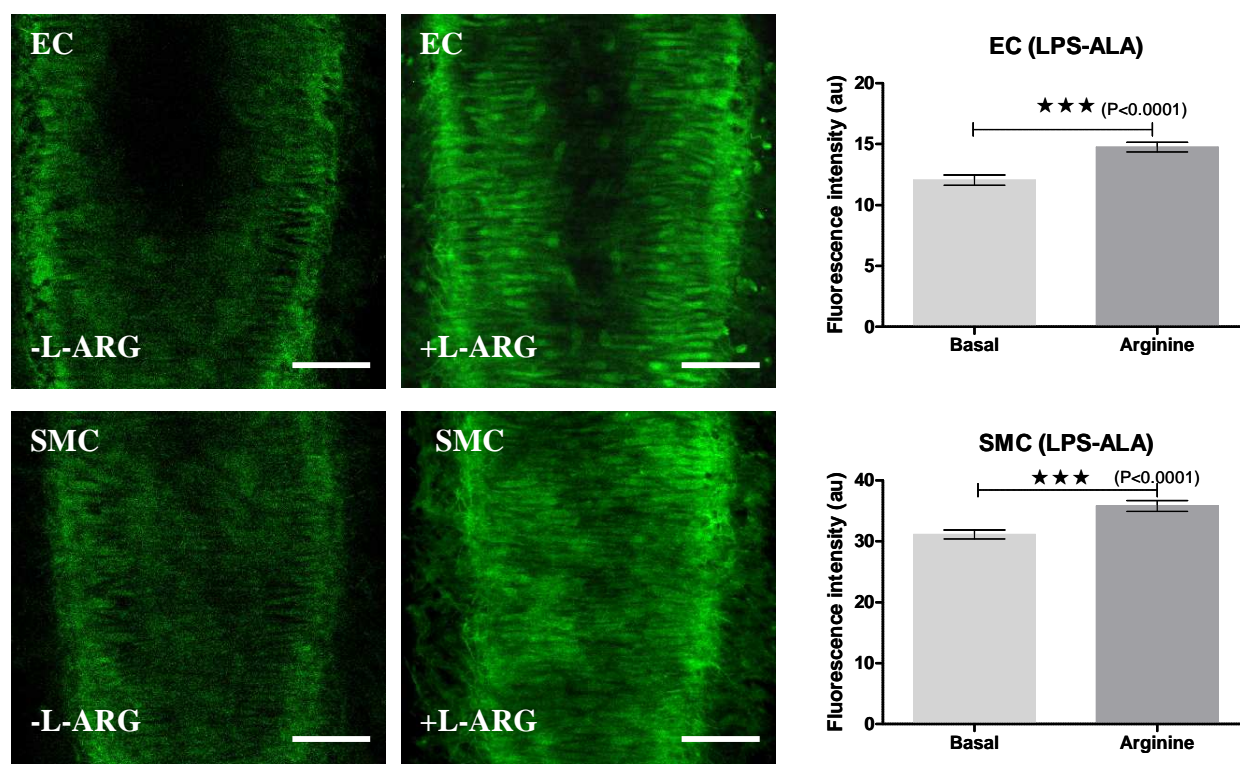


Fig. 34 Detection and quantification of NO produced in endotoxemic explanted murine carotid arteries ex vivo with and without arg supplementation; NO signal detected in smooth muscle cells (SMCs) and endothelial cells (ECs) of the tissue with 5 min incubation of $\text{Cu}_2\text{FL2E}$ ($20 \mu\text{M}$) and, subsequently 30min incubation of L-ARG ($67 \mu\text{M}$). Scale bars, $50 \mu\text{m}$.

In contradiction, during ongoing endotoxemia, L-arginine supplementation improved the localized NO production in both ECs (as seen by a significant increase in fluorescence intensity) and SMCs. The later could be due to either iNOS induced NO production in SMCs or the increased amount of NO diffused from ECs (**Fig. 34**). The participation of various NOS in context to this was not studied. Also the effect of

3. Results

extracellular arginine supplementation on microcirculation balance was not studied. However, the vasomotor response of the explanted carotid arteries (functionality) was assessed by simultaneous measurement of NO-related $\text{Cu}_2\text{FL2E}$ fluorescence and NO mediated vasomotor response (i.e. the change in luminal diameter). Luminal diameters were obtained from XZ images after 3D reconstruction. L-arginine supplementation (for 30 min), increased fluorescence intensity for both SMCs and ECs in endotoxemic arteries compared to normal arteries. The average luminal diameter of the endotoxemic arteries also increased (from; $100 \pm 10 \mu\text{m}$, to; $170 \pm 10 \mu\text{m}$) upon administration of arginine compared with normal arteries (from; $200 \pm 10 \mu\text{m}$, to; $200 \pm 20 \mu\text{m}$) (**Fig. 35**). Conclusively, $\text{Cu}_2\text{FL2E}$ -TPLSM can be considered to be an important tool for the visualization of modulated NO production in disease condition, and hence this approach could contribute to basic scientific research hugely, where NO is an important biomarker for cardiovascular complication. One can benefit from early diagnosis of modulated NO production in these vascular diseases.

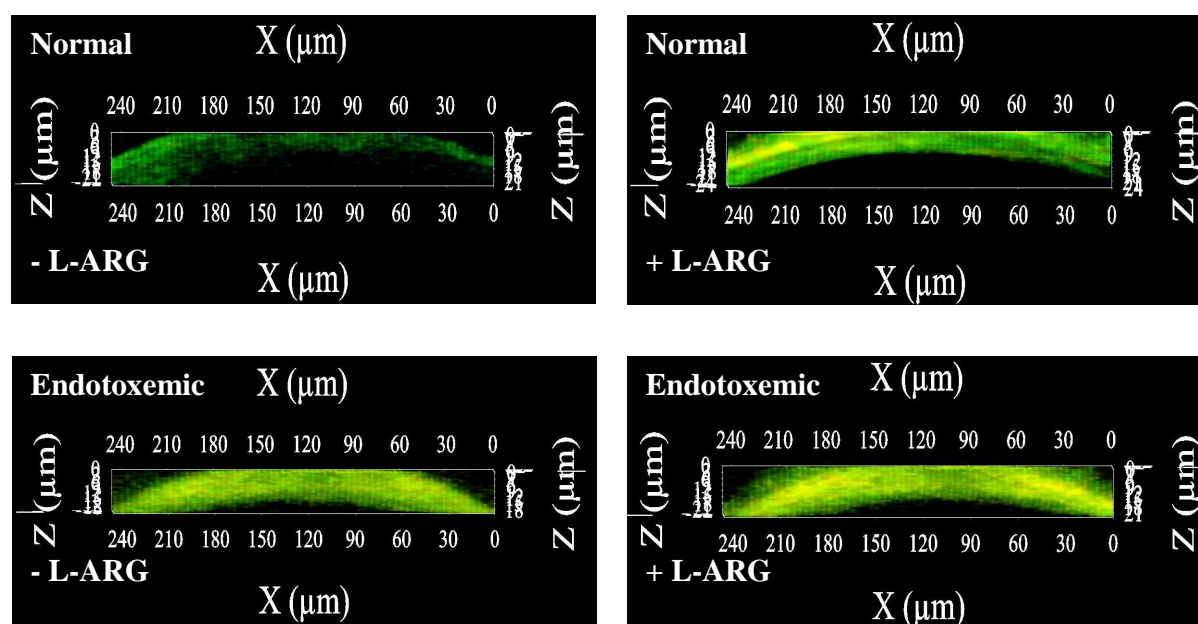


Fig. 35 Functional imaging of NO in endotoxemic arteries; 3D reconstruction of vessels with $\text{Cu}_2\text{FL2E}$ without/ with L-ARG.

3. Results

3.4.2 NO synthesis in normal and endotoxemic carotid artery of Arginase-1 knockout mouse ($Arg^{fl/fl}/Tie2-Cre^{tg/-}$): effect of arginine supplementation

Endothelial cells of the tissue specific $Arg^{fl/fl}/Tie2-Cre^{tg/-}$ mice ($Arg^{fl/fl}/Tie2-Cre^{tg/-}$ + LPS) exhibited more ex vivo NO production compared to the endothelial cells of the control mice (Control + LPS) (**Fig. 36**), however the origin (NOS2; iNOS or NOS3; eNOS) of the enhanced NO production needed to be unraveled.

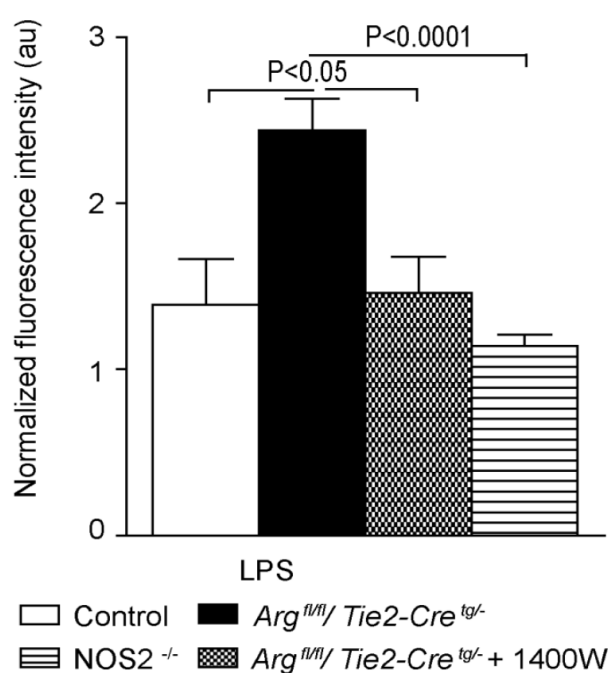


Fig. 36 Ex vivo NO production measured in carotid arteries of LPS-treated Control and $Arg^{fl/fl}/Tie2-Cre^{tg/-}$ mice. The endothelial cells in carotid arteries of $Arg^{fl/fl}/Tie2-Cre^{tg/-}$ mice exhibited significantly more ex vivo NO production compared to endothelial cells of Control and $NOS2^{-/-}$ mice. *In vivo* treatment with 1400W and in $Arg^{fl/fl}/Tie2-Cre^{tg/-}$ mice showed less ex vivo NO production compared to the $Arg^{fl/fl}/Tie2-Cre^{tg/-}$ (LPS-treated) group. NO production displayed as normalized fluorescence intensity (au).

3. Results

To test whether, the effects of arginase I depletion were dependent on the increased NOS2-mediated NO production, a selective NOS2 (iNOS) blocker, 1400W was administered. *In vivo* supplementation of 1400W in the *Arg^{fl/fl}/Tie2-Cre^{tg/+}* LPS group, resulted in significant lower ex vivo NO production in the endothelial cells of these animals, measured with two-photon microscopy (**Fig. 36**) and Cu₂FL2E. The NO-production observed in endothelial cells of the *Arg^{fl/fl}/Tie2-Cre^{tg/+}* + LPS+1400W carotid arteries was not significantly different from the concentrations observed in the endothelial cells of the Control+LPS carotid arteries.

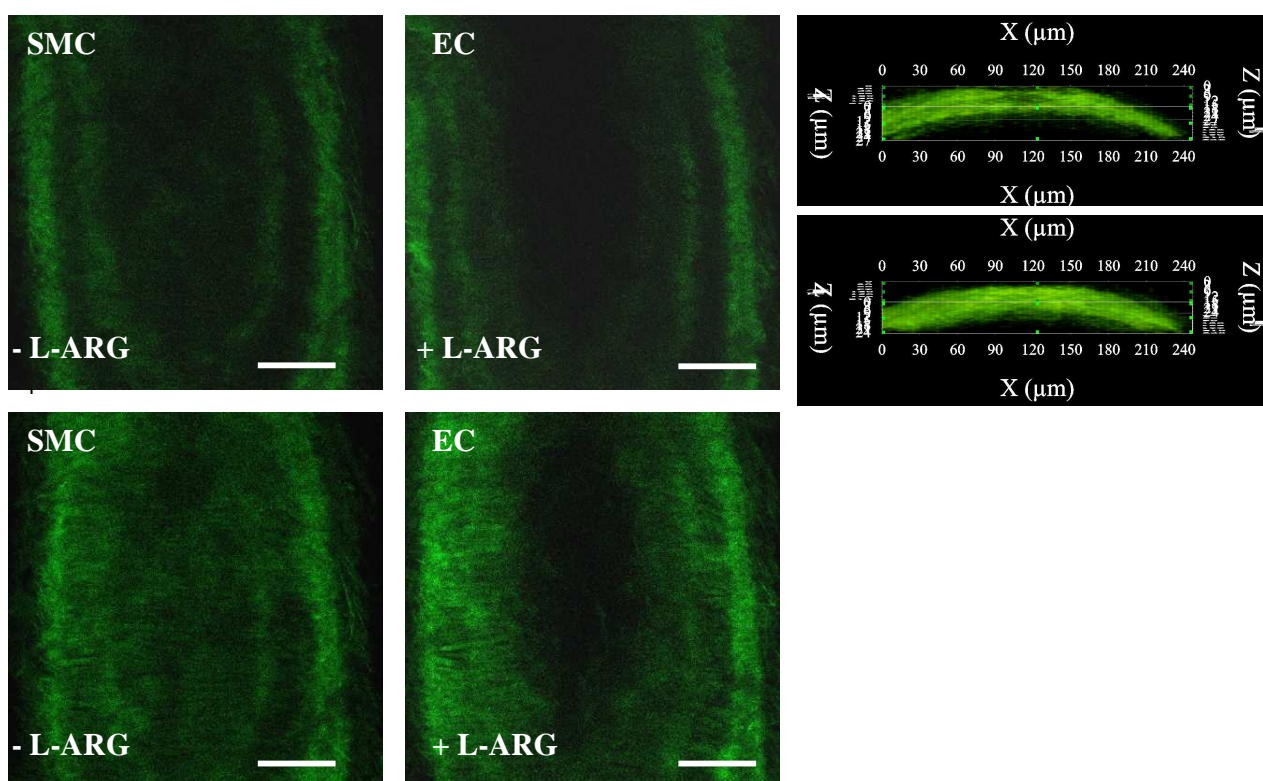


Fig. 37 Detection and quantification of NO produced in explanted murine *arg^{-/-}* carotid arteries ex vivo using Cu₂FL2E; NO signal detected in smooth muscle cells (SMCs) and endothelial cells (ECs) of the tissue with 5 min incubation of Cu₂FL2E (20 μM) and, subsequently 30min incubation of L-ARG (67 μM). Scale bars, 50 μm.

3. Results

In contrast to this, endothelial cells from *NOS2^{-/-}* mice displayed an ex vivo NO production, which was comparable to the NO production as observed in the Control animals (*NOS2^{-/-}* + LPS versus Control + LPS, n=3; P= 0.32; **Fig. 37**).

Cu₂FL2E –TPLSM imaging modality was used as the tool to investigate the role of arginine supplementation at sub-cellular level (structural-functional) during normal and endotoxemic condition in Arginase ^{-/-} mouse.

The results indicate that extracellular arginine supplementation at basal level *Arg^{fl/fl}/Tie2-Cre^{tg/-}* mice did not enhance NO signal in ECs and SMCs. The vasomotor response (i.e. the change in luminal diameter) indicates abrogation of NO production or its limited utilization for vasorelaxation as luminal diameter decrease (**Fig. 37**).

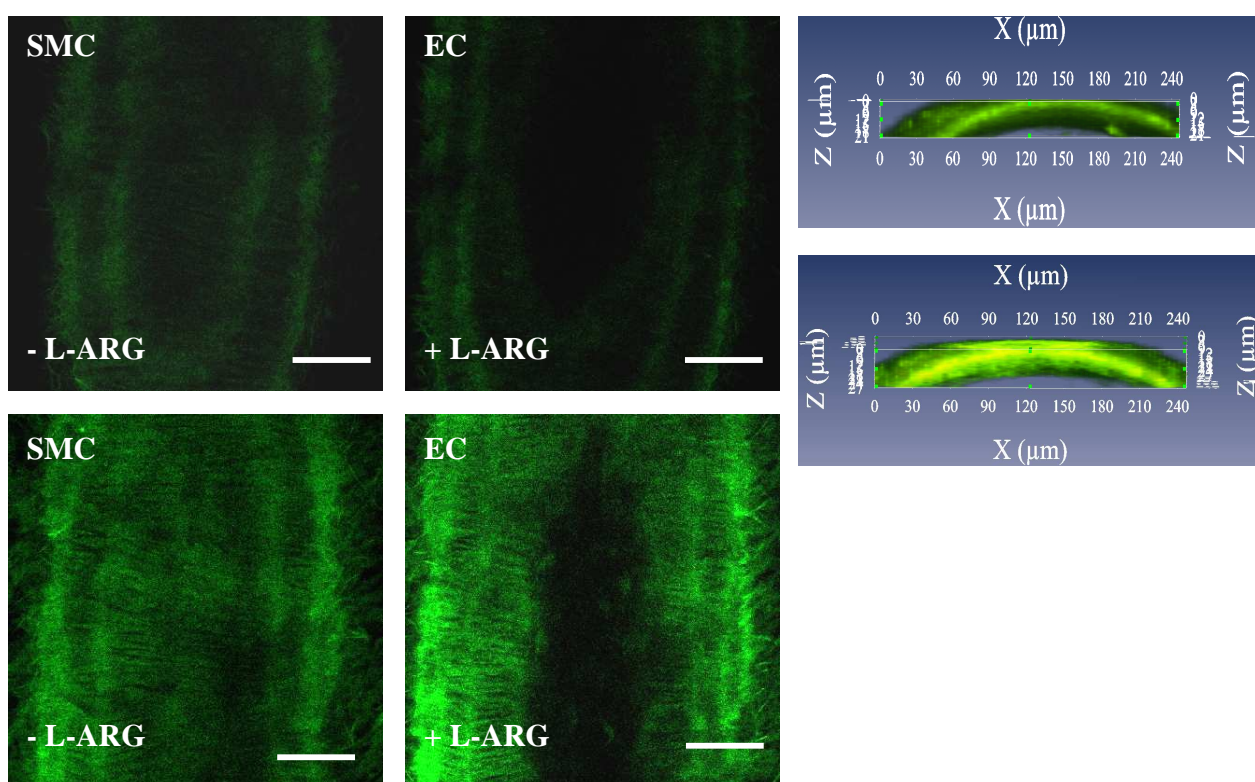


Fig. 38 Detection and quantification of NO produced in explanted murine *arg^{-/-}* carotid arteries (endotoxemic) ex vivo using Cu₂FL2E; NO signal detected in smooth muscle cells (SMCs) and endothelial cells (ECs) of the tissue with 5 min incubation of Cu₂FL2E (20 μM) and, subsequently 30min incubation of L-ARG (67 μM). Scale bars, 50 μm.

3. Results

In contradiction, during ongoing endotoxemia (*Arg^{fl/fl}/Tie2-Cre^{tg/+}* LPS mice), L-arginine supplementation improved the localized NO production in both ECs (as seen by a significant increase in fluorescence intensity) and also the luminal diameter increased (**Fig. 38**) as seen from 3D constructions. The average luminal diameter of the endotoxemic arteries also increased (from; $165 \pm 10 \mu\text{m}$, to; $195 \pm 10 \mu\text{m}$) upon administration of arginine compared with normal arteries (from; $205 \pm 10 \mu\text{m}$, to; $185 \pm 20 \mu\text{m}$).

Modulating the arginase activity during endotoxemia needs to aim at restoring the balance between arginase and arginine supplementation during inflammatory conditions as this may be the key to an improved endothelial function.

3.4.3 *In vitro* assessment of arginine supplementation on human coronary arterial endothelial cells

Results indicate that arginine is immensely important for cell survival, as lack of arginine in medium *in vitro* leads to substantial cell death on shear stress-induced endothelial NO-production. On supplementation with $400 \mu\text{M}$ arginine, there is comparable cell survival and increased NO production.

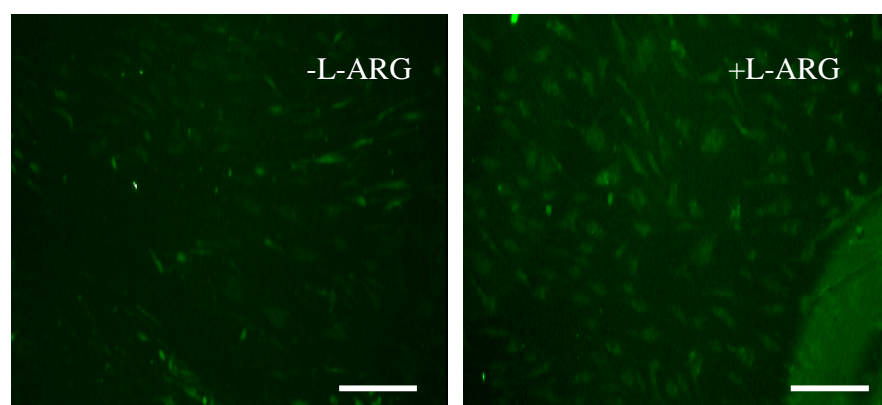


Fig. 39 Assessment of arginine supplementation on survival of HCAECs using $\text{Cu}_2\text{FL2E}$: NO signal detected in endothelial cells (ECs) of the tissue with 5 min incubation of $\text{Cu}_2\text{FL2E}$ ($20 \mu\text{M}$) and, subsequently 30min incubation of L-ARG ($67 \mu\text{M}$). Scale bars, $50 \mu\text{m}$.

3.5. *In vitro* thrombus imaging with carbon dot and TPLSM

Application of novel fluorescent nanoparticle conjugated peptide in thrombus imaging using Two-Photon Laser Scanning Microscopy (TPLSM) is highlighted in this study. Experiments showed strong fluorescence (red) from TAMRA clearly showing the fibrin network. Initially, no fluorescence was seen from C-Dots. Later on increasing the power of the laser, the fluorescence from the TAMRA bleached and fluorescence (blue) from C-Dot tended to increase in the fibrin network. Hence, it was clear that fibrin was labeled by this bilabeled peptide. Fluorescence from the C-Dot can be seen in the blue range of spectra and therefore it can be used as an important fluorophore as not many fluorophores are known in this range. The surface chemistry of these cDots can also be used to tailor drugs and can be used to target various sites in vascular tree when conjugated with disease specific ligands in relation to various cardiovascular diseases like atherosclerosis, hypertension etc.

3.5.1 Structure of the bi-labeled peptide

Activated factor XIII (FXIIIa) plays an important role in regulating the resistance of thrombi against fibrinolysis. FXIIIa covalently crosslinks alpha2 antiplasmin, a key inhibitor of plasmin-mediated fibrinolysis, to fibrin.

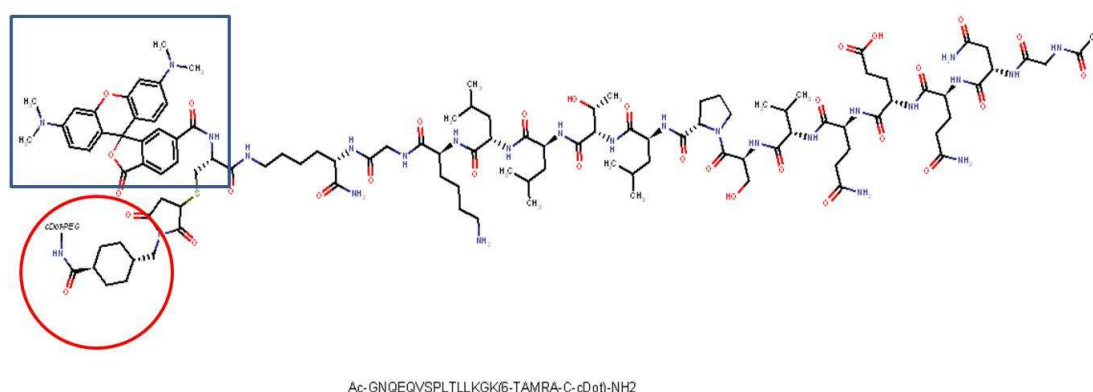


Fig. 40 Structure of A14 peptide conjugated with TAMRA (indicated with blue box) and C-dot (indicated with red circle) at the N-terminal of the peptide, showing proximity of C-dot and TAMRA conjugation on the peptide.

3. Results

Factor XIII specific ligand (peptide A14) has been coupled to TAMRA (6-carboxytetramethyl rhodamine dye) and cDot to visualize thrombus with two-photon microscopy (**Fig. 40**).

3.5.2 Characterization of fluorescent properties of C-Dot

Preliminary experiments were done with C-Dots using the Nanodrop photospectrometer to identify their fluorescence emission peaks. C-Dots were also used under two-photon microscopy to check their two-photon excitability. Additionally, their fluorescence lifetime was determined. Making use of surface chemistry of C-Dots, A14 peptide was prepared bilabeled with TAMRA (579nm emission) (RED) and C-Dot (439nm emission) (BLUE) to selectively target fibrin exposed on fresh thrombus in vitro.

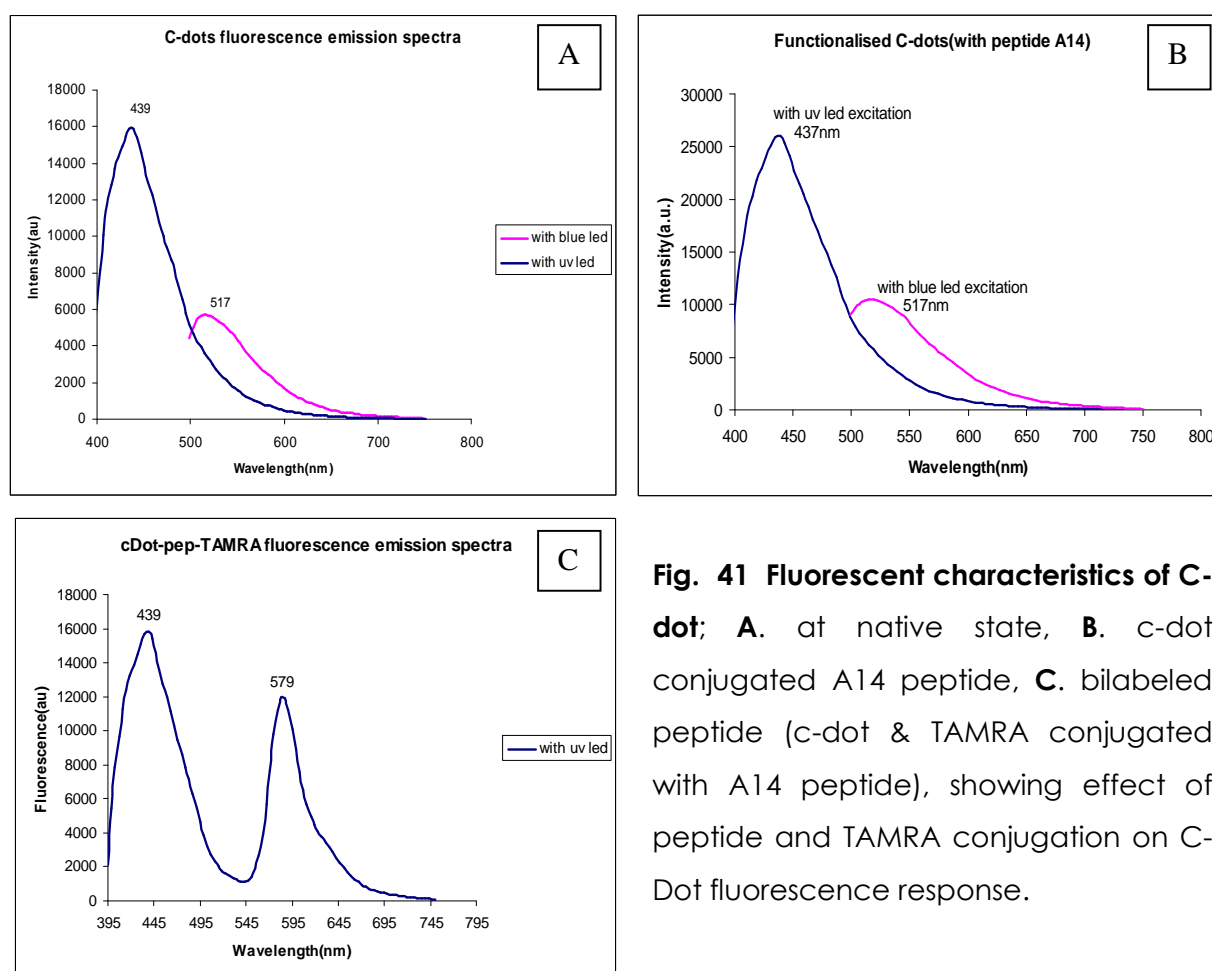


Fig. 41 Fluorescent characteristics of C-dot; **A.** at native state, **B.** c-dot conjugated A14 peptide, **C.** bilabeled peptide (c-dot & TAMRA conjugated with A14 peptide), showing effect of peptide and TAMRA conjugation on C-Dot fluorescence response.

3. Results

TAMRA is used as a control for cDot efficacy. Many experiments were performed using Nanodrop photospectrometer to check the effect of peptide and TAMRA on cDot fluorescence emission (**Fig. 41**). Using two-photon microscopy the following two-photon fluorescent characteristics were revealed for c-dots: optimal excitation: 775nm, emission: 460-470nm, fluorescence lifetime: 2.7ns.

3.5.3 Thrombus imaging with TPLSM and c-dot-TAMRA conjugated A14 peptide reveal c-dot and TAMRA as FRET pairs

A14 peptide conjugated to carbon dots (cDots) was used to target fibrin exposed on fresh thrombus in vitro. A14 is an antiplasmin based peptide and its utility to image fresh thrombi has been shown before. Our experiment showed strong fluorescence (red) from TAMRA clearly showing the fibrin network. Initially, no fluorescence was seen from cDots (**Fig. 42 (a)**). Later on increasing the power of the laser, the fluorescence from the TAMRA bleached and fluorescence (blue) from cDot tended to increase in the fibrin network (**Fig. 42 (b, c, and d)**).

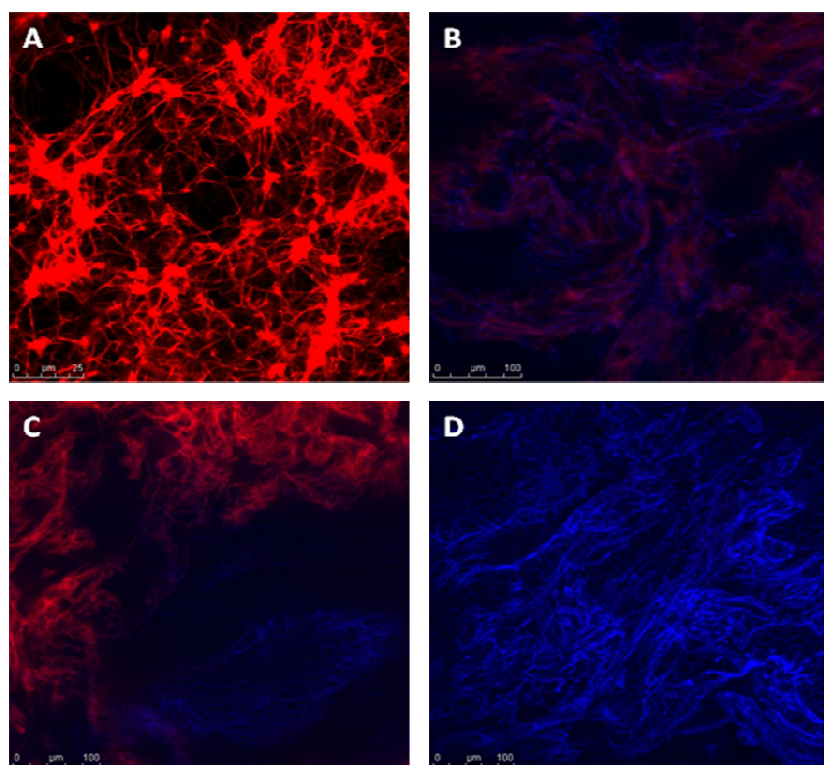


Fig. 42 Fluorescence from C-dot expressed on fibrin; fluorescence from cDot expressed by slow photobleaching of TAMRA, **A.** TAMRA expressed on fibrin, **B, C, D.** cDot expression on fibrin

3. Results

Hence, it was clear that fibrin was labeled by this bilabeled peptide. This also shows FRET (Fluorescence Resonance Energy Transfer) on play. This can be further confirmed by measuring the change in fluorescence lifetime of C-Dot and TAMRA individually. C-Dot and TAMRA can also be used as an important FRET pair as seen from the experiment. Fluorescence from the C-Dot can be seen in blue range of spectra and therefore it can be used as an important fluorophore as not many fluorophores are known in this range. However, further experiments need to be done to validate the data. Since carbon dot shows promise as a labelling dye, further experiment must be done where C-Dot will be conjugated alone with the peptide and targeted to fresh thrombus.

4. General discussion - future perspectives

The studies explore the feasibility of two-photon microscopy in unraveling structural and functional details in vasculature with high spatial and temporal resolution. Subcellular imaging from *in vitro* to *ex vivo* environment is addressed in the context of both nitric oxide imaging and thrombus imaging.

In the first part, we demonstrate the feasibility of using Cu₂FL2E as a direct, sensitive, and specific NO probe. Combined with TPLSM we describe a suitable imaging method for investigating NO biology in the vascular system.

NO is an important messenger that regulates a multitude of physiological functions within the vascular system. Abrogation of NO production in case of dysfunctional endothelium can result in cardiovascular diseases such as hypertension, atherosclerosis and sepsis. To study its role and (sub) cellular constitution, direct and specific NO-detection in living cells and tissues is a major requirement. The high diffusibility and short half-life of NO complicate real time detection. Several chemical methods are available to measure the oxidation products of NO, such as nitrite and nitrate, but detection of NO itself is still challenging. The lack of specific non-toxic NO probes has hampered the studies on important aspects of NO in cellular and tissue metabolism such as diffusion properties and depicting the exact source of NO production. In the present study, we establish the applicability of Cu₂FL2E to analyze NO dynamics in cells and vasculature. Superior characteristics of Cu₂FL2E such as non-toxicity, high specificity and sensitivity for NO make it an ideal probe. Cu₂FL2E selectively detects NO over H₂O₂ **(47)**, whereas DAF-2-DA failed to make this distinction (which is in agreement with literature **(45, 78, 118)**). Cu₂FL2E also detects nanomolar concentrations of NO produced in vascular endothelial cells with higher sensitivity than DAF-2-DA. Based on the rate of NO generation from SNAP (1.4 μM NO per minute at a concentration of 100 μM in PBS at pH 7.4 and 37°C) **(114, 115)**, a rough estimate of the NO detection limit can be made. Under the conditions employed in our sensitivity test, in which both Cu₂FL2E and DAF-2-DA are challenged with various concentrations of SNAP, Cu₂FL2E shows better sensitivity (significant change in fluorescence intensity with 2.5 μM of SNAP) by comparison to DAF-2-DA (significant change with 5 μM of SNAP). By calculating back for NO concentration, the lower end detection limit of Cu₂FL2E is ~35 nM, which is in the normal physiological

4. General discussion - future perspectives

range of stimulated NO levels in healthy tissue. This calibration procedure gives an insight into semi-quantification of basal and accelerated levels of NO signal. Therefore, we believe that Cu₂FL2E will also detect nanomolar concentrations of NO produced in vascular endothelial cells and arteries, which can be utilized in assaying NO contribution under normal and diseased conditions. We further show that *ex vivo* NO imaging in murine carotid arteries allows distinction of intimal (ECs) from medial (SMCs) NO signal. Although it is difficult to comment on the sources of NO generation and contribution, we speculate that ECs are the prime source of NO generation in the vessel wall (as results show significant changes in fluorescence in ECs when triggered with flow or ACh), but the capacity of SMCs to generate NO (i.e. by activation of iNOS) **(125, 126)** must also be considered (specially, in case of chemical triggers like H₂O₂) and its limited capacity when induced by flow is interesting. Along with NO mediated vasodilation, endothelium-derived hyperpolarizing factor (EDHF) participation in relaxation of various arteries is another interesting aspect to study in this context. EDHF's vasodilator action is of prime importance particularly when NO production is compromised. However, EDHF contribute mainly in small vessel dilation. Under our conditions, the carotids and aorta (with suitable controls) show vasorelaxation to be primarily NO-dependent.

By obtaining NO occupancy profiles in SMCs and ECs, we specifically addressed compartments and temporal profiles of NO production in the vasculature. A similar profile was obtained with ACh stimulations (data not shown). The temporal occupancy profile of NO in different cells plays a major role in vascular biology and pathology, as that determines NO participation in protective or pathologic role.

Quantitative differences in NO-signal *ex vivo*, as determined using Cu₂FL2E, correspond with measurements of vasodilation or vasoconstriction, in the absence or presence of L-NAME. This result not only establishes the viability of the mounted vessels, but also shows that Cu₂FL2E does not affect the enzymatic activity of the NO synthesis or of downstream pathways involved in SMC-relaxation. Thus, the use of Cu₂FL2E in combination with TPLSM (resolution and penetration depth) and mounting the arteries in the vessel chambers is a valuable method to analyze NO in vascular tissue with high specificity and cellular resolution.

4. General discussion - future perspectives

SNAP has been used by multiple investigators as one of the most widely used chemical sources for NO since there is no authentic stable source for NO (**46, 114, 115, 127**). SNAP releases NO and other thiol molecules almost instantaneously, at controlled rate (**128**). In contrast, for short time experiments, NONOates are not a suitable choice because of their slow dissociation rate, while solutions of NO can dissociate before reaching the probe. We evaluated the effect of SNAP on vascular endothelial cells loaded with probe, to check if on removal of SNAP the fluorescence of the probe is affected or not. A point of consideration in this study is the role of the Cu(II)/Cu(I) ion on NO release from S-nitrosothiols (SNAP) or by cells associated with activated eNOS. According to previous studies (**115, 127**), copper ions can decompose S-nitrosothiols more rapidly, thus speeding up NO release from SNAP. Therefore, we evaluated the influence of the copper ions on the release of NO from SNAP.

We found that the fluorescence response of DAF to NO (delivered by SNAP) in the presence of similar amounts of CuCl₂ as present in Cu₂FL2E did not change significantly. This result confirmed that there is no measurable influence of copper under the experimental conditions used in our studies. Use of copper chelators, NO scavengers and EPR measurement have already been shown by Lim *et al* (**46**) that confirmed no influence of copper in the measurements. However, we cannot completely exclude the possibility that fluorescence increase in stimulated cells results from activated eNOS was due to presence of copper-ions along with extracellular calcium (**128**). Nevertheless, control experiments, such as cells incubated with Cu₂FL2E, without stimulus did not exhibit significant fluorescence, indicating that Cu(I)/Cu(II) ions by themselves do not interfere with cellular NO imaging. In cells, copper released from Cu₂FL2E is likely scavenged rapidly by cellular components such as metallothionein or copper chaperones, minimizing the chance of copper ions to influence the cellular response. An intriguing question still to be answered concerns the contribution of subclasses NO synthases (NOS) to the total NO production in healthy and diseased vessels. This experimental methodology opens new avenues for further research on NO metabolism and its effect on vessel wall morphology and function. Direct visualization and measurement of NO would help to further elucidate its role as an important determinant of endothelium dysfunction in relation to diseases like atherosclerosis and hypertension.

4. General discussion - future perspectives

In this study, we have used healthy blood vessels and ECs in the absence of cardiovascular risk factors. With more complex morphology of the vessel wall as in an atherosclerotic lesion, visualization of NO is even more important.

In conclusion, NO analysis with Cu₂FL2E in combination with TPLSM allows specific detection and semi-quantification of endogenous NO production both *in vitro* and *ex vivo* with high spatial-temporal resolution. With the use of Cu₂FL2E and TPLSM we are able to unravel the structural-functional relationship of NO in the vessel wall. The presence of NO in various vascular cells could be monitored *ex vivo* for several physiological NO-stimuli. The presented analytical method for temporal-spatial kinetics of NO synthesis and the presence in the vascular wall provides a valid method to study the role of NO in vascular biology at an unprecedented level. Thus, the findings of this research hold key for future research and application in the field of basic medical biology.

In line with this study, Cu₂FL2E-TPLSM method was further applied to study modulated NO formation in endotoxemia. In this study, a newly developed prolonged murine endotoxemia model was used to investigate the disturbances of the arginine-NO metabolism and to investigate the role of L-arginine supplementation during ongoing endotoxemia. The results of the present investigation, in the second part, demonstrated that endothelial capacity to produce NO is restored by L-arginine supplementation in a prolonged murine endotoxemia model. However, its effect for microcirculatory improvement needs to be studied and validated. Finding ways to prevent or reverse endothelial activation can help reduce vascular complications. Also, investigation of endothelial specific arginase I deficiency in a prolonged *in vivo* model of murine endotoxemia by Cu₂FL2E-TPLSM demonstrated an enhanced NO production. Our findings reveal that the enhanced NO production was NOS2 derived in endothelial cells and tissue.

As seen from the results, the enhanced plasma arginine availability due to deficiency of arginase 1, did not influence the basal NO production. Thus, during basal conditions, enhanced plasma L-arginine availability did not influence the NOS3 derived NO

4. General discussion - future perspectives

production. In addition, an experimental L-arginine deficient state **(86, 87)** was used to determine the role of the tissue specific arginase-I on NOS3 derived NO.

LPS infusion in the *Arg^{fl/fl}/Tie2-Cre^{tg/-}* mice resulted in a significant increased NO production in endothelial cells. Since the remnant arginase-I activity in these tissue specific *Arg^{fl/fl}/Tie2-Cre^{tg/-}* mice is negligible, another important competitor for arginine availability may benefit from the arginase I deficiency instead of NOS3. The impaired inhibition of NOS2 activity, by arginase-I, is suggested to play the leading part in the detrimental outcome of this study. Normally, arginase-I competes with NOS2 for substrate **(105, 129, 130)** and regulates the NOS2 translation and expression, especially in the endothelium, which restrains the inflammatory response **(131)**. This knowledge led to investigate whether *in vivo* NOS2 inhibition would positively influence the NO production and microcirculation. *In vivo* suppression of NOS2 with 1400W revealed lower tissue (endothelial cells) NO production, suggesting the enhanced NO production to be NOS2 derived in the *Arg^{fl/fl}/Tie2-Cre^{tg/-}* mice. Endothelial / hematopoietic arginase-I deficient (*Arg^{fl/fl}/Tie2-Cre^{tg/-}*) knock-out mice exhibited an enhanced by an enhanced NO production in endothelial cells under basal and endotoxemic conditions. Selective NOS2 inhibition in endotoxemic *Arg^{fl/fl}/Tie2-Cre^{tg/-}* mice prevented the enhanced inflammatory response and NO production, which strengthened our findings, that NOS2 benefits from the arginase-I tissue specific deficiency during endotoxemia.

In conclusion, arginase I plays a crucial role in controlling NOS2 during inflammation in endothelial cells, and modulating the arginase activity during endotoxemia needs to be performed with great precautions.

Therefore, future studies need to focus on the fragile balance between arginase and NOS2 during inflammatory conditions as this may be the key to an improved endothelial function.

In the final part, we presented work on CDots conjugated peptide that can affordably image thrombus formation. In this study, an alpha2-antiplasmin based peptide was used conjugated with C-Dot (as a fluorescent marker) to visualize early stage of thrombus formation. Activated factor XIII (FXIIIa) covalently crosslinks alpha2-antiplasmin to fibrin in early stage thrombus. Thus, *in vitro* generated thrombi were targeted with this new

4. General discussion - future perspectives

conjugated agent to visualize fibrins expressed on fresh thrombus. With very interesting set of experiments, binding of this agent to fresh thrombi were observed. TAMRA and C-Dot evolved to be FRET pairs from our experiment, and a novel biomarking strategy was developed. A challenge for biomarking, based on luminescent materials, has been the development of structures (C-Dot) with highly visible emissions for precise imaging, combined with nanoscale dimensions for suitable targetting.

The surface chemistry of these CDots can also be used to tailor drugs and can be used to target various sites in vascular tree when conjugated with disease specific ligands. This will prove its importance in clinical platform as it will not only help in imaging but drugs attached to it will help to resist the progression of disease. It can also be used to target atherosclerotic plaques. Biodistribution study of this CDot peptide in mice needs to be optimized for assessing its binding capabilities and it will also show the biocompatibility of the conjugate in the body or if it induces certain other reponses. The most important use of this CDot peptide conjugate in comparison to qdot-peptide conjugate is that it increases the time window during which this can be used for thrombus detection as CDot is resistant to photobleaching and photoblinking. The CDot peptide conjugate prepared here specifically binds to fibrin expressed on fresh thrombus. Using the surface chemistry of the CDots other peptide could be tagged that specifically binds to receptors expressed on organized (old) thrombus. Alpha 2b beta 3 integrin receptor expressed in platelet on an organized thrombus may be targeted and imaged. This will help in a comparative analysis of thrombi using CDot – peptide conjugate. *In vivo* imaging is another possible exploration of this method to image thrombus. The surface chemistry of CDots also gives option to attach Gd-complexes so that it can be used as bimodal agents in fluorescence imaging and in MRI. Determination of the optimal dosage is another important study that needs to be standardized.

5. Summary

The domain of the vascular biology is a complex system consisting of different types of blood vessels, cells, and signaling molecules. It is now recognized that these vessels and molecules are part of a subtle regulatory system with differential properties along the vascular tree. Altered production of these molecules is a molecular clue for dysfunctionality of cells or alterations of vessel properties that may lead to various acute and chronic diseases. Current knowledge of such vascular alterations is mostly based on histological studies of isolated samples that have lost their viability. Functional properties of various compounds are still largely unknown. Better understanding of the functionality of these molecules in the context of cardiovascular functioning can increase insight in early stage of disease condition. Thus studying these properties *in vivo* or in viable arteries *ex vivo* is indispensable. This thesis focuses on the vessel wall of large murine arteries and cultured cell systems using TPLSM as an imaging tool for studying alterations in vessel wall properties as well as important molecules and their functional consequences.

In this thesis, I first addressed the concept of NO imaging in vasculature with a novel method. Nitric oxide analysis with Cu₂FL2E in combination with TPLSM allowed specific detection and semi-quantification of endogenous NO production both *in vitro* and *ex vivo*. With the use of Cu₂FL2 and TPLSM we were able to unravel the structural-functional relationship of NO in the vessel wall. Presence of NO in various vascular cells could be monitored *ex vivo* for several physiological NO-stimuli. The Cu₂FL2E-TPLSM approach provides a valid method to study the role of NO in vascular biology at an unprecedented level and can enable investigation of the regulatory pathways in the complex interplay between NO and vascular (dys)function.

In the second part, NO production was studied with TPLSM in murine endotoxemia. Impact of arginine supplementation in wild type and ARG-1 ^{-/-} mouse, in NO metabolism was investigated. A disturbed arginine-nitric oxide metabolism is associated with endotoxemia. Therefore, the effect of L-arginine supplementation on eNOS-induced intracellular NO production was studied in wild type and a non-lethal prolonged endotoxemia model in mice. TPLSM revealed that the L-arginine supplementation restored intracellular NO production during endotoxemia.

5. Summary

However, further investigation is needed to find out if this NO improves the microcirculation during endotoxemia. Arginase-I also contributes to endothelial dysfunction during endotoxemia as it competes with NOS3 for arginine availability. Therefore, I investigated the effects of cell-specific arginase-1 deficiency on the arginine availability, the NOS3-derived NO production during murine endotoxemia. Arginase-I plays a crucial role in controlling NOS2 during inflammation in endothelial cells. Modulating the arginase activity resulted in an inflammatory response an increased NO production by NOS2. Therefore, modulating arginase activity during endotoxemia needs to aim at restoring the balance between arginase and NOS2 during inflammatory conditions, as this may be the key to an improved endothelial function.

In the final part, visualization of fresh thrombus formation has been described using fibrin-targeted peptide conjugated with C-Dot. Thrombosis plays a major role in several vascular diseases and early detection of thrombus formation is a hitherto unmet requirement in clinical practice. Further validation of this method might help in translation of early detection strategy of thrombus in clinical scenario.

In general discussion, I contemplate various ideas regarding the topics described and open new avenues and possible future outcomes for application of these novel studies. I conclude that the described techniques (in the forefront of TPLSM imaging) offer a new and different view on healthy and diseased arteries and provide new insight in various structural and functional properties of vessels. Further development of these techniques holds potential for future applications in both a scientific and clinical environment.

6. Zusammenfassung

Das Gebiet der Gefäßbiologie ist ein komplexes System, bestehend aus verschiedenen Typen von Blutgefäßen, Zellen und Signalmolekülen. Diese Gefäße und Moleküle sind Teil eines subtilen regulatorischen Systems mit verschiedenen Eigenschaften. Eine Störung der Produktion dieser Moleküle ist der Initiator von Dysfunktionalität von Zellen oder Veränderungen der Blutgefäßeigenschaften, die zu verschiedenen akuten und chronischen Erkrankungen führen können. Derzeitige Erkenntnisse solcher Gefäßveränderungen basieren vor allem auf histologischen Studien von isolierten Gewebeproben, welche durch die verschiedenen Fixierungsmethoden ihre Lebensfähigkeit verloren haben. Die funktionellen Eigenschaften der verschiedenen Stoffe noch weitgehend unbekannt. Ein besseres Verständnis der Funktion dieser Moleküle im Bezug auf die Herz-Kreislauf-Funktionen können einen besseren Einblick in das frühe Stadium der Krankheitszustand ermöglichen. Somit sind diesbezügliche Studien *in vivo* oder in lebensfähigen Arterien *ex vivo* ist unverzichtbar. Diese Arbeit konzentriert sich auf die Gefäßwand von murinen Hauptarterien und *in vitro* kultivierten Zellsystemen mit TPLSM als Bildgebungsmethode, um die Veränderung der Gefäßwandeigenschaften sowie wichtige Moleküle und deren funktionelle Konsequenzen zu untersuchen.

In dieser Arbeit visualisieren ich Stickstoffmonoxid (NO) in Gefäßen mit einem neuartigen Verfahren. Stickoxid-Analyse mit Cu₂FL2E in Kombination mit TPLSM erlaubt den spezifischen Nachweis und semi-Quantifizierung der endogenen NO-Produktion *in vitro* und *ex vivo*. Durch den Einsatz von Cu₂FL2 und TPLSM konnten wir den strukturellen und funktionalen Einfluss von NO in der Gefäßwand entwirren. Die Anwesenheit von NO in verschiedenen vaskulären Zellen konnte *ex vivo* für mehrere physiologische NO-Reize beobachtet werden. Der Cu₂FL2E-TPLSM Ansatz bietet eine passende Methode, um die Rolle von NO in der vaskulären Biologie zu studieren und ermöglicht die Untersuchung der Regulationsmechanismen in dem komplexen Zusammenspiel zwischen NO und vaskuläre (Dys)-Funktion.

Im zweiten Teil wurde die NO-Produktion in Mäuse mit Endotoxinämie mittels TPLSM untersucht. Auswirkungen von Arginin im NO-Metabolismus wurde in Wildtyp und ARG -1^{-/-} Mäuse untersucht. Ein gestörter Arginin-Stickstoffmonoxid Stoffwechsel ist mit

6.Zusammenfassung

Endotoxinämie verbunden. Aus diesem Grund wurde die Wirkung von L-Arginin Zusatz auf eNOS-induzierte intrazelluläre NO-Produktion in Wildtyp und nicht-tödliche verlängerte Endotoxämie in Mäusen untersucht. TPLSM zeigte, dass L-Arginin Zusatz bei Endotoxinämie die intrazellulären NO-Produktion wiederherstellte. Allerdings sind weitere Untersuchungen erforderlich, um zu zeigen ob NO die Mikrozirkulation bei Endotoxinämie verbessert. Arginase-I trägt auch zu einer endothelialen Dysfunktion bei Endotoxinämie bei, da es mit NOS3 um Arginin konkurriert. Wir haben daher die Auswirkungen des zellspezifischen Arginase-1-Mangels im Bezug auf die Arginin Verfügbarkeit untersucht und die NOS3-abhängige NO-Produktion während der murinen Endotoxinämie. Arginase-I spielt eine entscheidende Rolle bei der Regulierung von NOS2 während der Entzündung in Endothelzellen. Die Veränderung der Arginaseaktivität führte zu einer Entzündungsreaktion und einer erhöhten NO-Produktion durch NOS2. Daher muss die Steuerung der Arginase-Aktivität unter entzündlichen Bedingungen während Endotoxinämie gezielt auf die Wiederherstellung des Gleichgewichts zwischen Arginase und NOS2 zielen, da dies der Schlüssel zu verbesserten Endothelfunktion sein kann.

Im letzten Teil wird die Visualisierung von Thrombusbildung durch ein Fibrin-spezifisches Peptid konjugiert mit C-Dots beschrieben. Thrombose spielt eine wichtige Rolle in verschiedenen Gefäßerkrankungen und die Früherkennung von Thrombusbildung ist ein bisher unerfüllten Anforderungen in der klinischen Praxis. Weitere Untersuchungen und Validierung dieser Methode könnte der Translation dieser Thrombus-Früherkennungsstrategie in klinischen Szenarios helfen.

In der allgemeinen Diskussion betrachten wir verschiedene Ideen über die Themen beschrieben und eröffnen neue Möglichkeiten, zukünftige Ergebnisse für die Anwendung dieser neuartigen Studien. Wir schlussfolgern, dass die beschriebenen Techniken (in vorderster Front TPLSM imaging) einen neuen und anderen Blick auf gesunden und kranken Arterien bietet und neue Einblicke in den verschiedenen strukturellen und funktionellen Eigenschaften von Blutgefäßen. Die Weiterentwicklung dieser Techniken hat Potential für zukünftige Anwendungen in sowohl einer wissenschaftlichen als auch klinischen Umfeld.

7. Acknowledgements

In Abraham Lincoln's words "And in the end, it's not the years in your life that count. It's the life in your years." On this note, the seemingly simple part of writing thesis (i.e. Acknowledgement) appears an herculean task to me, as my heart is overwhelmed with intense emotions, and words fail short. This makes writing it a challenge. First and foremost, I would like to thank all the people who inspired my thoughts and enriched my faith in science and love for mankind.

The data presented in my Ph.D. thesis were conducted at the Two-photon imaging Lab., Cardiovascular Research Institute Maastricht (CARIM), Netherlands. Other educational training, courses and seminars were conducted by both CARIM and the Institute for Molecular Cardiovascular Research (IMCAR), RWTH-Aachen, Germany. The experimental work was carried out between October 2008 and March 2012. I would like to show my gratitude to Professor Dr. Christian Weber, Director of IMCAR (former) who gave me the opportunity to work in this project. I am grateful to Professor Dr. Mark J. Post (former acting Director of CARIM) for his constructive comments and for his important support throughout my work. Moreover, Professor Post looked closely at the final version of the thesis, correcting it and offering suggestions for improvement.

I am heartily thankful to my supervisor, Professor Dr. Marc AMJ van Zandvoort whose understanding, encouragement, and support from the initial to the final level enabled me to develop an understanding of the subject. His guidance has been of great value for me and has provided a good basis for the present thesis and gave me untiring help and zeal during my difficult moments. I also thank him for conceiving ideas with me and helping develop those ideas into various projects that are presented in this thesis. I also thank him for being my examiner on my PhD examination committee and heading the imaging unit and help developing the unit with joint efforts. Above all, Marc as a person has always instilled the spirit of life - by all happiness and smile. My sincere thanks are due to the official supervisor, Professor Dr. Jurgen Bernhagen, for his detailed review, constructive criticism and excellent advice during the preparation of this thesis. I also thank him for being my examiner on my PhD examination committee. Special note of thanks for his excellent management of our graduate school (EuCAR 1). Thanks to Prof. Tilman Hackeng for taking care of the graduate school too and also for his important suggestions and helps in the Carbon dot project.

7.Acknowledgements

I wish to express my warm and sincere thanks to Dr. Daniel G.M. Molin, who introduced me to the field of vascular cell cultures and Dr. Nynke van den Akker, who gave me important guidance during my first steps into cell culturing and fluorescence microscopy. They both believed in me as a scientist and their ideals and concepts have had a remarkable influence on my entire career in the scientific field. They were immensely supportive and reliable guides. They also contributed in planning experiments with me, writing and correcting manuscript and providing immense support in cell culture, griess assay and flow experiments, and in interpretation of results. My present and former colleagues from CARIM supported me in my research work by discussing science, projects and by giving various important suggestions. I want to thank Iulia, for all her genuine interest, care, and understanding when I needed in my work and life. I thank Remco, Lenneke, Kim, Sietze, Wim, Timo, Vivianne, and Pieter for all their help, support, interest and valuable hints.

Special vote of thanks to Pieter van den Vijder for preparing the CDot conjugated peptide used in the study and thanks to Prof.Tilman Hackeng for his suggestions and support in this project. Especially I am thankful to my colleague Nina Wijnands and Prof. Martijn Poeze whose work contributed to this thesis. They developed the prolonged endotoxemic mouse models and the knock out models presented in this thesis. Jugular vein cannulation and surgical proceedings in endotoxemia model was performed by Nina. I also want to thank Jeroen and Anneke for all their technical assistance, for their amity and a lot of help. Their help in setting up of microscope and maintenance, software development and taking care of laboratory goods and ordering was of great help. I thank Frau Mayer, Claire and Heike for their kind help in secretarial work and immense care. For all administrative issues, their contribution is highly appreciable.

I am highly grateful to all my external collaborators; Prof. Stephen J. Lippard (Massachusetts Institute of Technology, USA) for kindly providing the copper based probe used in nitric oxide imaging study. I am also thankful to him and his colleagues Prof.Pluth, and Prof.McQuade for their help in writing manuscript and valuable suggestions. My gratitude for Prof.Ya ping Sun (Clemson University, USA) for kindly providing the CDots.

7.Acknowledgements

I am grateful to all my EuCAR colleagues; Wu, Adelina, Elena, Baixue, Martin, Yaw, Sebastian, Annette, Patricia, Anne, Emma for wonderful time I spent with you. Your companionship and warmth was always comfortable to be with for discussions, meetings, conferences and made the venture enjoyable. Wu's efforts to follow up the NO story and to carry on the collaborative project by performing two-photon microscopy are highly appreciable.

The work presented in this thesis was largely supported by the DFG (German Scientific Organization) Grant for EuCAR GRK 1508/1 to IMCAR and by NWO (Dutch Scientific Organization) to CARIM. The Leica TPLSM was obtained via a grant (No.902-16-276) from the medical section of NWO. This research was performed within the Vital Imaging Unit CARIM.

My beloved friends and their rich friendship was an essential part of my life. Without their encouragement and understanding it would have been impossible for me to finish this work. I thank them as they made this period enjoyable and motivating for me. Thank you Subhasish, for contemplating each other's ideas both with future prospect and hopeless ones. Your fond brotherhood, and discussing work and everyday life became a part of my life. I shall always cherish the memorable days of vacations, sports and fun. Hope, our friendship grows more in coming years. Thanks Oindrilla, for all delicious foods, care and support, and fond friendship. Sameera, thank you for your friendly bond and hours of chat to discuss life, badminton game, and for the nice food that you cooked. Thank you Subrata, for always being by my side and for your friendship. Thanks Santosh, Priyanka, Praveen and Ramesh for adding all the fun and support when needed. Without your love, patience and support during my stay abroad for research, the journey, thick and thin, in good moments and bad ones, would have never been accomplished. Therefore, cheers! to all my wonderful friends.

I offer my regards and blessings to all the people behind the scenes, those who supported me in any respect during the completion of the project.

Last, but not least, I owe my loving thanks to my parents, my sister and my grandmother for their love, constant support, and care they have provided me throughout my life. For making me believe in myself and always giving the positive support needed. I dedicate this book to them.

7.Acknowledgements

With the lines of Rabindranath Tagore, *“Where words come out from the depth of truth; Where tireless striving stretches its arms towards perfection; Where the clear stream of reason has not lost its way into the dreary desert sand of dead habit, Where the mind is led forward by thee into ever-widening thought and action—”,* I bid my deepest gratitude to each and one, who contributed positively to my work and my life. Like others, when I moved to this city, I carried dreams along with me, and now I am happy that I shall carry my dreams and memories too further.

Mitrajit Ghosh

8. References

- (1) Furchgott, R. F., and Zawadzki, J. V. (1980) The obligatory role of endothelial cells in the relaxation of arterial smooth muscle by acetylcholine. *Nature* **288**, 373-376
- (2) Palmer, R. M., Ferrige, A. G., and Moncada, S. (1987) Nitric oxide release accounts for the biological activity of endothelium-derived relaxing factor. *Nature* **327**, 524-526
- (3) Ignarro, L. J., Buga, G. M., Wood, K. S., Byrns, R. E., and Chaudhuri, G. (1987) Endothelium-derived relaxing factor produced and released from artery and vein is nitric oxide. *Proc Natl Acad Sci U S A* **84**, 9265-9269
- (4) Koshland, D. E., Jr. (1992) The molecule of the year. *Science* **258**, 1861
- (5) SoRelle, R. (1998) Nobel prize awarded to scientists for nitric oxide discoveries. *Circulation* **98**, 2365-2366
- (6) Radomski, M. W., and Moncada, S. (1993) The biological and pharmacological role of nitric oxide in platelet function. *Adv Exp Med Biol* **344**, 251-264
- (7) Radomski, M. W., Palmer, R. M., and Moncada, S. (1987) Endogenous nitric oxide inhibits human platelet adhesion to vascular endothelium. *Lancet* **2**, 1057-1058
- (8) Radomski, M. W., Palmer, R. M., and Moncada, S. (1987) The anti-aggregating properties of vascular endothelium: interactions between prostacyclin and nitric oxide. *Br J Pharmacol* **92**, 639-646
- (9) Radomski, M. W., Palmer, R. M., and Moncada, S. (1990) An L-arginine/nitric oxide pathway present in human platelets regulates aggregation. *Proc Natl Acad Sci U S A* **87**, 5193-5197
- (10) Garg, U. C., and Hassid, A. (1989) Nitric oxide-generating vasodilators and 8-bromo-cyclic guanosine monophosphate inhibit mitogenesis and proliferation of cultured rat vascular smooth muscle cells. *J Clin Invest* **83**, 1774-1777
- (11) Palmer, R. M., Ashton, D. S., and Moncada, S. (1988) Vascular endothelial cells synthesize nitric oxide from L-arginine. *Nature* **333**, 664-666

8. References

- (12) Sessa, W. C., Garcia-Cardena, G., Liu, J., Keh, A., Pollock, J. S., Bradley, J., Thiru, S., Braverman, I. M., and Desai, K. M. (1995) The Golgi association of endothelial nitric oxide synthase is necessary for the efficient synthesis of nitric oxide. *J Biol Chem* **270**, 17641-17644
- (13) Pollock, J. S., Nakane, M., Buttery, L. D., Martinez, A., Springall, D., Polak, J. M., Forstermann, U., and Murad, F. (1993) Characterization and localization of endothelial nitric oxide synthase using specific monoclonal antibodies. *Am J Physiol* **265**, C1379-1387
- (14) Balligand, J. L., and Cannon, P. J. (1997) Nitric oxide synthases and cardiac muscle. Autocrine and paracrine influences. *Arterioscler Thromb Vasc Biol* **17**, 1846-1858
- (15) Forstermann, U., Boissel, J. P., and Kleinert, H. (1998) Expressional control of the 'constitutive' isoforms of nitric oxide synthase (NOS I and NOS III). *FASEB J* **12**, 773-790
- (16) Blum-Degen, D., Heinemann, T., Lan, J., Pedersen, V., Leblhuber, F., Paulus, W., Riederer, P., and Gerlach, M. (1999) Characterization and regional distribution of nitric oxide synthase in the human brain during normal ageing. *Brain Res* **834**, 128-135
- (17) Yun, H. Y., Dawson, V. L., and Dawson, T. M. (1997) Nitric oxide in health and disease of the nervous system. *Mol Psychiatry* **2**, 300-310
- (18) Hoffman, R. A., Zhang, G., Nussler, N. C., Gleixner, S. L., Ford, H. R., Simmons, R. L., and Watkins, S. C. (1997) Constitutive expression of inducible nitric oxide synthase in the mouse ileal mucosa. *Am J Physiol* **272**, G383-392
- (19) Guo, F. H., De Raeve, H. R., Rice, T. W., Stuehr, D. J., Thunnissen, F. B., and Erzurum, S. C. (1995) Continuous nitric oxide synthesis by inducible nitric oxide synthase in normal human airway epithelium in vivo. *Proc Natl Acad Sci U S A* **92**, 7809-7813
- (20) Mannick, J. B., Asano, K., Izumi, K., Kieff, E., and Stamler, J. S. (1994) Nitric oxide produced by human B lymphocytes inhibits apoptosis and Epstein-Barr virus reactivation. *Cell* **79**, 1137-1146
- (21) Zamora, R., Vodovotz, Y., and Billiar, T. R. (2000) Inducible nitric oxide synthase and inflammatory diseases. *Mol Med* **6**, 347-373

8. References

- (22) Shah, A. M. (2000) Inducible nitric oxide synthase and cardiovascular disease. *Cardiovasc Res* **45**, 148-155
- (23) Fukuto, J. M., and Chaudhuri, G. (1995) Inhibition of constitutive and inducible nitric oxide synthase: potential selective inhibition. *Annu Rev Pharmacol Toxicol* **35**, 165-194
- (24) Anggard, E. (1994) Nitric oxide: mediator, murderer, and medicine. *Lancet* **343**, 1199-1206
- (25) Radomski, M. W., Palmer, R. M., and Moncada, S. (1987) Comparative pharmacology of endothelium-derived relaxing factor, nitric oxide and prostacyclin in platelets. *Br J Pharmacol* **92**, 181-187
- (26) Murad, F., Mittal, C. K., Arnold, W. P., Katsuki, S., and Kimura, H. (1978) Guanylate cyclase: activation by azide, nitro compounds, nitric oxide, and hydroxyl radical and inhibition by hemoglobin and myoglobin. *Adv Cyclic Nucleotide Res* **9**, 145-158
- (27) Bolotina, V. M., Najjibi, S., Palacino, J. J., Pagano, P. J., and Cohen, R. A. (1994) Nitric oxide directly activates calcium-dependent potassium channels in vascular smooth muscle. *Nature* **368**, 850-853
- (28) Blatter, L. A., Taha, Z., Mesaros, S., Shacklock, P. S., Wier, W. G., and Malinski, T. (1995) Simultaneous measurements of Ca²⁺ and nitric oxide in bradykinin-stimulated vascular endothelial cells. *Circ Res* **76**, 922-924
- (29) Neufeld, G., Cohen, T., Gengrinovitch, S., and Poltorak, Z. (1999) Vascular endothelial growth factor (VEGF) and its receptors. *FASEB J* **13**, 9-22
- (30) Govers, R., and Rabelink, T. J. (2001) Cellular regulation of endothelial nitric oxide synthase. *Am J Physiol Renal Physiol* **280**, F193-206
- (31) Razani, B., Engelman, J. A., Wang, X. B., Schubert, W., Zhang, X. L., Marks, C. B., Macaluso, F., Russell, R. G., Li, M., Pestell, R. G., Di Vizio, D., Hou, H., Jr., Kneitz, B., Lagaud, G., Christ, G. J., Edelmann, W., and Lisanti, M. P. (2001) Caveolin-1 null mice are viable but show evidence of hyperproliferative and vascular abnormalities. *J Biol Chem* **276**, 38121-38138

8. References

- (32) Misko, T. P., Schilling, R. J., Salvemini, D., Moore, W. M., and Currie, M. G. (1993) A fluorometric assay for the measurement of nitrite in biological samples. *Anal Biochem* **214**, 11-16
- (33) Rao, A. M., Dogan, A., Hatcher, J. F., and Dempsey, R. J. (1998) Fluorometric assay of nitrite and nitrate in brain tissue after traumatic brain injury and cerebral ischemia. *Brain Res* **793**, 265-270
- (34) Nakatsubo, N., Kojima, H., Sakurai, K., Kikuchi, K., Nagoshi, H., Hirata, Y., Akaike, T., Maeda, H., Urano, Y., Higuchi, T., and Nagano, T. (1998) Improved nitric oxide detection using 2,3-diaminonaphthalene and its application to the evaluation of novel nitric oxide synthase inhibitors. *Biol Pharm Bull* **21**, 1247-1250
- (35) Gunasekar, P. G., Kanthasamy, A. G., Borowitz, J. L., and Isom, G. E. (1995) Monitoring intracellular nitric oxide formation by dichlorofluorescein in neuronal cells. *J Neurosci Methods* **61**, 15-21
- (36) Imrich, A., and Kobzik, L. (1997) Fluorescence-based measurement of nitric oxide synthase activity in activated rat macrophages using dichlorofluorescein. *Nitric Oxide* **1**, 359-369
- (37) Soh, N., Katayama, Y., and Maeda, M. (2001) A fluorescent probe for monitoring nitric oxide production using a novel detection concept. *Analyst* **126**, 564-566
- (38) Barker, S. L., Clark, H. A., Swallen, S. F., Kopelman, R., Tsang, A. W., and Swanson, J. A. (1999) Ratiometric and fluorescence-lifetime-based biosensors incorporating cytochrome c' and the detection of extra- and intracellular macrophage nitric oxide. *Anal Chem* **71**, 1767-1772
- (39) Franz, K. J., Singh, N., Spingler, B., and Lippard, S. J. (2000) Aminotroponiminates as ligands for potential metal-based nitric oxide sensors. *Inorg Chem* **39**, 4081-4092
- (40) Franz, K. J., Singh, N., and Lippard, S. J. (2000) Metal-Based NO Sensing by Selective Ligand Dissociation *Angew Chem Int Ed Engl* **39**, 2120-2122

8. References

- (41) Meineke, P., Rauen, U., de Groot, H., Korth, H. G., and Sustman, R. (2000) Nitric oxide detection and visualization in biological systems. Applications of the FNOCT method. *Biol Chem* **381**, 575-582
- (42) Batz, M., Korth, H. G., Meineke, P., and Sustmann, R. (1999) Fluorescence detection of nitric oxide based on cheletropic spin traps. *Methods Enzymol* **301**, 532-539
- (43) Kojima, H., Nakatsubo, N., Kikuchi, K., Kawahara, S., Kirino, Y., Nagoshi, H., Hirata, Y., and Nagano, T. (1998) Detection and imaging of nitric oxide with novel fluorescent indicators: diaminofluoresceins. *Anal Chem* **70**, 2446-2453
- Kojima H, Nakatsubo N, Kikuchi K, Kawahara S, Kirino Y, Nagoshi H, Hirata Y & Nagano T. Detection and imaging of nitric oxide with novel fluorescent indicators: diaminofluoresceins. *Anal. Chem.* 1998; 70(13), 2446-2453
- (44) Kojima, H., Hirotsani, M., Nakatsubo, N., Kikuchi, K., Urano, Y., Higuchi, T., Hirata, Y., and Nagano, T. (2001) Bioimaging of nitric oxide with fluorescent indicators based on the rhodamine chromophore. *Anal Chem* **73**, 1967-1973
- (45) von Bohlen and Halbach, O. (2003) Nitric oxide imaging in living neuronal tissues using fluorescent probes. *Nitric Oxide* **9**, 217-228.
- (46) Lim, M.H., Xu, D. and Lippard, S.J. (2006) Visualization of nitric oxide in living cells by a copper-based fluorescent probe. *Nat Chem Biol* **2**, 375-380.
- (47) McQuade, L. E., Ma, J., Lowe, G., Ghatpande, A., Gelperin, A., and Lippard, S. J. Visualization of nitric oxide production in the mouse main olfactory bulb by a cell-trappable copper(II) fluorescent probe. *Proc Natl Acad Sci U S A* **107**, 8525-8530
- (48) Sato, M., Hida, N., and Umezawa, Y. (2005) Imaging the nanomolar range of nitric oxide with an amplifier-coupled fluorescent indicator in living cells. *Proc Natl Acad Sci U S A*. **102**, 14515-14520.
- (49) Saraiva, J., Marotta-Oliveira, S. S., Cicillini, S. A., Eloy Jde, O., and Marchetti, J. M. (2011) Nanocarriers for nitric oxide delivery. *J Drug Deliv* **2011**, 936438

8. References

- (50) Yokoyama, H., Fujii, S., Yoshimura, T., Ohya-Nishiguchi, H., and Kamada, H. (1997) In vivo ESR-CT imaging of the liver in mice receiving subcutaneous injection of nitric oxide-bound iron complex. *Magn Reson Imaging* **15**, 249-253
- (51) Nagano, T. (1999) Practical methods for detection of nitric oxide. *Luminescence* **14**, 283-290
- (52) Townsend, D. W., and Beyer, T. (2002) A combined PET/CT scanner: the path to true image fusion. *Br J Radiol* 75 Spec No, S24-30
- (53) Shao, Y., Cherry, S. R., Farahani, K., Meadors, K., Siegel, S., Silverman, R. W., and Marsden, P. K. (1997) Simultaneous PET and MR imaging. *Phys Med Biol* **42**, 1965-1970
- (54) Ley, K., Laudanna, C., Cybulsky, M. I., and Nourshargh, S. (2007) Getting to the site of inflammation: the leukocyte adhesion cascade updated. *Nat Rev Immunol* **7**, 678-689
- (55) Reitsma, S., Slaaf, D. W., Vink, H., van Zandvoort, M. A., and oude Egbrink, M. G. (2007) The endothelial glycocalyx: composition, functions, and visualization. *Pflugers Arch* **454**, 345-359
- (56) Megens, R. T., Reitsma, S., Schiffers, P. H., Hilgers, R. H., De Mey, J. G., Slaaf, D. W., oude Egbrink, M. G., and van Zandvoort, M. A. (2007) Two-photon microscopy of vital murine elastic and muscular arteries. Combined structural and functional imaging with subcellular resolution. *J Vasc Res* **44**, 87-98
- (57) Ritman, E. L., and Lerman, A. (2007) The dynamic vasa vasorum. *Cardiovasc Res* **75**, 649-658
- (58) Hirsh, J., and Fuster, V. (1994) Guide to anticoagulant therapy. Part 1: Heparin. American Heart Association. *Circulation* **89**, 1449-1468
- (59) Hirsh, J., and Fuster, V. (1994) Guide to anticoagulant therapy. Part 2: Oral anticoagulants. American Heart Association. *Circulation* **89**, 1469-1480

8. References

- (60) Miserus R.J., Dirksen A., Douma K., van Zandvoort M.A.M.J., Daemen M.J.A.P., Heeneman S., Kooi E. and Hackeng T.M (2007) Molecular Imaging of thrombi using a bimodal A2-antiplasmin -based contrast agent. *Journal of Thrombosis and Haemostasis* **5**.
- (61) Prinzen, L., Miserus, R. J., Dirksen, A., Hackeng, T. M., Deckers, N., Bitsch, N. J., Megens, R. T., Douma, K., Heemskerk, J. W., Kooi, M. E., Frederik, P. M., Slaaf, D. W., van Zandvoort, M. A., and Reutelingsperger, C. P. (2007) Optical and magnetic resonance imaging of cell death and platelet activation using annexin a5-functionalized quantum dots. *Nano Lett* **7**, 93-100
- (62) Cao, L., Wang, X., Meziani, M. J., Lu, F., Wang, H., Luo, P. G., Lin, Y., Harruff, B. A., Veca, L. M., Murray, D., Xie, S. Y., and Sun, Y. P. (2007) Carbon dots for multiphoton bioimaging. *J Am Chem Soc* **129**, 11318-11319
- (63) Yang, S. T., Cao, L., Luo, P. G., Lu, F., Wang, X., Wang, H., Meziani, M. J., Liu, Y., Qi, G., and Sun, Y. P. (2009) Carbon dots for optical imaging in vivo. *J Am Chem Soc* **131**, 11308-11309
- (64) Göppert-Mayer, M. (1931) Über Elementarakte mit zwei Quantensprüngen. *Ann. Phys.*, **9**:273-295
- (65) Masters, B.R. and P.T. So (2004) Antecedents of two-photon excitation laser scanning microscopy. *Microsc Res Tech* **63**, 3-11
- (66) Sako, Y., Sekihata, A., Yanagisawa, Y., Yamamoto, M., Shimada, Y., Ozaki, K., and Kusumi, A. (1997) Comparison of two-photon excitation laser scanning microscopy with UV-confocal laser scanning microscopy in three-dimensional calcium imaging using the fluorescence indicator Indo-1. *J Microsc* **185**, 9-20
- (67) Iborra, F., Cook, P. R., and Jackson, D. A. (2003) Applying microscopy to the analysis of nuclear structure and function. *Methods* **29**, 131-141
- (68) Piston, D.W. (1999) Imaging living cells and tissues by two-photon excitation microscopy. *Trends Cell Biol* **9**, 66-69.
- (69) Zipfel, W. R., Williams, R. M., and Webb, W. W. (2003) Nonlinear magic: multiphoton microscopy in the biosciences. *Nat Biotechnol* **21**, 1369-1377

8. References

- (70) van Zandvoort, M., Engels, W., Douma, K., Beckers, L., Oude Egbrink, M., Daemen, M., and Slaaf, D. W. (2004) Two-photon microscopy for imaging of the (atherosclerotic) vascular wall: a proof of concept study. *J Vasc Res* **41**, 54-63
- (71) Konig, K. (2000) Multiphoton microscopy in life sciences. *J Microsc* **200**, 83-104
- (72) Tauer, U. (2002) Advantages and risks of multiphoton microscopy in physiology. *Exp Physiol* **87**, 709-714
- (73) Moncada, S., and Higgs, E. A. (2006) The discovery of nitric oxide and its role in vascular biology. *Br J Pharmacol* **147** Suppl 1, S193-201
- (74) Yuan, S. Y. (2006) New insights into eNOS signaling in microvascular permeability. *Am J Physiol Heart Circ Physiol* **291**, H1029-1031
- (75) Boo, Y. C., and Jo, H. (2003) Flow-dependent regulation of endothelial nitric oxide synthase: role of protein kinases. *Am J Physiol Cell Physiol* **285**, C499-508
- (76) Sato, M., Hida, N., and Umezawa, Y. (2005) Imaging the nanomolar range of nitric oxide with an amplifier-coupled fluorescent indicator in living cells. *Proc Natl Acad Sci U S A* **102**, 14515-14520
- (77) Wiklund, N. P., Iversen, H. H., Leone, A. M., Celtek, S., Brundin, L., Gustafsson, L. E., and Moncada, S. (1999) Visualization of nitric oxide formation in cell cultures and living tissue. *Acta Physiol Scand* **167**, 161-166
- (78) Hong, H., Sun, J., and Cai, W. (2009) Multimodality imaging of nitric oxide and nitric oxide synthases. *Free Radic Biol Med* **47**, 684-698
- (79) Nagano, T., and Yoshimura, T. (2002) Bioimaging of nitric oxide. *Chem Rev* **102**, 1235-1270
- (80) van Zandvoort, M., Engels, W., Douma, K., Beckers, L., Oude Egbrink, M., Daemen, M., and Slaaf, D. W. (2004) Two-photon microscopy for imaging of the (atherosclerotic) vascular wall: a proof of concept study. *J Vasc Res* **41**, 54-63
- (81) Luiking, Y. C., Engelen, M. P., and Deutz, N. E. (2010) Regulation of nitric oxide production in health and disease. *Curr Opin Clin Nutr Metab Care* **13**, 97-104

8. References

- (82) Flam, B. R., Eichler, D. C., and Solomonson, L. P. (2007) Endothelial nitric oxide production is tightly coupled to the citrulline-NO cycle. *Nitric Oxide* **17**, 115-121
- (83) Luiking, Y. C., Poeze, M., Ramsay, G., and Deutz, N. E. (2009) Reduced citrulline production in sepsis is related to diminished de novo arginine and nitric oxide production. *Am J Clin Nutr* **89**, 142-152
- (84) Kubes, P., and McCafferty, D. M. (2000) Nitric oxide and intestinal inflammation. *Am J Med* **109**, 150-158
- (85) Buga, G. M., Singh, R., Pervin, S., Rogers, N. E., Schmitz, D. A., Jenkinson, C. P., Cederbaum, S. D., and Ignarro, L. J. (1996) Arginase activity in endothelial cells: inhibition by NG-hydroxy-L-arginine during high-output NO production. *Am J Physiol* **271**, H1988-1998
- (86) Luiking, Y. C., and Deutz, N. E. (2007) Exogenous arginine in sepsis. *Crit Care Med* **35**, S557-563
- (87) Luiking, Y. C., Poeze, M., Dejong, C. H., Ramsay, G., and Deutz, N. E. (2004) Sepsis: an arginine deficiency state? *Crit Care Med* **32**, 2135-2145
- (88) Chen, K., Inoue, M., Wasa, M., Fukuzawa, M., Kamata, S., and Okada, A. (1997) Expression of endothelial constitutive nitric oxide synthase mRNA in gastrointestinal mucosa and its downregulation by endotoxin. *Life Sci* **61**, 1323-1329
- (89) Kvietys, P. R., and Granger, D. N. (2012) Role of reactive oxygen and nitrogen species in the vascular responses to inflammation. *Free Radic Biol Med* **52**, 556-592
- (90) Poeze, M., Bruins, M. J., Kessels, F., Luiking, Y. C., Lamers, W. H., and Deutz, N. E. (2011) Effects of L-arginine pretreatment on nitric oxide metabolism and hepatosplanchnic perfusion during porcine endotoxemia. *Am J Clin Nutr* **93**, 1237-1247
- (91) Lu, J. L., Schmiede, L. M., 3rd, Kuo, L., and Liao, J. C. (1996) Downregulation of endothelial constitutive nitric oxide synthase expression by lipopolysaccharide. *Biochem Biophys Res Commun* **225**, 1-5

8. References

- (92) Liu, S. F., Adcock, I. M., Old, R. W., Barnes, P. J., and Evans, T. W. (1996) Differential regulation of the constitutive and inducible nitric oxide synthase mRNA by lipopolysaccharide treatment in vivo in the rat. *Crit Care Med* **24**, 1219-1225
- (93) Soeters, P. B., Hallemeesch, M. M., Bruins, M. J., van Eijk, H. M., and Deutz, N. E. (2002) Quantitative in vivo assessment of arginine utilization and nitric oxide production in endotoxemia. *Am J Surg* **183**, 480-488
- (94) Hollenberg, S. M., Broussard, M., Osman, J., and Parrillo, J. E. (2000) Increased microvascular reactivity and improved mortality in septic mice lacking inducible nitric oxide synthase. *Circ Res* **86**, 774-778
- (95) Nathan, C., and Xie, Q. W. (1994) Nitric oxide synthases: roles, tolls, and controls. *Cell* **78**, 915-918
- (96) Vissers, Y. L., Debats, I. B., Luiking, Y. C., Jalan, R., van der Hulst, R. R., Dejong, C. H., and Deutz, N. E. (2004) Pros and cons of L-arginine supplementation in disease. *Nutr Res Rev* **17**, 193-210
- (97) Shen, L. J., Beloussow, K., and Shen, W. C. (2005) Accessibility of endothelial and inducible nitric oxide synthase to the intracellular citrulline-arginine regeneration pathway. *Biochem Pharmacol* **69**, 97-104
- (98) Bode-Boger, S. M., Boger, R. H., Galland, A., Tsikas, D., and Frolich, J. C. (1998) L-arginine-induced vasodilation in healthy humans: pharmacokinetic-pharmacodynamic relationship. *Br J Clin Pharmacol* **46**, 489-497
- (99) Boger, R. H., and Bode-Boger, S. M. (2001) The clinical pharmacology of L-arginine. *Annu Rev Pharmacol Toxicol* **41**, 79-99
- (100) Fukatsu, K., Ueno, C., Maeshima, Y., Hara, E., Nagayoshi, H., Omata, J., Mochizuki, H., and Hiraide, H. (2004) Effects of L-arginine infusion during ischemia on gut blood perfusion, oxygen tension, and circulating myeloid cell activation in a murine gut ischemia/reperfusion model. *JPEN J Parenter Enteral Nutr* **28**, 224-230; discussion 230-221
- (101) Jeyabalan, G., Klune, J. R., Nakao, A., Martik, N., Wu, G., Tsung, A., and Geller, D. A. (2008) Arginase blockade protects against hepatic damage in warm ischemia-reperfusion. *Nitric Oxide* **19**, 29-35

8. References

- (102) Durante, W., Johnson, F. K., and Johnson, R. A. (2007) Arginase: a critical regulator of nitric oxide synthesis and vascular function. *Clin Exp Pharmacol Physiol* **34**, 906-911
- (103) Ochoa, J. B., Bernard, A. C., O'Brien, W. E., Griffen, M. M., Maley, M. E., Rockich, A. K., Tsuei, B. J., Boulanger, B. R., Kearney, P. A., and Morris Jr, S. M., Jr. (2001) Arginase I expression and activity in human mononuclear cells after injury. *Ann Surg* **233**, 393-399
- (104) Kim, J. H., Bugaj, L. J., Oh, Y. J., Bivalacqua, T. J., Ryoo, S., Soucy, K. G., Santhanam, L., Webb, A., Camara, A., Sikka, G., Nyhan, D., Shoukas, A. A., Ilies, M., Christianson, D. W., Champion, H. C., and Berkowitz, D. E. (2009) Arginase inhibition restores NOS coupling and reverses endothelial dysfunction and vascular stiffness in old rats. *J Appl Physiol* **107**, 1249-1257
- (105) Morris, S. M., Jr. (2005) Arginine metabolism in vascular biology and disease. *Vasc Med* **10**, S83-87
- (106) Vanhoutte, P. M. (2008) Arginine and arginase: endothelial NO synthase double crossed? *Circ Res* **102**, 866-868
- (107) Morris, S. M., Jr. (2009) Recent advances in arginine metabolism: roles and regulation of the arginases. *Br J Pharmacol* **157**, 922-930
- (108) El Kasmi, K. C., Qualls, J. E., Pesce, J. T., Smith, A. M., Thompson, R. W., Henao-Tamayo, M., Basaraba, R. J., Konig, T., Schleicher, U., Koo, M. S., Kaplan, G., Fitzgerald, K. A., Tuomanen, E. I., Orme, I. M., Kanneganti, T. D., Bogdan, C., Wynn, T. A., and Murray, P. J. (2008) Toll-like receptor-induced arginase 1 in macrophages thwarts effective immunity against intracellular pathogens. *Nat Immunol* **9**, 1399-1406
- (109) Morris, S. M., Jr. (2007) Arginine metabolism: boundaries of our knowledge. *J Nutr* **137**, 1602S-1609S
- (110) Chicoine, L. G., Paffett, M. L., Young, T. L., and Nelin, L. D. (2004) Arginase inhibition increases nitric oxide production in bovine pulmonary arterial endothelial cells. *Am J Physiol Lung Cell Mol Physiol* **287**, L60-68

8. References

- (111) Van den Bossche, J., Lamers, W. H., Koehler, E. S., Geuns, J. M., Alhonen, L., Uimari, A., Pirnes-Karhu, S., Van Overmeire, E., Morias, Y., Brys, L., Vereecke, L., De Baetselier, P., and Van Ginderachter, J. A. (2012) Pivotal Advance: Arginase-1-independent polyamine production stimulates the expression of IL-4-induced alternatively activated macrophage markers while inhibiting LPS-induced expression of inflammatory genes. *J Leukoc Biol* **91**, 685-699
- (112) Carrillo, A., Chamorro, S., Rodriguez-Gago, M., Alvarez, B., Molina, M. J. Rodriguez-Barbosa, J. I., Sanchez, A., Ramirez, P., Munoz, A., Dominguez, J., Parrilla, P., and Yelamos, J. (2002) Isolation and characterization of immortalized porcine aortic endothelial cell lines. *Vet Immunol Immunopathol* **89**, 91-98
- (113) Yamada, M., Lamping, K. G., Duttaroy, A., Zhang, W., Cui, Y., Bymaster, F. P., McKinzie, D. L., Felder, C. C., Deng, C. X., Faraci, F. M., and Wess, J. (2001) Cholinergic dilation of cerebral blood vessels is abolished in M(5) muscarinic acetylcholine receptor knockout mice. *Proc Natl Acad Sci U S A* **98**, 14096-14101
- (114) Ouyang, J., Hong, H., Shen, C., Zhao, Y., Ouyang, C., Dong, L., Zhu, J., Guo, Z., Zeng, K., Chen, J., Zhang, C., and Zhang, J. (2008) A novel fluorescent probe for the detection of nitric oxide in vitro and in vivo. *Free Radic Biol Med* **45**, 1426-1436
- (115) Feelisch, M. (1993) The Biochemical Pathways of Nitric-Oxide Formation from Nitrovasodilators - Appropriate Choice of Exogenous NO Donors and Aspects of Preparation and Handling of Aqueous NO Solutions. *J Cardiovasc Pharm* **17**, S25-S33
- (116) Tian, J., Hou, Y., Lu, Q., Wiseman, D. A., Vasconcelos Fonesca, F., Elms, S., Fulton, D. J., and Black, S. M. (2010) A novel role for caveolin-1 in regulating endothelial nitric oxide synthase activation in response to H₂O₂ and shear stress. *Free Radic Biol Med* **49**, 159-170
- (117) Sartoretto, J. L., Kalwa, H., Pluth, M. D., Lippard, S. J., and Michel, T. (2011) Hydrogen peroxide differentially modulates cardiac myocyte nitric oxide synthesis. *Proc Natl Acad Sci U S A* **108**, 15792-15797

8. References

- (118) Cai, H., Li, Z., Dikalov, S., Holland, S. M., Hwang, J., Jo, H., Dudley, S. C., Jr., and Harrison, D. G. (2002) NAD(P)H oxidase-derived hydrogen peroxide mediates endothelial nitric oxide production in response to angiotensin II. *J Biol Chem* **277**, 48311-48317
- (119) Thomas, S. R., Chen, K., and Keane, J. F., Jr. (2002) Hydrogen peroxide activates endothelial nitric-oxide synthase through coordinated phosphorylation and dephosphorylation via a phosphoinositide 3-kinase-dependent signaling pathway. *J Biol Chem* **277**, 6017-6024
- (120) Kuzkaya, N., Weissmann, N., Harrison, D. G., and Dikalov, S. (2003) Interactions of peroxynitrite, tetrahydrobiopterin, ascorbic acid, and thiols: implications for uncoupling endothelial nitric-oxide synthase. *J Biol Chem* **278**, 22546-22554
- (121) Jay B. Fox Jr. Kinetics and mechanisms of the Griess reaction. *Analytical Chemistry* **1979**, 1493-1502
- (122) Zhang, Q., Malik, P., Pandey, D., Gupta, S., Jagnandan, D., Belin de Chantemele, E., Banfi, B., Marrero, M. B., Rudic, R. D., Stepp, D. W., and Fulton, D. J. (2008) Paradoxical activation of endothelial nitric oxide synthase by NADPH oxidase. *Arterioscler Thromb Vasc Biol* **28**, 1627-1633
- (123) Lu, X., and Kassab, G. S. (2004) Nitric oxide is significantly reduced in ex vivo porcine arteries during reverse flow because of increased superoxide production. *J Physiol* **561**, 575-582
- (124) Wijnands, K. A., Vink, H., Briede, J. J., van Faassen, E. E., Lamers, W. H., Buurman, W. A., and Poeze, M. (2012) Citrulline a more suitable substrate than arginine to restore NO production and the microcirculation during endotoxemia. *PLoS One* **7**, e37439
- (125) Buchwalow, I. B., Podzuweit, T., Bocker, W., Samoilova, V. E., Thomas, S., Wellner, M., Baba, H. A., Robenek, H., Schnekenburger, J., and Lerch, M. M. (2002) Vascular smooth muscle and nitric oxide synthase. *Faseb J* **16**, 500-508

8. References

- (126) Zadeh, M. S., Kolb, J. P., Geromin, D., D'Anna, R., Boulmerka, A., Marconi, A., Dugas, B., Marsac, C., and D'Alessio, P. (2000) Regulation of ICAM-1/CD54 expression on human endothelial cells by hydrogen peroxide involves inducible NO synthase. *J Leukoc Biol* **67**, 327-334
- (127) Singh, R. J., Hogg, N., Joseph, J., and Kalyanaraman, B. (1996) Mechanism of nitric oxide release from S-nitrosothiols. *J Biol Chem* **271**, 18596-18603
- (128) Demura, Y., Ameshima, S., Ishizaki, T., Okamura, S., Miyamori, I., and Matsukawa, S. (1998) The activation of eNOS by copper ion (Cu²⁺) in human pulmonary arterial endothelial cells (HPAEC). *Free Radic Biol Med* **25**, 314-320
- (129) Berkowitz, D. E., White, R., Li, D., Minhas, K. M., Cernetich, A., Kim, S., Burke, S., Shoukas, A. A., Nyhan, D., Champion, H. C., and Hare, J. M. (2003) Arginase reciprocally regulates nitric oxide synthase activity and contributes to endothelial dysfunction in aging blood vessels. *Circulation* **108**, 2000-2006
- (130) Bachetti, T., Comini, L., Francolini, G., Bastianon, D., Valetti, B., Cadei, M., Grigolato, P., Suzuki, H., Finazzi, D., Albertini, A., Curello, S., and Ferrari, R. (2004) Arginase pathway in human endothelial cells in pathophysiological conditions. *J Mol Cell Cardiol* **37**, 515-523
- (131) Munder, M. (2009) Arginase: an emerging key player in the mammalian immune system. *Br J Pharmacol* **158**, 638-651

9. Curriculum Vitae

Personal profile:

Name: Mitrajit Ghosh

Date of Birth: 21-11-1983

Marital status: Single

Gender: Male

Nationality: Indian

Education and Qualification:

De- Nobili School, Mugma, Dhanbad, India. High School (I.C.S.E. Board, New Delhi) May 2000

De- Nobili School, Mugma, Dhanbad, India. Intermediate (I.S.C. Board, New Delhi) in Physics, Chemistry, Maths, and Biology. May 2002

St. Joseph's College, Bangalore University, Bangalore, India.
Bachelors Degree in Science (B.Sc.) in Bioscience
(Subjects: Microbiology, Chemistry, Botany) June 2002- 2005

CMRIMS, Bangalore University, Bangalore, India.
Masters Degree in Science (M.Sc.) in Microbiology. June 2005-2007

Cardiovascular Research Institute of Maastricht
(Maastricht University, the Netherlands) and
Institute for Molecular Cardiovascular Research
(RWTH University, Germany). *Doctorate studies.* October 2008-present

Work experience

USA-INDIA collaborated research project (2007-2008)

Sponsorship:

Cromoz.Inc., North Carolina, USA and Indian Institute of Technology, Kanpur, (IIT-Kanpur) India.

Place: Department of Bio-inorganic Chemistry, IIT- Kanpur, India.

Designation of appointment: Research Associate.

Scientific advisor: Prof. Dr. Sabyasachi Sarkar (Department of Chemistry), IIT-Kanpur, India.

9. Curriculum Vitae

Research Exposures:

- National Institute of Oceanography, Shwarde Pharmaceuticals, UB Group (Goa, India)
Presented visit report as requirement towards Master's Degree May 2007
- National Dairy Research Centre (Bangalore, India)
Presented visit report as requirement towards Bachelor's Degree May 2005
- National Institute of Advanced Studies (Indian Institute of Science, Bangalore, India).
Two weeks summer training program.
TOPIC: "Understanding Science". May 2004
- St. Joseph's College (Bangalore, India) (*with visit to Taramani Research Centre, Chennai*). Project in Genetics
TOPIC: "Dermatoglyphics analysis of allergic patients". June-July 2003
- Indian Institute of Technology-Kanpur (Kanpur, India). Assignment work on "Severe Acute Respiratory Syndrome (SARS)". May 2003

Meetings/Conferences attended:

- Gordon Research Seminar & Conference 2012- Endothelial Cell Phenotypes in Health & Disease, Lucca (Barga), Italy (*poster presentation*) July – August 2012
- DFG-IRTG On site Review, Aachen, Germany (*Oral & poster presentation*) July 2012
- Biomedica 2012-The European Life sciences Summit, Liege, Belgium (*poster presentation*) April 2012
- Cardiovascular Network Retreat 2012, Geissen, Germany (*Oral presentation*) March 2012
- Joint meeting of The European Society for Microcirculation (ESM) and The German Society of Microcirculation and Vascular Biology (GFMVB), Munich, Germany (*Oral presentation*) October 2011
- 6th European Molecular Imaging Meeting, Leiden, the Netherlands (*Oral presentation*) June 2011
- Biomedical Engineering Research Day 2011, Technical University Eindhoven, the Netherlands (*poster presentation*) May 2011
- Approaching the Clinic: Nitrite and Nitrate Pathophysiology and Therapy, Atlanta, Georgia, United States of America (*poster presentation*) May 2011

9. Curriculum Vitae

- Focus on Microscopy (FOM) Conference 2011, Konstanz, Germany
(*poster presentation*) April 2011
- The Cardiovascular Conference, Nordwijkerhout, the Netherlands
(*poster presentation*) March 2011
- Life Sciences Career Event, Maastricht University, Maastricht, the Netherlands
(*poster presentation*) March 2011
- CARIM Day, Maastricht University, the Netherlands
(*poster presentation*) November 2010
- Annual Symposium of the DFG Graduate-School "EuCAR", Aachen, Germany
(*Oral presentation*) October 2010
- Annual Congress of European Society of Intensive Care Medicine (ESICM), Barcelona, Spain
(*poster presentation*) October 2010
- Netherlands Heart Foundation's one week PhD training program in Vascular Biology
(Arnhem, the Netherlands) (*poster presentation*) October 2010
- 9th World Congress for Microcirculation – Maison de la Chimie, Paris, France- "Young Investigator Symposium" on Vascular Biology (*Oral presentation*) September 2010
- First British Heart Foundation sponsored - Vascular Biology Summer School, Bristol, United Kingdom (*Oral and poster presentation*) July 2010
- 16th International Vascular Biology Meeting (IVBM), Los Angeles, California, United States of America (*poster presentation*) June 2010
- Netherlands Heart Foundation's one week PhD training program in Thrombosis and Haemostasis (Arnhem, the Netherlands) (*poster presentation*) October 2009
- 12th Dutch Atherosclerosis Society, Symposium (Ede, the Netherlands) March 2009
- National Conference at Oxford College (Bangalore, India)
TOPIC: Molecular Breakthroughs in Diagnostic Microbiology. April 2007

Awards and honors

Travel award for Gordon Research Seminar & Conference, Lucca (Braga), Italy.

Has been awarded with merit certificate (St. Joseph's College, Bangalore, India) during Bachelor study of science for scoring first class marks.

9. Curriculum Vitae

Honorarium awardee fellow at National Institute of Advanced Studies (IISc Bangalore, India) for summer program.

Publications

Journals:

01. M Ghosh, NMS van den Akker, KAP Wijnands, C Weber, Lindsey E. McQuade , Michael D. Pluth , Stephen J. Lippard , Mark J Post, DGM Molin, MAMJ van Zandvoort **(2013)**. Specific visualization of nitric oxide in the vasculature with a copper (II) fluorescent probe and two-photon microscopy. **PLoS ONE** (accepted)

02. Sonkar S.K., **Ghosh M**, Roy M, Begum A and Sarkar S. **(2012)**, Carbon nano-onions as nontoxic and high performance fluorescing agents in food chain – an in vivo study from unicellular *Escherichia coli* to multicellular *Caenorhabditis elegans*. **Mater. Express 2, 105-114 (with cover image)**.

03. Ghosh, M., Sonkar, S. K., Saxena, M. and Sarkar, S. **(2011)**, Carbon Nano-onions for Imaging the Life Cycle of *Drosophila Melanogaster*. **Small, 7: 3170–3177 (with frontispiece)**.

04. Sonkar S.K., **Ghosh M**, Muller A and Sarkar S. Unprecedented Giant Spherical Hollow Aggregates by Substrate Templated Assembly of {Mo₇₂Fe₃₀} Keplerates. (submitted)

05. Wijnands KAP, Hoeksema M, Meesters D M , Akker van den NMS, Molin DGM, Briedé JJ, **Ghosh M**, Köhler E S, Winther P de M, Buurman W A, Lamers W H, Poeze M. Detrimental effects of Arginase-1 deficiency on vascular function and NOS3 mediated NO production during endotoxemia.(submitted)

06. Kristien J.A. Lemmens, Bregje van de Wier, Nathalie Vaes, **Mitrajit Ghosh**, Marc AMJ van Zandvoort, Wim J.F. van der Vijgh, Aalt Bast and Guido R.M.M. Haenen. The direct antioxidant effect of the flavonoid monoHER. (submitted)

9. Curriculum Vitae**Conference proceedings:**

Abstract; **M Ghosh**, NMS van den Akker, C Weber, DGM Molin, MAMJ van Zandvoort **(2011)** Direct imaging and visualization of nitric oxide in cells and arteries with a copper (II) fluorescent probe and two-photon microscopy. **Nitric Oxide, Vol. 24 (May 2011), S17.**

Abstract; **M Ghosh**, NMS van den Akker, C Weber, M.J.Post, DGM Molin, MAMJ van Zandvoort **(2011)** Specific visualization of nitric oxide in cells and arteries with a copper based fluorescent probe and two-photon microscopy. **J Vasc Res 2011; 48(Suppl.1):4-356 (DOI: 10.1159/000332604).**